Final Report

FDOT Contract No.: BED31-977-12
UF Contract No.: AWD13557

Determination of in-situ rock density and strength with SH-Love wave tomography

Principal Investigators:
Khiem Tran, Ph.D.
Michael McVay, Ph.D.

Researchers:
Minh Nhat Tran (Ph.D. student)
Bingkun Yang (Ph.D. student)
Kunyu Yang, Ph.D.

Department of Civil and Coastal Engineering
Engineering School of Sustainable Infrastructure and Environment
University of Florida
P.O. Box 116580
Gainesville, Florida 32611-6580

Developed for the

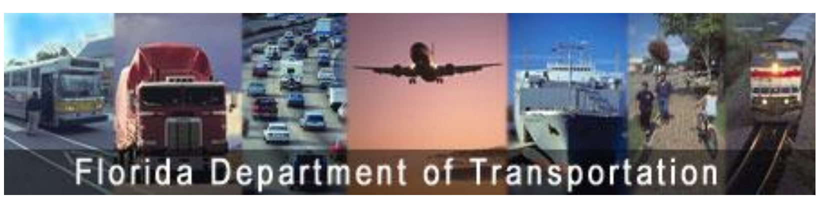

Kelly Shishlova, P.E., Project Manager

May 2025

DISCLAIMER

The opinions, findings, and conclusions expressed in this publication are those of the authors and not necessarily those of the Florida Department of Transportation or the U.S. Department of Transportation.

Prepared in cooperation with the State of Florida Department of Transportation and the U.S. Department of Transportation.

SI (MODERN METRIC) CONVERSION FACTORS (from FHWA)

APPROXIMATE CONVERSIONS TO SI UNITS

SYMBOL	WHEN YOU KNOW	MULTIPLY BY	TO FIND	SYMBOL
LENGTH				
in	inches	25.4	millimeters	mm
ft	feet	0.305	meters	m
yd	yards	0.914	meters	m
mi	miles	1.61	kilometers	km

SYMBOL	WHEN YOU KNOW	MULTIPLY BY	TO FIND	SYMBOL
AREA				
in^2	square inches	645.2	square millimeters	mm^2
ft^2	square feet	0.093	square meters	m^2
yd^2	square yard	0.836	square meters	m^2
ac	acres	0.405	hectares	ha
mi^2	square miles	2.59	square kilometers	km^2

SYMBOL	WHEN YOU KNOW	MULTIPLY BY	TO FIND	SYMBOL
VOLUME				
fl oz	fluid ounces	29.57	milliliters	mL
gal	gallons	3.785	liters	L
ft^3	cubic feet	0.028	cubic meters	m^3
yd^3	cubic yards	0.765	cubic meters	m^3
NOTE: volumes greater than 1000 L shall be shown in m^3				

SYMBOL	WHEN YOU KNOW	MULTIPLY BY	TO FIND	SYMBOL
MASS				
oz	ounces	28.35	grams	g
lb	pounds	0.454	kilograms	kg
T	short tons (2000 lb)	0.907	megagrams (or "metric ton")	Mg (or "t")

SYMBOL	WHEN YOU KNOW	MULTIPLY BY	TO FIND	SYMBOL
TEMPERATURE (exact degrees)				
°F	Fahrenheit	5 (F-32)/9 or (F-32)/1.8	Celsius	°C

SYMBOL	WHEN YOU KNOW	MULTIPLY BY	TO FIND	SYMBOL
ILLUMINATION				
fc	foot-candles	10.76	lux	lx
fl	foot-Lamberts	3.426	candela/m^2	cd/m^2

SYMBOL	WHEN YOU KNOW	MULTIPLY BY	TO FIND	SYMBOL
FORCE and PRESSURE or STRESS				
Lbf*	poundforce	4.45	newtons	N
kip	kip force	1000	pounds	lbf
lbf/in^2	poundforce per square inch	6.89	kilopascals	kPa

APPROXIMATE CONVERSIONS TO SI UNITS

SYMBOL	WHEN YOU KNOW	MULTIPLY BY	TO FIND	SYMBOL
LENGTH				
mm	millimeters	0.039	inches	in
m	meters	3.28	feet	ft
m	meters	1.09	yards	yd
km	kilometers	0.621	miles	mi

SYMBOL	WHEN YOU KNOW	MULTIPLY BY	TO FIND	SYMBOL
AREA				
mm^2	square millimeters	0.0016	square inches	in^2
m^2	square meters	10.764	square feet	ft^2
m^2	square meters	1.195	square yards	yd^2
ha	hectares	2.47	acres	ac
km^2	square kilometers	0.386	square miles	mi^2

SYMBOL	WHEN YOU KNOW	MULTIPLY BY	TO FIND	SYMBOL
VOLUME				
mL	milliliters	0.034	fluid ounces	fl oz
L	liters	0.264	gallons	gal
m^3	cubic meters	35.314	cubic feet	ft^3
m^3	cubic meters	1.307	cubic yards	yd^3

SYMBOL	WHEN YOU KNOW	MULTIPLY BY	TO FIND	SYMBOL
MASS				
g	grams	0.035	ounces	oz
kg	kilograms	2.202	pounds	lb
Mg (or "t")	megagrams (or "metric ton")	1.103	short tons (2000 lb)	T

SYMBOL	WHEN YOU KNOW	MULTIPLY BY	TO FIND	SYMBOL
TEMPERATURE (exact degrees)				
°C	Celsius	1.8C+32	Fahrenheit	°F

SYMBOL	WHEN YOU KNOW	MULTIPLY BY	TO FIND	SYMBOL
ILLUMINATION				
lx	lux	0.0929	foot-candles	fc
cd/m^2	candela/m^2	0.2919	foot-Lamberts	fl

SYMBOL	WHEN YOU KNOW	MULTIPLY BY	TO FIND	SYMBOL
FORCE and PRESSURE or STRESS				
N	newtons	0.225	poundforce	lbf
kPa	kilopascals	0.145	poundforce per square inch	lbf/in^2

*SI is the symbol for International System of Units. Appropriate rounding should be made to comply with Section 4 of ASTM E380.
(Revised March 2003)

TECHNICAL REPORT DOCUMENTATION PAGE

1. Report No.	2. Government Accession No.	3. Recipient's Catalog No.
4. Title and Subtitle Determination of in-situ rock density and strength with SH-Love wave tomography		5. Report Date May 2025 6. Performing Organization Code
7. Authors Khiem T. Tran, Michael McVay, Minh N. Tran, Bingkun Yang, and Kunyu Yang		8. Performing Organization Report No.
9. Performing Organization Name and Address University of Florida – Dept. of Civil and Coastal Engineering Engineering School of Sustainable Infrastructure and Environment 365 Weil Hall – P.O. Box 116580 Gainesville, FL 32611-6580		10. Work Unit No. (TRAIS) 11. Contract or Grant No. BED31-977-12
12. Sponsoring Agency Name and Address Florida Department of Transportation 605 Suwannee Street, MS 30 Tallahassee, FL 32399		13. Type of Report and Period Covered Final Report 10/1/2022 – 05/30/2025 14. Sponsoring Agency Code
15. Supplementary Notes		

16. Abstract

Acquiring detailed information on in situ rock density and its variability is essential for the design of shallow foundations. For instance, mass density influences rock strength and its stress-strain behavior in most Florida limestone formations. Moreover, all rock formations are heterogeneous, with density variations occurring on different scales both vertically and horizontally and porosities exceeding twenty percent. Traditional invasive methods, such as core sampling, provide valuable data but are limited by their invasive nature and restricted spatial coverage. This often leads to gaps in the data, potentially compromising the foundation design, especially in heterogeneous formations like those found in Florida In this project, a new seismic method, SH-Love full-waveform inversion (SH-Love FWI), was developed for determination of rock density over large areas, eliminating the need for extensive borings. The method takes advantage of the high sensitivity of horizontal shear (SH) and Love waves to material mass density and simultaneously inverts mass density and S-wave velocity (Vs), which can be used to compute elastic moduli for foundation design. Validation through synthetic modeling demonstrated its capability to resolve complex subsurface profiles, including thin, high-density layers. Field experiments at three Florida sites confirmed the method's efficacy, accurately characterizing subsurface profiles up to 18-m depth with submeter resolution. Seismic-derived densities closely matched rock core results, confirming SH-Love FWI as a reliable tool for determination of in situ rock density. Standalone GUI software for SH-Love FWI analysis has been developed and transferred to FDOT for future use.

Keywords: geotechnical site characterization, full-waveform inversion, rocks, density, SH- and Love-waves, strength of materials.

17. Key Words	18. Distribution Statement		
Geotechnical site characterization, full-waveform inversion, rocks, density, SH- and Love-waves, strength of materials.	No restrictions.		
19. Security Classif. (of this report) Unclassified	20. Security Classif. (of this page) Unclassified	21. No. of Pages 130	22. Price

Form DOT F 1700.7 (8-72) Reproduction of completed page authorized

ACKNOWLEDGMENTS

The researchers would like to thank the Florida Department of Transportation (FDOT) for the financial support to carry out this research and the State Materials Office in Gainesville and District 2 Geotechnical Materials Group for providing access and assisting with field tests.

EXECUTIVE SUMMARY

Detailed information on in situ rock density, layering, and associated variability is important for the design and construction of shallow foundations. For instance, the recent FDOT project BDV31-977-51 has shown that mass density (or unit weight) controls rock strength as well as its stress-strain behavior for most Florida limestone formations. In addition, all rock formations are heterogeneous with density varying both vertically and horizontally with porosity generally greater than twenty percent. Traditional invasive methods, such as core sampling, are expensive and provide limited coverage. This often leads to gaps in the data, potentially compromising the foundation design, especially in heterogeneous formations like those found in Florida

To address the issue, this project has developed a new seismic method, 2D SH-Love full-waveform inversion (2D SH-Love FWI) and its algorithm for determination of in situ rock density over large areas. The algorithm consists of the forward simulation of elastic horizontal shear (SH) and Love waves, and adjoint-state optimization for model updating (inversion) to extract material density and S-wave velocity. For field experiments, SH and Love waves are generated by applying a horizontal source (e.g., horizontally striking sledgehammer on a shear beam) and recorded by an array of horizontal geophones on the ground surface. The recorded waveform data are then analyzed to independently extract the density and S-wave velocity of the subsurface materials.

There are three main advantages of this SH-Love wave approach. First, it has been well recognized that SH and Love waves (horizontal source) are much more sensitive to material density than vertical S-wave, P-wave, and Rayleigh waves (P-SV) (vertical source), and thus the density can be extracted more accurately. Second, SH-Love wave simulation requires much less computing time (30% that of P-SV waves), and the 2D SH-Love FWI analysis can be performed quickly (20 minutes) in the field. Lastly and most importantly, both the mass density and S-wave

velocity (Vs) are characterized. Thus, shear (G) and Young (E) moduli can be computed for determination of shallow foundation's settlement and bearing capacity and other geotechnical analyses.

For validation of the seismic method, field experiments were conducted at three Florida sites (Bell, CR 250, and Kanapaha). Seismic tests were performed along multiple test lines up to 120 ft in length, and rock core samples were collected for comparison. The acquired seismic data were analyzed by the SH-Love FWI algorithm to extract subsurface density and Vs profiles up to 60-ft depth. The seismic-derived densities showed strong agreement with those obtained from rock core samples for all three test sites, confirming SH-Love FWI as a reliable tool for determination of in situ rock density. Finally, standalone GUI software for SH-Love FWI analysis has been developed and transferred to FDOT for future use.

TABLE OF CONTENTS

Table of Contents Page

DISCLAIMER ii

SI (MODERN METRIC) CONVERSION FACTORS (from FHWA) iii

TECHNICAL REPORT DOCUMENTATION PAGE v

ACKNOWLEDGMENTS vi

EXECUTIVE SUMMARY vii

LIST OF FIGURES xi

Chapter 1 – INTRODUCTION 1

1.1 Background 1
1.2 Outline of the study 3

Chapter 2 – DEVELOPMENT OF SH-LOVE FWI ALGORITHM (TASK 1) 4

2.1 Introduction 4
2.2 Methodology 4
2.2.1 Forward simulation 5
2.2.2 Model update 6
2.3 Synthetic experiment on a deep model of 18-m depth 10
2.3.1 Test configuration and setup 10
2.3.2 Inversion analysis and results 12
2.4 High resolution synthetic experiment on a model of 9-m depth 17
2.4.1 Test configuration and setup 17
2.4.2 Inversion analysis and results 18
2.5 Conclusion 23

Chapter 3 – OPTIMIZATION OF TEST CONFIGURATIONS AND WAVE CHARACTERISTICS (TASK 2) 25

3.1 Introduction 25
3.2 Synthetic experiment on deep model of 18-m depth 26
3.2.1 Test configuration 26
3.2.2 Results for test configuration 1 (24 receivers, 25 shots) 28
3.2.3 Results for test configuration 2 (24 receivers, 13 shots) 32
3.2.4 Results for test configuration 3 (12 receivers, 13 shots) 35
3.2.5 Results for test configuration 4 (12 receivers, 7 shots) 38
3.3 Synthetic experiment on shallow model of 9-m depth 42
3.3.1 Test configuration 42
3.3.2 Results for test configuration 1 (24 receivers, 25 shots) 44

3.3.3 Results for test configuration 2 (24 receivers, 13 shots) 47
3.3.4 Results for test configuration 3 (12 receivers, 13 shots) 50
3.3.5 Results for test configuration 4 (12 receivers, 7 shots) 53
3.4 Conclusion 57

Chapter 4 – VERIFICATION OF SH-LOVE FWI ALGORITHM WITH FIELD EXPERIMENTS (TASK 3)..59

4.1 Introduction..59
4.2 Bell site 59
4.3 CR 250 site 67
4.4 Kanapaha site...74
4.5 Conclusion 81

Chapter 5 – DEVELOPMENT OF DATA REDUCTION AND INTERPRETATION MODULE (TASK 4) 82

5.1 Introduction..82
5.2 Summary of software development and validation 82
5.3 Conclusion 83

Chapter 6 – SUMMARY 84

6.1 General...84
6.2 Development of SH-Love FWI algorithm 84
6.3 Optimization of field test configurations and wavefield characteristics 85
6.4 Verification of SH-Love FWI algorithm with field experiments 85
6.5 Development of data reduction and interpretation module 86

REFERENCES 87

Appendix: Software Manual 91

1. Introduction...91
2. Input parameters 92
3. Input data 94
4. Preprocessing...97
5. Spectral analysis 102
6. Initial model...103
7. Inversion 104
Run inversion...104
Multiple runs 111
8. Save and open inversion projects 112

LIST OF FIGURES

Figure page

Figure 2.1. Synthetic model: (a) true model used for generating synthetic data and (b) initial model at the beginning of iteration. 11

Figure 2.2. Acquisition geometry used for synthetic experiment 12

Figure 2.3. Synthetic model: normalized least squares error versus the inversion iteration number. 13

Figure 2.4. Synthetic model: waveform comparison for the first shot: (a) observed data and estimated data associated with the initial model, (b) observed data and estimated data associated with the final inverted model, (c) residual associated with the initial model, and (d) residual associated with final inverted model. 14

Figure 2.5. Synthetic model: (a) inverted results of the first run, and (b) inverted results of the second run. 16

Figure 2.6. Synthetic model: comparison of S-wave velocity at distances of (a) X=18 m and (b) X=27 m and density at distances (c) X=18 m and (d) X=27 m. 17

Figure 2.7. Synthetic model: (a) true model used for generating synthetic data, (b) initial model at the beginning of iteration. 19

Figure 2.8. Synthetic model: normalized least squares error versus the inversion iteration number. 20

Figure 2.9. Synthetic model: waveform comparison for the first shot: (a) observed data and estimated data associated with the initial model, (b) observed data and estimated data associated with the final inverted model, (c) residual associated with the initial model, and (d) residual associated with final inverted model. 21

Figure 2.10. Synthetic model: (a) inverted results of the first run, and (b) inverted results of the second run. 22

Figure 2.11. Synthetic model: comparison of S-wave velocity at distances of (a) X=9 m and (b) X=13.5 m, and density at distances (c) X=9 m and (d) X=13.5 m. 23

Figure 3.1. Synthetic deep model: (a) true model used for generating synthetic data, (b) initial model at the beginning of iteration. 27

Figure 3.2. Test configuration 1: 24 receivers and 25 shots 27

Figure 3.3. Test configuration 2: 24 receivers and 13 shots 27

Figure 3.4. Test configuration 3: 12 receivers and 13 shots 28

Figure 3.5. Test configuration 4: 12 receivers and 7 shots 28

Figure 3.6. Synthetic model of density (kg/m^3) and S-wave velocity (m/s): (a) inverted model at 5-25 Hz and (b) inverted model at 5-40 Hz (deep model, 24 receivers and 25 shots). 29

Figure 3.7. Synthetic model (deep model, 24 receivers and 25 shots): comparison of density at distances of (a) X=18 m and (b) X=27 m, and S-wave velocity at distances (c) X=18 m and (d) X=27 m...30

Figure 3.8. Synthetic model: normalized least squares error versus the inversion iteration number (deep model, 24 receivers and 25 shots)...31

Figure 3.9. Synthetic model (deep model, 24 receivers and 25 shots): waveform comparison for the first shot: (a) observed data and estimated data associated with the initial model, (b) observed data and estimated data associated with the final inverted model, (c) residual associated with the initial model, and (d) residual associated with final inverted model. 32

Figure 3.10. Synthetic model of density (kg/m^3) and S-wave velocity (m/s): (a) inverted model at 5-25 Hz and (b) inverted model at 5-40 Hz (deep model, 24 receivers and 13 shots). 33

Figure 3.11. Synthetic model (deep model, 24 receivers and 13 shots): comparison of density at distances of (a) X=18 m and (b) X=27 m and S-wave velocity at distances (c) X=18 m and (d) X=27 m. 34

Figure 3.12. Synthetic model: normalized least squares error versus the inversion iteration number (deep model, 24 receivers and 13 shots)...34

Figure 3.13. Synthetic model (deep model, 24 receivers and 13 shots): waveform comparison for the first shot: (a) observed data and estimated data associated with the initial model, (b) observed data and estimated data associated with the final inverted model, (c) residual associated with the initial model, and (d) residual associated with final inverted model...35

Figure 3.14. Synthetic model of density (kg/m^3) and S-wave velocity (m/s): (a) inverted model at 5-25 Hz and (b) inverted model at 5-40 Hz (deep model, 12 receivers and 13 shots). 36

Figure 3.15. Synthetic model (deep model, 12 receivers and 13 shots): comparison of density at distances of (a) X=18 m and (b) X=27 m and S-wave velocity at distances (c) X=18 m and (d) X=27 m. 36

Figure 3.16. Synthetic model: normalized least squares error versus the inversion iteration number (deep model, 12 receivers and 13 shots)...37

Figure 3.17. Synthetic model (deep model, 12 receivers and 13 shots): waveform comparison for the first shot: (a) observed data and estimated data associated with the initial model, (b) observed data and estimated data associated with the final inverted model, (c) residual associated with the initial model, and (d) residual associated with final inverted model...38

Figure 3.18. Synthetic model of density (kg/m^3) and S-wave velocity (m/s): (a) inverted model at 5-25 Hz and (b) inverted model at 5-40 Hz (deep model, 12 receivers and 7 shots). 39

Figure 3.19. Synthetic model (deep model, 12 receivers and 7 shots): comparison of density at distances of (a) X=18 m and (b) X=27 m and S-wave velocity at distances (c) X=18 m and (d) X=27 m...40

Figure 3.20. Synthetic model: normalized least squares error versus the inversion iteration number (deep model, 12 receivers and 7 shots)..40

Figure 3.21. Synthetic model (deep model, 12 receivers and 7 shots): waveform comparison for the first shot: (a) observed data and estimated data associated with the initial model, (b) observed data and estimated data associated with the final inverted model, (c) residual associated with the initial model, and (d) residual associated with final inverted model. 41

Figure 3.22. Synthetic shallow model: (a) true model used for generating synthetic data and (b) initial model at the beginning of iteration. 43

Figure 3.23. Test configuration 1: 24 receivers and 25 shots 43

Figure 3.24. Test configuration 2: 24 receivers and 13 shots 44

Figure 3.25. Test configuration 3: 12 receivers and 13 shots 44

Figure 3.26. Test configuration 4: 12 receivers and 7 shots 44

Figure 3.27. Synthetic model of density (kg/m^3) and S-wave velocity (m/s): (a) inverted model at 10-50 Hz and (b) inverted model at 10-80 Hz (shallow model, 24 receivers and 25 shots). 45

Figure 3.28. Synthetic model (shallow model, 24 receivers and 25 shots): comparison of density at distances of (a) X=9 m and (b) X=13.5 m and S-wave velocity at distances (c) X=9 m and (d) X=13.5 m. 46

Figure 3.29. Synthetic model: normalized least squares error versus the inversion iteration number (shallow model, 24 receivers and 25 shots)..46

Figure 3.30. Synthetic model (shallow model, 24 receivers and 25 shots): waveform comparison for the first shot: (a) observed data and estimated data associated with the initial model, (b) observed data and estimated data associated with the final

inverted model, (c) residual associated with the initial model, and (d) residual associated with final inverted model..47

Figure 3.31. Synthetic model of density (kg/m^3) and S-wave velocity (m/s): (a) inverted model at 10-50 Hz and (b) inverted model at 10-80 Hz (shallow model, 24 receivers and 13 shots). 48

Figure 3.32. Synthetic model (shallow model, 24 receivers and 13 shots): comparison of density at distances of (a) X=9 m and (b) X=13.5 m and S-wave velocity at distances (c) X=9 m and (d) X=13.5 m. 49

Figure 3.33. Synthetic model: normalized least squares error versus the inversion iteration number (shallow model, 24 receivers and 13 shots)..49

Figure 3.34. Synthetic model (shallow model, 24 receivers and 13 shots): waveform comparison for the first shot: (a) observed data and estimated data associated with the initial model, (b) observed data and estimated data associated with the final inverted model, (c) residual associated with the initial model, and (d) residual associated with final inverted model..50

Figure 3.35. Synthetic model of density (kg/m^3) and S-wave velocity (m/s): (a) inverted model at 10-50 Hz and (b) inverted model at 10-80 Hz (shallow model, 12 receivers and 13 shots). 51

Figure 3.36. Synthetic model (shallow model, 12 receivers and 13 shots): comparison of density at distances of (a) X=9 m and (b) X=13.5 m and S-wave velocity at distances (c) X=9 m and (d) X=13.5 m. 52

Figure 3.37. Synthetic model: normalized least squares error versus the inversion iteration number (shallow model, 12 receivers and 13 shots)..52

Figure 3.38. Synthetic model (shallow model, 12 receivers and 13 shots): waveform comparison for the first shot: (a) observed data and estimated data associated with the initial model, (b) observed data and estimated data associated with the final inverted model, (c) residual associated with the initial model, and (d) residual associated with final inverted model..53

Figure 3.39. Synthetic model of density (kg/m^3) and S-wave velocity (m/s): (a) Inverted model at 10-50 Hz and (b) Inverted model at 10-80 Hz (shallow model, 12 receivers and 7 shots). 54

Figure 3.40. Synthetic model (shallow model, 12 receivers and 7 shots): comparison of density at distances of (a) X=9 m and (b) X=13.5 m and S-wave velocity at distances (c) X=9 m and (d) X=13.5 m. 55

Figure 3.41. Synthetic model: normalized least squares error versus the inversion iteration number (shallow model, 12 receivers and 7 shots)..55

Figure 3.42. Synthetic model (shallow model, 12 receivers and 7 shots): waveform comparison for the first shot: (a) observed data and estimated data associated with the initial model, (b) observed data and estimated data associated with the final inverted model, (c) residual associated with the initial model, and (d) residual associated with final inverted model..56

Figure 4.1. Bell site: test setup with a line of geophones 60

Figure 4.2. Bell site: two test lines and boring location..61

Figure 4.3. Bell site: data acquisition geometry. 61

Figure 4.4. Bell site: wave excitation by striking sledgehammer to shear-beam pressed by a vehicle-wheel. 62

Figure 4.5. Bell site: spectral image of measured data. 62

Figure 4.6. Bell site: initial models of density and Vs used for both test lines. 63

Figure 4.7. Bell site: waveform comparison of observed and estimated data from the final inverted model: (a) line 1 and (b) line 2. 64

Figure 4.8. Bell site: density and Vs profile for (a) line 1 and (b) line 2......................................65

Figure 4.9. Bell site: shear and Young's modulus calculated from inverted results for (a) line 1 and (b) line 2 66

Figure 4.10. Bell site: comparison of density from seismic testing with that of rock coring samples...67

Figure 4.11. (a) New seismic shear source and (b) zoom-in shear box 68

Figure 4.12. CR 250 site: (a) site map with locations of two test lines and coring (yellow star) and (b) acquisition geometry used for both test lines. 69

Figure 4.13. CR 250 site: (a) spectral image and (b) initial models of density and Vs used for both test lines. 70

Figure 4.14. CR 250 site: waveform comparison of observed and estimated data from the final inverted model for the first shot: (a) line 1 and (b) line 2. 71

Figure 4.15. CR 250 site: density and Vs profile for (a) line 1 and (b) line 2. 72

Figure 4.16. CR 250 site: shear and Young's modulus for (a) line 1 and (b) line 2......................72

Figure 4.17. CR 250 site: comparison of density from seismic testing with that of rock coring samples. The coring location is 10 ft away from each of the two test lines. 74

Figure 4.18. Kanapaha site: field experiment 75

Figure 4.19. Kanapaha site: locations of three test lines and two borings B21 and B22..............75

Figure 4.20. Kanapaha site: data acquisition geometry. 76

Figure 4.21. Kanapaha site: waveform comparison of observed and estimated data for the first shot: (a) line 1, (b) line 2, and (c) line 3. 77

Figure 4.22. Kanapaha site: density and Vs profiles for (a) line 1, (b) line 2, and (c) line 3. 78

Figure 4.23. Kanapaha site: Shear and Young's modulus calculated from inverted results for (a) line 1, (b) line 2, and (c) line 3. 79

Figure 4.24. Comparison of density from seismic testing with that of rock coring samples, (a) Boring 22 and (b) Boring 21. 80

Chapter 1 – INTRODUCTION

1.1 Background

The design and construction of shallow foundations rely heavily on accurate subsurface information, particularly regarding rock density and variability. For instance, mass density influences rock strength and its stress-strain behavior in most limestone formations in Florida, USA (Nguyen et al., 2019). Moreover, Florida rock formations are often heterogeneous, with density variations occurring on different scales both vertically and horizontally and porosities exceeding twenty percent. Traditional invasive methods, such as core sampling, provide valuable data but are limited by their invasive nature and restricted spatial coverage. This often leads to gaps in the data, potentially compromising the foundation design, especially in heterogeneous formations like those found in Florida. As the demand for more precise and comprehensive subsurface characterization increases, non-invasive techniques like seismic full-waveform inversion (FWI) offer a promising alternative. This study aims to develop a 2D SH-Love full-waveform inversion (FWI) method for determination of rock density and moduli over a large volume without the need for extensive borings.

Seismic techniques have long been employed in geophysical surveys to infer the properties of subsurface materials (Virieux & Operto, 2009). The evolution of these techniques has led to the development of full-waveform inversion (FWI), which utilizes the entire waveform recorded by seismic sensors to produce high-resolution models of subsurface properties. Unlike traditional seismic methods that rely solely on analyses of travel times or dispersion characteristics, FWI leverages the full complexity of seismic waves, making it capable of resolving finer details of subsurface structures. Iteratively minimizing the discrepancy between measured and simulated waveform data, seismic FWI can retrieve properties such as wave velocities, moduli, and even mass density.

For FWI applications at geotechnical scales (depths of tens of meters), most studies have focused on vertical S-wave, P-wave, and Rayleigh waves (PSV wavefields), including 2D FWI (Groos et al., 2017; Tran et al., 2013; Tran & Sperry, 2018) and 3D FWI (Fathi et al., 2015; Nguyen & Tran, 2018; Smith et al., 2019; Tran et al., 2019, 2020; Mirzanejad et al., 2020, 2021). Although PSV wavefields can be conveniently generated by vertical impacts (e.g., sledgehammers or drop weights), they are dominated by Rayleigh-wave components, which are not sensitive to material density. Therefore, it is not possible to accurately extract density from the inversion of Rayleigh-wave-dominated wavefields, and density is often fixed or correlated with S-wave velocity during FWI of PSV wavefields (Tran et al., 2019).

More recently, the focus has expanded to include SH- and Love-waves (Pan et al., 2018, 2016; Dokter et al., 2017; Wittkamp et al., 2019; Köhn et al., 2019; Chen et al., 2021; Chen & Tran, 2021). SH and Love waves have shown promise in the field of geotechnical engineering. These waves, generated by horizontal shear motions, are less affected by fluid content and more sensitive to the rigidity and density of the medium through which they travel. This sensitivity makes them ideal for applications where detailed information about rock density and shear strength is critical. Moreover, being independent of P-wave velocity (Aki & Richards, 1980), SH and Love waves require fewer input parameters and equations for waveform simulation than PSV waves, reducing computing time to about 30% of that needed for FWI of PSV wavefields (Dokter et al., 2017). The use of SH and Love waves in FWI can reduce the computational load and enhance the accuracy of inverted mass density.

1.2 Outline of the study

To extract mass density from seismic data, this study developed a 2D SH-Love FWI method and verified it with field experiments for determination of rock density, focusing on characterizing rock layers needed for design of shallow foundations. Field experiments of shear-wave seismic testing and rock coring were conducted at three Florida sites. Seismic data were analyzed by the 2D SH-Love FWI method, and densities from seismic data were compared to those from rock cores to assess the method’s capabilities. This is the first study that reports a direct comparison of densities obtained from seismic data and rock coring samples.

The 2D SH-Love FWI method was first developed and optimized as documented in chapters 2 and 3, respectively. The method was then applied to field experimental data at three Florida sites and verified by invasive tests (rock coring samples), (chapter 4). Finally, the GUI software of the 2D SH-Love FWI was developed, together with its user manual, for FDOT's future uses (chapter 5).

Chapter 2 – DEVELOPMENT OF SH-LOVE FWI ALGORITHM (TASK 1)

2.1 Introduction

This project is to develop an advanced SH-Love full waveform inversion (2D SH-Love FWI) method, which can characterize mass density and S-wave velocity of subsurface soil or rock at foot-scale to at least 30 ft depth. The horizontal shear (SH) and Love waves are generated by applying a horizontal source (e.g., horizontally striking on a shear beam) and recorded by an array of horizontal geophones on the ground surface. The recorded waveform data are then analyzed to independently extract density and S-wave velocity of the subsurface materials. Knowing both density (ρ) and S-wave velocity (Vs), shear (G) and Young (E) moduli can be computed (Equations 1 and 2) for determination of shallow foundation's settlement and bearing capacity, and other geotechnical analyses. It is noted that the mass properties (density or unit weight and Young's Modulus) are required for both bearing and settlement estimates of a footing.

$$G = \rho V_s^2 \tag{1}$$

$$E = 2G(1 + \mu) \tag{2}$$

This task is to develop the 2D SH-Love FWI algorithm and test it with synthetic datasets generated from realistic soil or rock profiles. The algorithm is then optimized and verified on field experimental data.

2.2 Methodology

We have successfully developed the 2D SH-Love FWI method and its algorithm. The algorithm consists of the forward simulation of elastic SH- and Love-waves, and adjoint-state optimization for model updating (inversion) to extract mass density and Vs profiles. Synthetic experiments are used to test the capability of the developed SH-Love FWI method. Details on the analytical formula and numerical implementation are presented as follows.

2.2.1 Forward simulation

The 2D SH- and Love-wave propagation in isotropic elastic medium is simulated using the first-order elastic wave equations (Virieux, 1984) based on stress equilibrium (Equation 3) and Hooke's elastic theory (Equations 4 & 5).

$$\rho(x,z)\frac{\partial v_y}{\partial t} = \frac{\partial \sigma_{xy}}{\partial x} + \frac{\partial \sigma_{yz}}{\partial z} + f_y. \tag{3}$$

$$\frac{\partial \sigma_{xy}}{\partial t} = \mu(x,z)\frac{\partial v_y}{\partial x}. \tag{4}$$

$$\frac{\partial \sigma_{yz}}{\partial t} = \mu(x,z)\frac{\partial v_y}{\partial z}. \tag{5}$$

where x and z denote the horizontal distance and depth in x- z -plane, respectively, y denotes the direction perpendicular to the x- z -plane. v_y is the particle velocity in the y-direction, σ_{xy} and σ_{yz} are the shear stresses. Parameters ρ and μ represent the mass density and the shear modulus, respectively, and f_y is the force of the excited source in the y-direction.

The perfectly matched layer (PML) developed by (Komatitsch & Martin, 2007) is used for boundary truncation. Specifically, the PMLs are applied at the bottom and vertical boundaries to absorb outgoing waves. For the free surface condition, the stress-imaging technique (Levander, 1988) is used. As for the initial condition, the particle velocity and stress are set to zero at time zero.

2.2.2 Model update

For model updating, the adjoint-state approach is adopted to minimize waveform residuals between the observed and estimated data. The residual between observed and estimated waveform data from shot *s* and receiver *r* is defined as:

$$\Delta \mathbf{d}_{\mathrm{s,r}} = \mathbf{D}_{\mathrm{s,r}}(\mathbf{m}) - \mathbf{d}_{\mathrm{s,r}} \tag{6}$$

where $d_{s,r}$ is the observed (measured) data from field experiment. $\mathbf{D}_{\mathrm{s,r}}(\mathbf{m})$ is the estimated data from the forward modelling for model **m** (Vs and density). The objective function is computed as the least-squares error E(**m**):

$$\mathrm{E}(\mathbf{m}) = \frac{1}{2}\Delta \mathbf{d}^{\mathrm{T}}\Delta \mathbf{d} \tag{7}$$

where Δ**d** is a column vector combining residuals $\Delta \mathbf{d}_{\mathrm{s,r}}$ from all shots and receivers. T denotes vector transpose.

The gradients for S-wave velocity (Vs) and density (ρ) are based on the adjoint-state method (Plessix, 2006) as:

$$\frac{\partial \mathrm{E}}{\partial \mathrm{V_s}} = -\frac{2}{\mathrm{V_s^3}\rho}\sum_{\mathrm{i=1}}^{\mathrm{Ns}}\int_0^{\mathrm{T}} \mathrm{dt}(\sigma_{\mathrm{xy}}^{\mathrm{f}}\sigma_{\mathrm{xy}}^{\mathrm{b}} + \sigma_{\mathrm{yz}}^{\mathrm{f}}\sigma_{\mathrm{yz}}^{\mathrm{b}}) \tag{8}$$

$$\frac{\partial \mathrm{E}}{\partial \rho} = -\frac{1}{\mathrm{V_s^2}\rho^2}\sum_{\mathrm{i=1}}^{\mathrm{Ns}}\int_0^{\mathrm{T}} \mathrm{dt}(\sigma_{\mathrm{xy}}^{\mathrm{f}}\sigma_{\mathrm{xy}}^{\mathrm{b}} + \sigma_{\mathrm{yz}}^{\mathrm{f}}\sigma_{\mathrm{yz}}^{\mathrm{b}} + \mathrm{V_s^2}\rho^2\frac{\partial \mathrm{v_y}}{\partial \mathrm{t}}\mathrm{u_y^b}) \tag{9}$$

where σ_{xy}^{f} and σ_{yz}^{f} denote the shear stresses in the forward propagated wavefield, σ_{xy}^{b} and σ_{yz}^{b} are the shear stresses in the back-propagated residual wavefield from receivers, v_y denotes the particle velocity in the forward wavefield, u_y^b denotes the particle displacement in the back-propagated wavefield, and Ns is the number of sources.

As FWI is a highly nonlinear and ill-posed inverse problem, regularization is particularly important to maintain optimization stability, especially for cases of sharp contrasts in material properties. The Tikhonov regularization (Tikhonov & Arsenin, 1977) is used to mitigate the ill-posed problem by smoothing the gradients as:

$$\left(\frac{\partial \mathrm{E}}{\partial \mathrm{V_s}}\right)_{\mathrm{r}} = \frac{\partial \mathrm{E}}{\partial \mathrm{V_s}} + \lambda_1 \mathbf{D}\mathrm{V_s} \tag{10}$$

$$\left(\frac{\partial \mathrm{E}}{\partial \rho}\right)_{\mathrm{r}} = \frac{\partial \mathrm{E}}{\partial \rho} + \lambda_2 \mathbf{D}\rho \tag{11}$$

where **D** is the 2D Laplacian matrix, whose elements are either 1, -4 or 0. The size of matrix **D** is $\mathrm{N} \times \mathrm{N}$ (N is the number of reconstructed parameters or cells). Coefficients λ_1 and λ_2 are the scaling factors between the regularization term and the gradient term, and we determine them similar to (Fathi et al., 2015) as:

$$\lambda_1 = \mathrm{R}\frac{\left\|\frac{\partial \mathrm{E}}{\partial \mathrm{V_s}}\right\|}{\|\mathbf{D}\mathrm{V_s}\|}, \lambda_2 = \mathrm{R}\frac{\left\|\frac{\partial \mathrm{E}}{\partial \rho}\right\|}{\|\mathbf{D}\rho\|} \tag{12}$$

where $\|\cdot\|$ represents the Euclidean norm. R is a factor controlling model smoothness, with the higher value leading the smoother model.

Inversion analyses are done with increasing ranges of data's frequency. The first analysis begins with larger regularization levels on low frequency data (e.g., 5 to 50 Hz). This produces smooth inverted models with fewer artifacts, and it is necessary for the early inversion stage with large residuals. The second analysis then uses smaller regularization levels on high frequency data (e.g., 5 to 80 Hz) and the result from the first analysis as the initial model. The smaller regularization level is better for sharp contrast imaging and characterization (e.g., 1 foot weak layer between two strong layers at Bell site). However, it tends to create more inversion artifacts and should be only used when residuals are relatively small such as those in the second analysis. The various regularization levels will allow imaging the sharp contrasts with minimal artifacts. We have conducted several trial runs, and the R value is selected as 0.3 at the first iteration and linearly decreased during inversion to 0.1 at the last iteration.

To minimize the least-squares error, S-wave velocity and density parameters are iteratively updated along the steepest-descent directions (Nocedal & Wright, 2006) as:

$$\mathrm{V_{s}}_{\mathrm{n+1}} = \mathrm{V_{s}}_{\mathrm{n}} - \alpha_{\mathrm{n}} \mathbf{H}_{\mathrm{n}}^{-1} \left(\frac{\partial \mathrm{E}}{\partial \mathrm{V_s}}\right)_{\mathrm{r}} \tag{13}$$

$$\rho_{\mathrm{n+1}} = \rho_{\mathrm{n}} - \beta_{\mathrm{n}} \mathbf{H}_{\mathrm{n}}^{-1} \left(\frac{\partial \mathrm{E}}{\partial \rho}\right)_{\mathrm{r}} \tag{14}$$

In the above equations, n denotes the iteration number, α_{n} and β_{n} are the optimal step lengths obtained independently by parabolic fitting (Nocedal & Wright, 2006). $\mathbf{H}_n^{-1}$ represents the inverse of Hessian matrix, which is the second derivative of the objective function. To limit the challenging computation of the complete Hessian, we adopt its approximation (Zhang et al., 2012) as:

$$\mathbf{H}_{\mathrm{n}}^{-1} = \left(\lambda + \sqrt{\mathrm{W_s}(\mathrm{x}, \mathrm{x_s}) \mathrm{W_r}(\mathrm{x})}\right)^{-1} \tag{15}$$

Where:

$$\lambda = \epsilon \max_{x}\left(\sqrt{W_s(x, x_s)W_r(x)}\right) \tag{16}$$

where $W_s(x, x_s)$ is the wave energy of the forward wavefield, excited at source location x_s and sampled at location x. Similarly, $W_r(x)$ is the wave energy of the back-propagated residual wavefield (excited at all receiver locations) and sampled at location x. λ is used to avoid the inverse of infinitesimals, and ϵ is set as 0.1 in this study. The inverse Hessian acts as a weighting function (larger values for deeper cells) to partially balance model updates during inversion. It helps suppress shallow inversion artifacts and resolve deeper structures.

In Equations 13 and 14, α_n and β_n are the optimal step lengths for Vs and density at the n-th iteration, respectively. They are obtained separately by parabolic fitting (Nocedal & Wright, 2006). Specifically, density is fixed when searching for α_n and Vs is fixed when searching for β_n. We use three points (high, low, and high) to form a parabolic curve for the fitting. The first point is associated with the step length of zero and the current misfit. The search of the second point (low) is done with four trial step lengths that perturb the parameter of 2%, 1%, 0.5% and 0.25%. If the second point is not found for one parameter (misfit increasing for all four trials), its step length is assigned to zero (no parameter update) and only update the other parameter in the current iteration. If the second point is not found for both parameters (Vs and density), the inversion is stopped. The search of the third point (high) is also done up to four trial step lengths that perturb the parameter of 0.5%, 1%, 2% and 4% from the second point. If the third point is not found (misfit decreasing for all four trials), we simply update the parameter of 1% for the current iteration to avoid potential overshooting.

2.3 Synthetic experiment on a deep model of 18-m depth

2.3.1 Test configuration and setup

The developed SH- and Love-waves full-waveform inversion (SH-Love FWI) algorithm is first tested on a synthetic experiment. The experiment starts with an assumed synthetic model, referred to as the true model, which represents a possible in situ field condition. This true model is used in the forward simulation, and its response to surface strikes (i.e., synthetic data) is recorded and assumed to represent the field data. The data are then used in the FWI algorithm, and the inverted result is compared with the true model for assessment of the algorithm's accuracy.

The synthetic model (Figure 2.1a) represents a challenging reverse soil profile of three undulating layers. The top, middle, and bottom layers have Vs of 300, 150, and 500 m/s and a density of 1,800, 1,600, and 2,000 kg/m^3, respectively. This is a valid assumption for near-surface characterization based on FDOT project BDV31-977-51 (McVay et al., 2019). Unlike P-waves that can propagate through water in soil or rock, S-waves only propagate through the soil or rock skeleton, as they need particle contact to transfer shear stress (no shear transfer in water). The more compact the soil or rock mass (higher mass density), the higher the Vs, generally. This synthetic model represents a common subsurface profile in Florida, for example, a soft soil layer located buried between a stiff soil layer and a weathered limestone layer.

For synthetic data simulation, the acquisition geometry consisted of 24 receivers and 25 sources (shots), each located at 1.5-m (5 ft) spacing on the free surface (Figure 2.2). The 18 m × 36 m (60 ft × 120 ft) medium was discretized into 48 × 96 grids with the spacing of 0.375 m (1.25 ft). A Ricker source wavelet was used to generate synthetic waveform data, which were then assumed as the measured data for inversion.

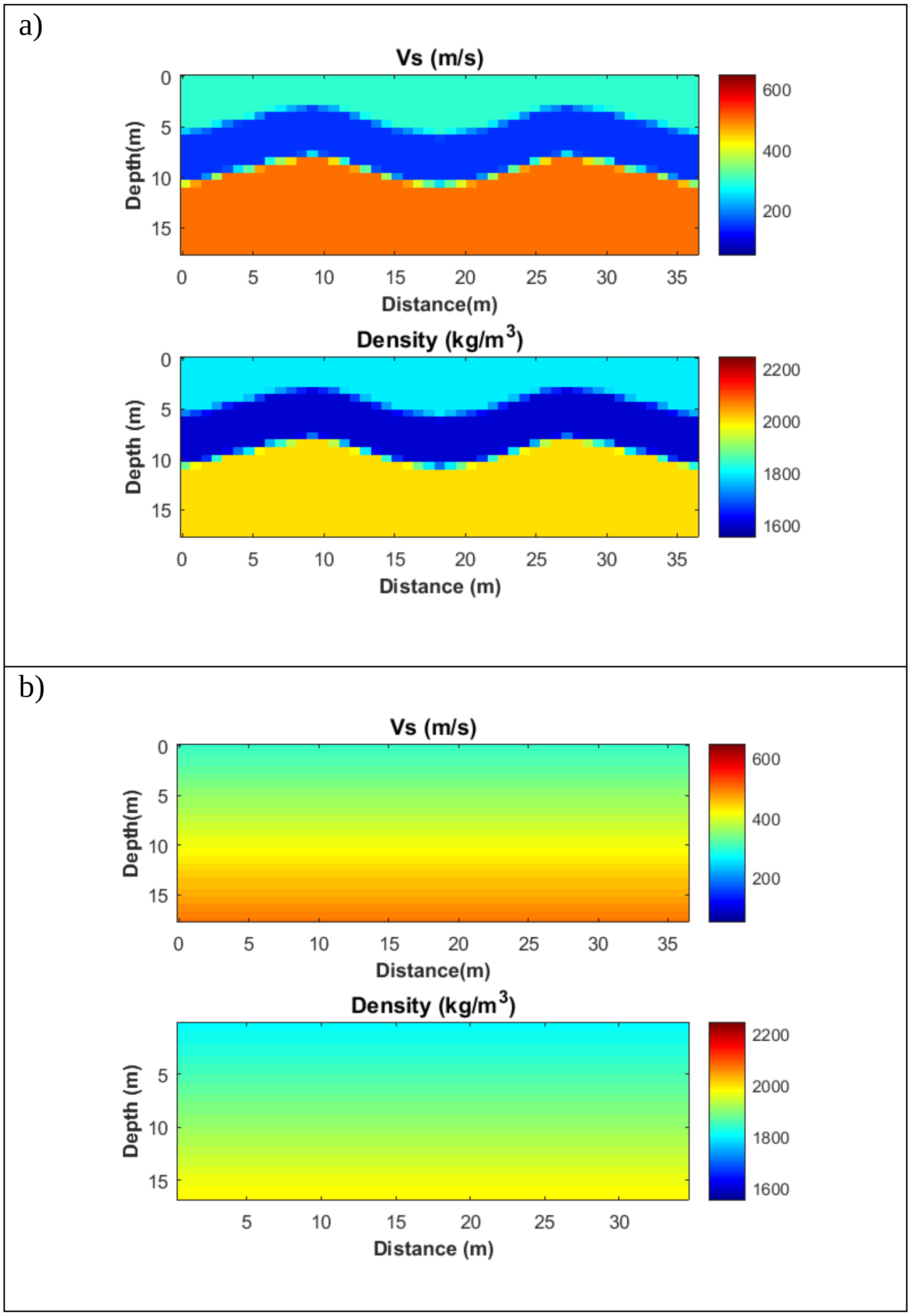

Figure 2.1. Synthetic model: (a) true model used for generating synthetic data and (b) initial model at the beginning of iteration.

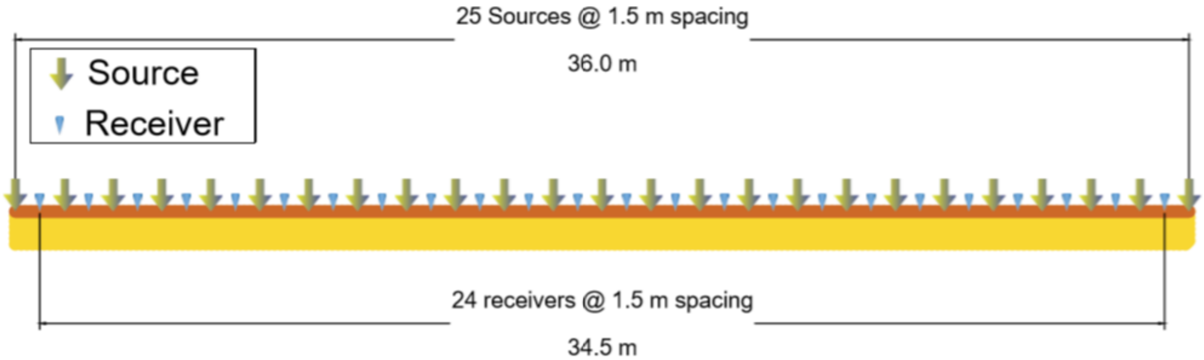

Figure 2.2. Acquisition geometry used for synthetic experiment

2.3.2 Inversion analysis and results

A 1D model (Figure 2.1b) was selected as the initial model for Vs, with the value linearly increasing from 300 m/s at the free surface to 500 m/s at the bottom of the domain. Such a profile can be estimated from the spectral analysis of the measured data. Unlike wave velocities, there is no visual indication of material density in the wavefields. Assuming mass density is positively correlated to Vs (validated in FDOT project BDV31-977-51), the initial model of density is taken as linearly increasing from 1,800 kg/m^3 on the top to 2,000 kg/m^3 at the bottom of the domain.

Next, two inversion runs were performed on data at two frequency ranges: 5 to 25 Hz and 5 to 40 Hz, beginning with the lower frequencies. The first run started with the initial model (Figure 2.1b), and the inverted result of the first run was then used as the input model for the second run. For accurate wave modelling, cell sizes of 0.75 m (2.5 ft) and 0.375 m (1.25 ft) were used for wave simulation and model updating in the first and second runs, respectively. The inversion was set to stop when it reached a predefined maximum number (50) of iterations, or no optimal step length is found (no better model), or the least squares error decreases less than 0.1% for 10 iterations. Both runs stopped at the predefined maximum number of 50 iterations. The entire inversion process took about 55 minutes (15 for first run and 40 for second run) on a desktop computer (Dell Precision 5820 Tower, Intel Xeon CPU W-2145, 8 cores with 3.70 GHz each, 64-GB RAM).

Normalized least-squares error for the two runs is shown in Figure 2.3. The error decreased substantially during inversion from 1.0 at the first iteration to 0.001 at the final iteration. It is noted that the error jumped at the beginning of the second run. This is because the model was not yet ready to propagate the higher frequency data (shorter wavelengths).

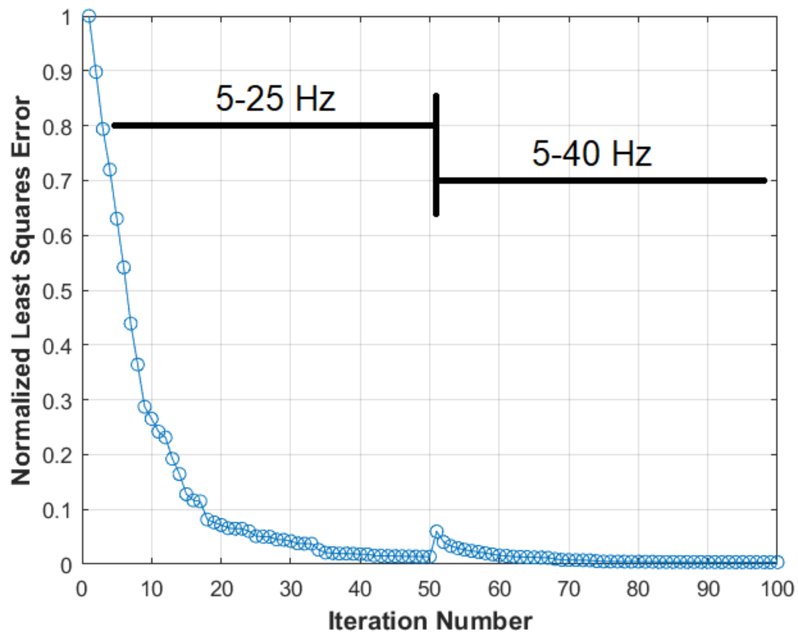

Figure 2.3. Synthetic model: normalized least squares error versus the inversion iteration number.

Figure 2.4 compares the observed waveform data against the estimated waveform data from the initial and final inverted model for the first shot. The waveform match improved significantly during inversion. The observed and final estimated waveform data are almost identical. The final residuals are close to zero for all the receivers.

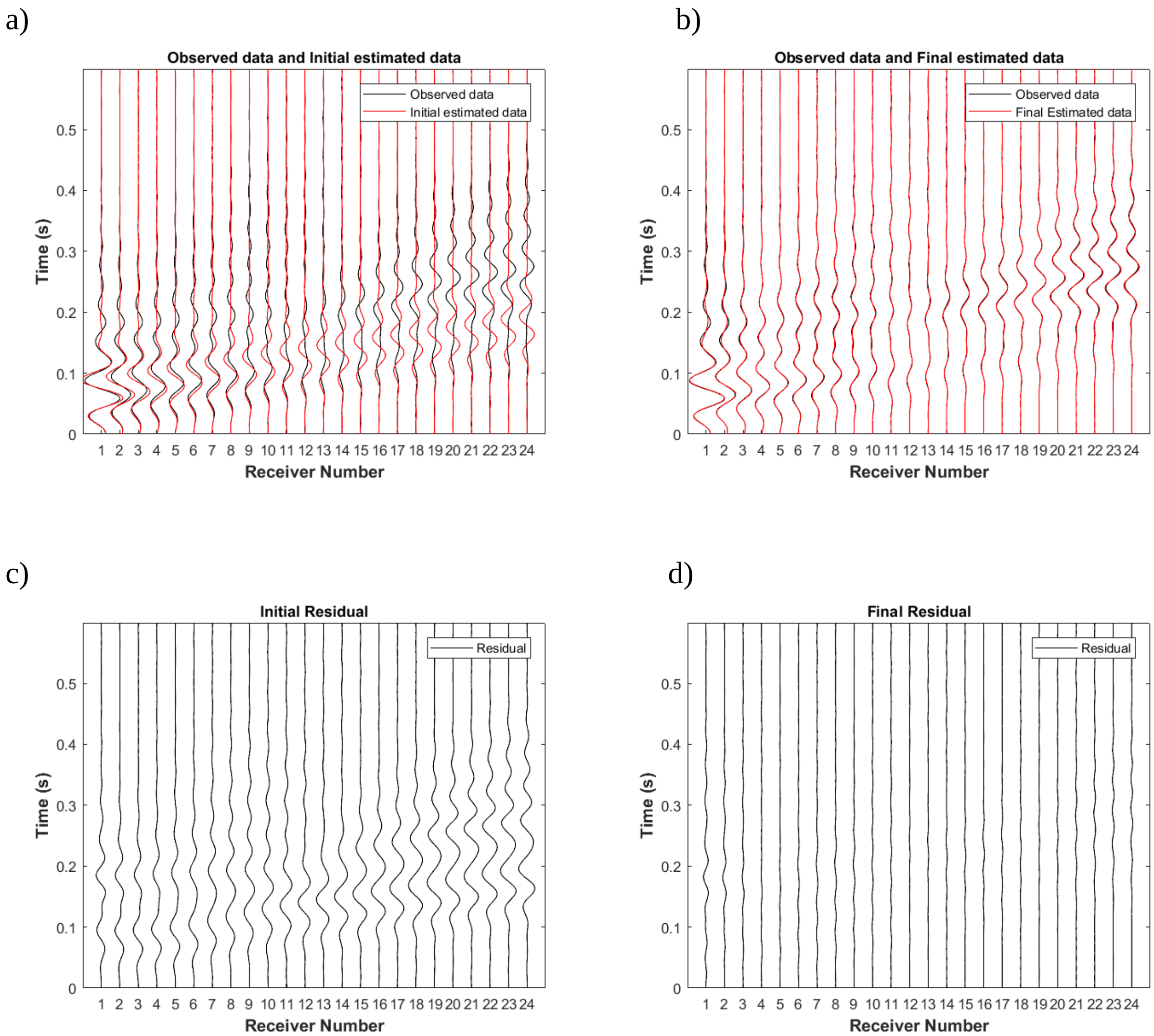

Figure 2.4. Synthetic model: waveform comparison for the first shot: (a) observed data and estimated data associated with the initial model, (b) observed data and estimated data associated with the final inverted model, (c) residual associated with the initial model, and (d) residual associated with final inverted model.

The results of the first and second inversion runs are shown in

Figure 2.5a and Figure 2.5b, respectively. The inverted result from the first run clearly shows the three undulating layers. Introducing higher frequency data in the second run improved the resolution between the layers greatly. Compared to the true model (Figure 2.1a), the true Vs and density values of all three layers are recovered, and the layer interfaces are imaged. The recovery of Vs profile is somewhat better than that of density, because the waveform data is more sensitive to Vs.

Next, a detailed comparison of Vs and density is presented in Figure 2.6 for two locations at the middle and right of the medium at distances of 18 m and 27 m. Compared with the initial values, Vs and density changed significantly during the inversion. Evidently, the final inverted Vs and density agree well with their true values at both locations. There are some discrepancies in Vs and density at the bottom of the model. This is mostly due to weak signal coverage in that zone. In addition, the implemented Tikhonov regularization always produces a smooth inverted model that leads to mismatch of Vs and density near the layer interfaces. Nevertheless, the presented FWI successfully invert both Vs and density of the challenging velocity-reversal model with acceptable accuracy.

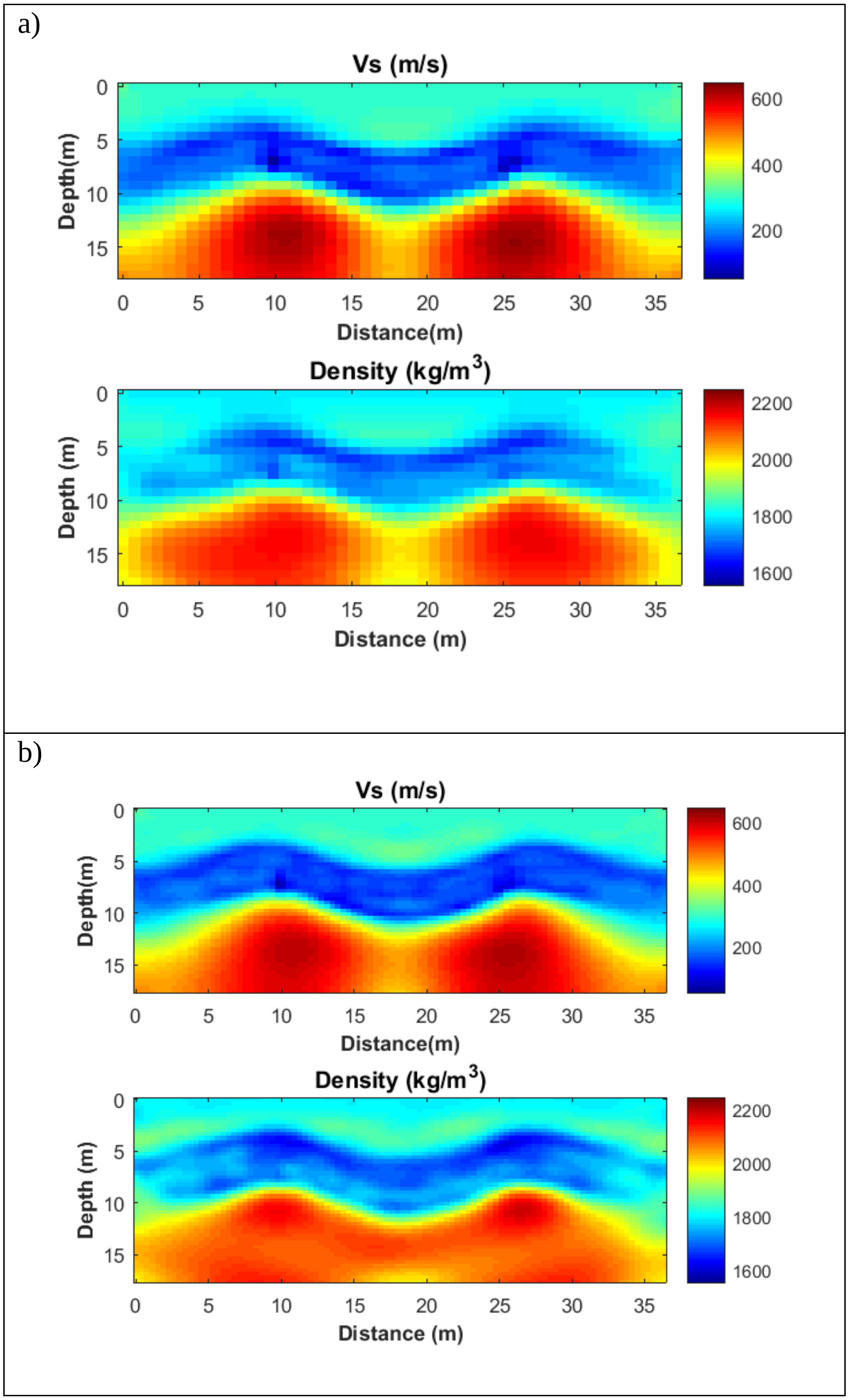

Figure 2.5. Synthetic model: (a) inverted results of the first run, and (b) inverted results of the second run.

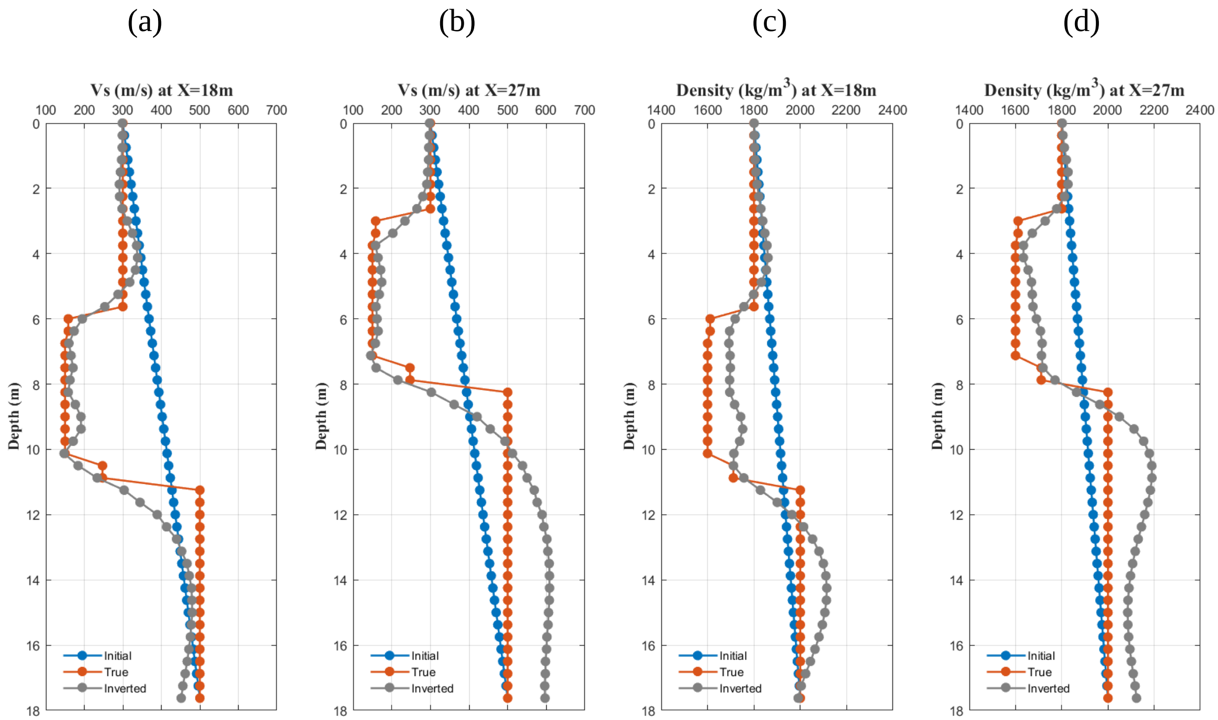

Figure 2.6. Synthetic model: comparison of S-wave velocity at distances of (a) X=18 m and (b) X=27 m and density at distances (c) X=18 m and (d) X=27 m.

2.4 High resolution synthetic experiment on a model of 9-m depth

2.4.1 Test configuration and setup

Characterizing a highly variable soil or rock profile to a depth of 30 ft at high resolution (i.e., inches) for a shallow foundation design (e.g., Bell, Florida, which had a thin weak weathered layer between competent rock layers) is of great interest. For the high resolution (i.e., inches), the developed SH-Love FWI algorithm was run on a 30-ft depth (9 m) domain with waveform data up to 80 Hz in the analysis. Note that 80 Hz was the highest frequency that could be generated in the field and propagate at least a distance of 60 ft, or twice the targeted depth needed for investigation. The objective was to relate the characterized resolution with depth as a function of receiver and shot spacing.

The synthetic dataset was generated from the forward simulation (Equations 3–5) on an assumed model (true model) consisting of four variable layers of high and low mass density and S-wave velocity, representing a challenging in situ field situation. The true model (Figure 2.7a) included four high and low velocity layers with Vs of 200, 300, 150, and 500 m/s and density of 1,500, 1,800, 1,600, and 2,000 kg/m^3, from the top to bottom respectively. For synthetic data simulation, the acquisition geometry consisted of 24 receivers and 25 sources (shots), both located at 0.75-m spacing (2.5 ft) on the free surface.

2.4.2 Inversion analysis and results

A 1D gradient initial model of Vs (Figure 2.7b) was selected with increasing values with depth from 200 m/s to 500 m/s. Assuming mass density is positively correlated to Vs, the initial model of density was taken as linearly increasing from 1,500 kg/m^3 on the top to 2,000 kg/m^3 at the bottom.

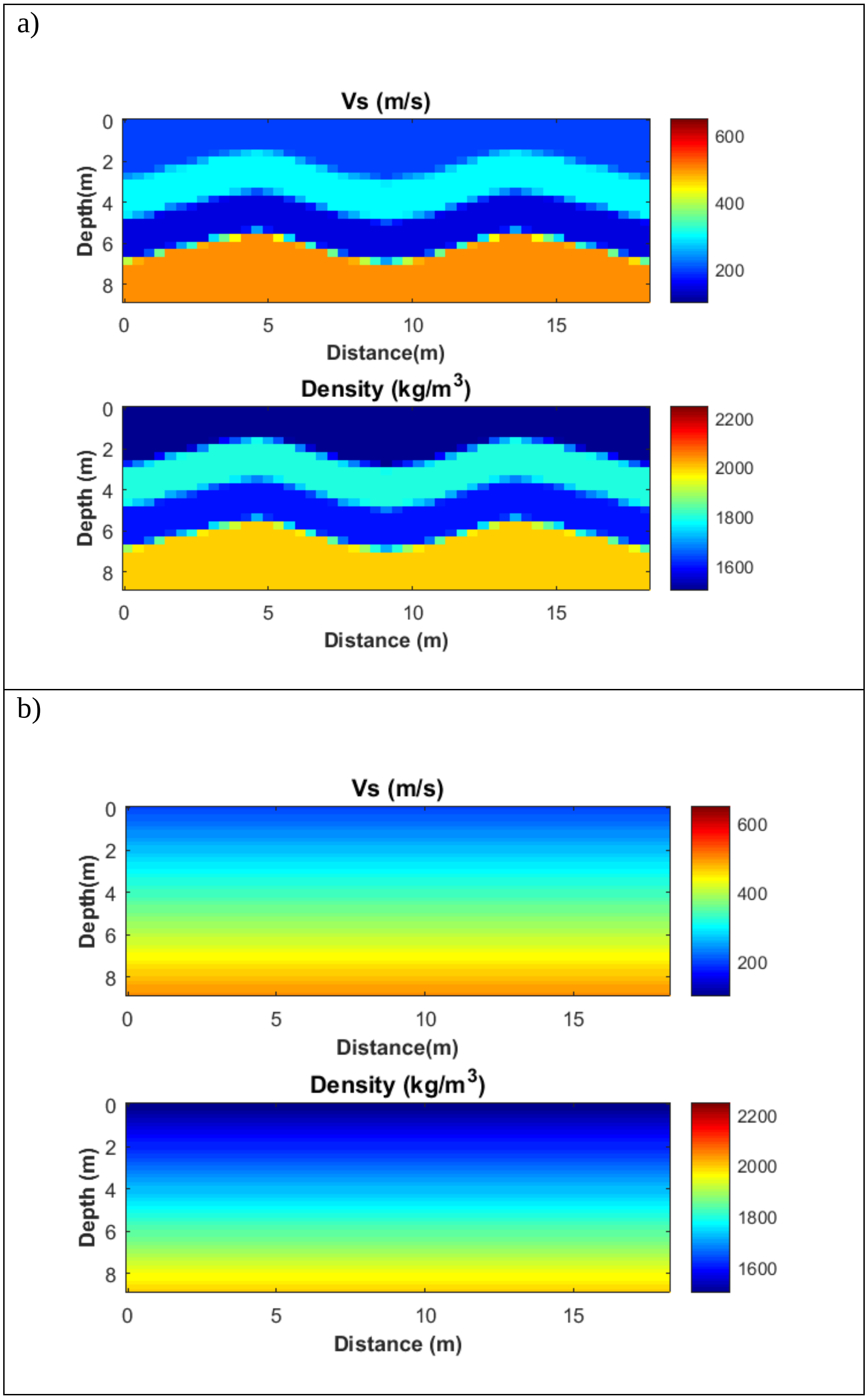

Figure 2.7. Synthetic model: (a) true model used for generating synthetic data, (b) initial model at the beginning of iteration.

The two observed data sets of 30 Hz and 40 Hz sources were filtered through frequency ranges of 10 to 50 Hz and 10 to 80 Hz, respectively and used in the two inversion stages. The medium was discretized in pixels of 0.375 m (15 in.) and 0.1875 m (7.5 in.) in the first and second runs, respectively. The inversion process stops either when it reaches a maximum of 50 iterations or when the error decreases less than 0.1% for 10 iterations. The two inversion stages ended after 50 iterations. Figure 2.8 illustrates the normalized least squares error during inversion, which gradually decreases from 1.0 to approximately 0.001 by the end.

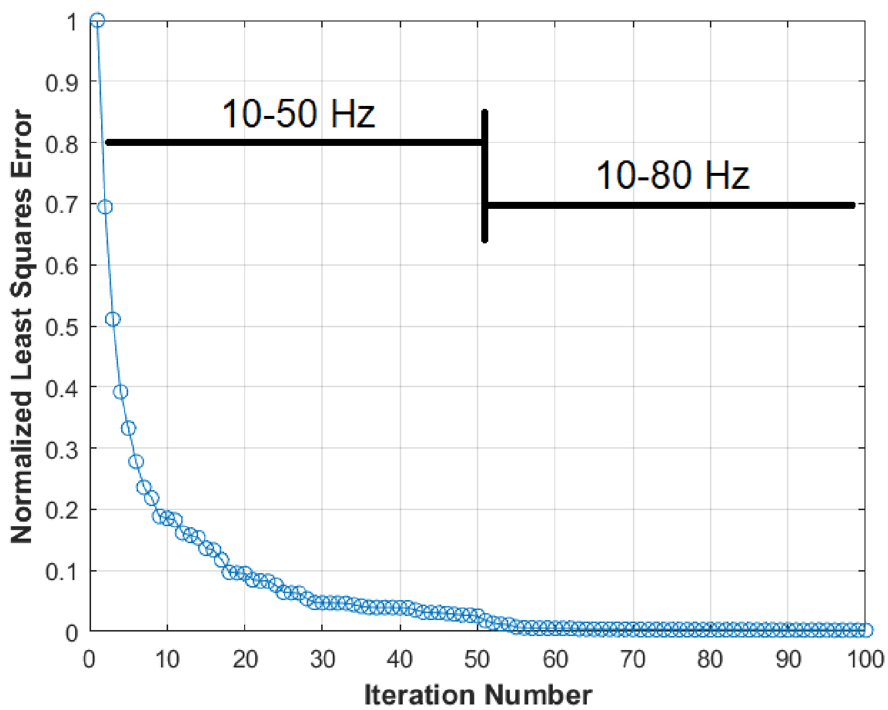

Figure 2.8. Synthetic model: normalized least squares error versus the inversion iteration number.

The comparison of the observed data against the initial and final estimated data (Figure 2.9a and b) shows the substantial improvement of waveform match. The residual decreased significantly from the initial (Figure 2.9c) to the final values (Figure 2.9d) during inversion.

Figure 2.10a and b represent the inverted results of the first and second inversion stages, respectively. The first stage successfully identifies all four layers in terms of Vs and density. The second stage further enhances the results obtained in the first stage, achieving a higher resolution (7.5 in pixel). The layer interfaces, Vs and density values were all characterized. Due to higher sensitivity to the waveform data, the recovery of Vs profile is somewhat better than that of density.

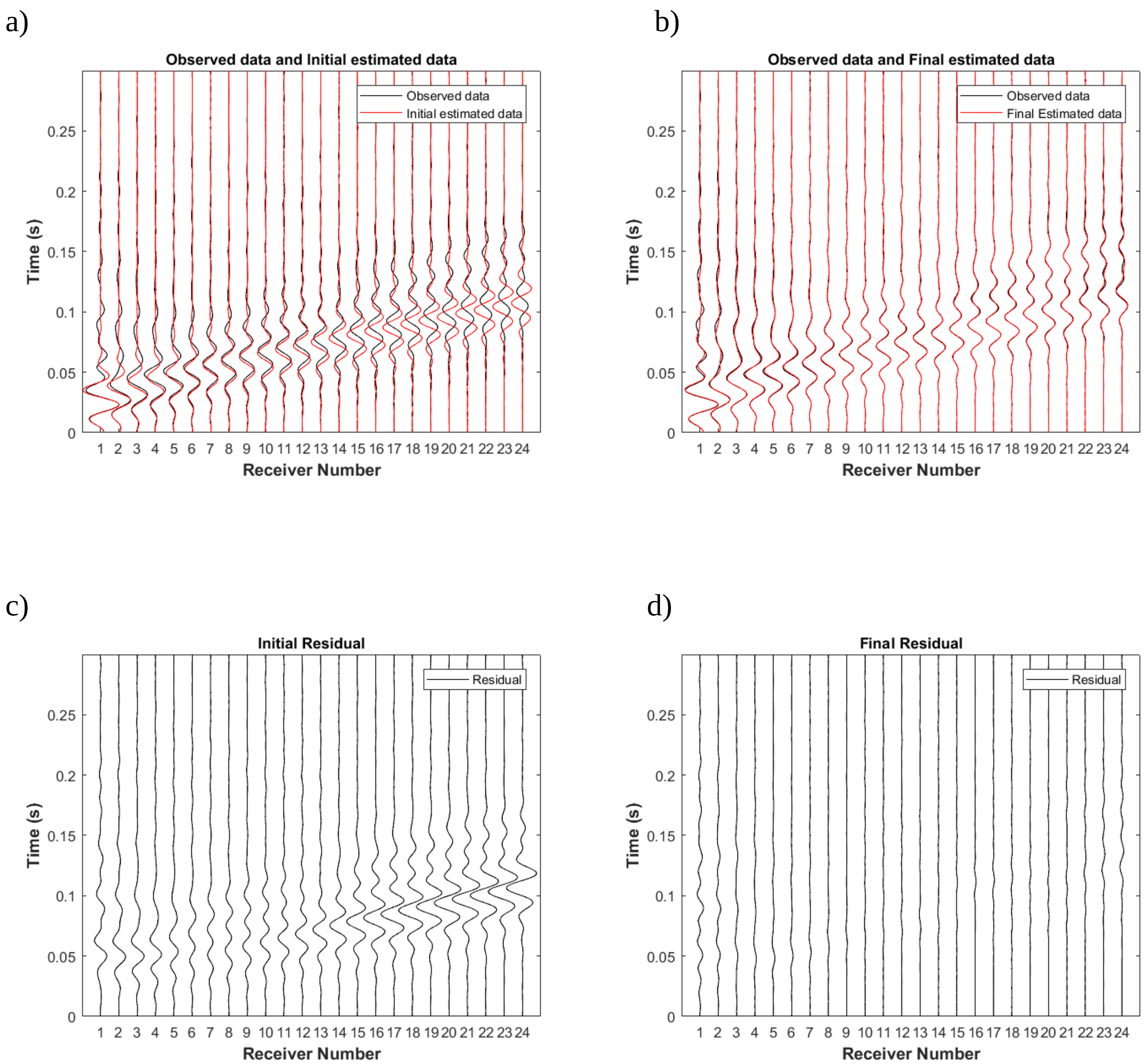

Figure 2.9. Synthetic model: waveform comparison for the first shot: (a) observed data and estimated data associated with the initial model, (b) observed data and estimated data associated with the final inverted model, (c) residual associated with the initial model, and (d) residual associated with final inverted model.

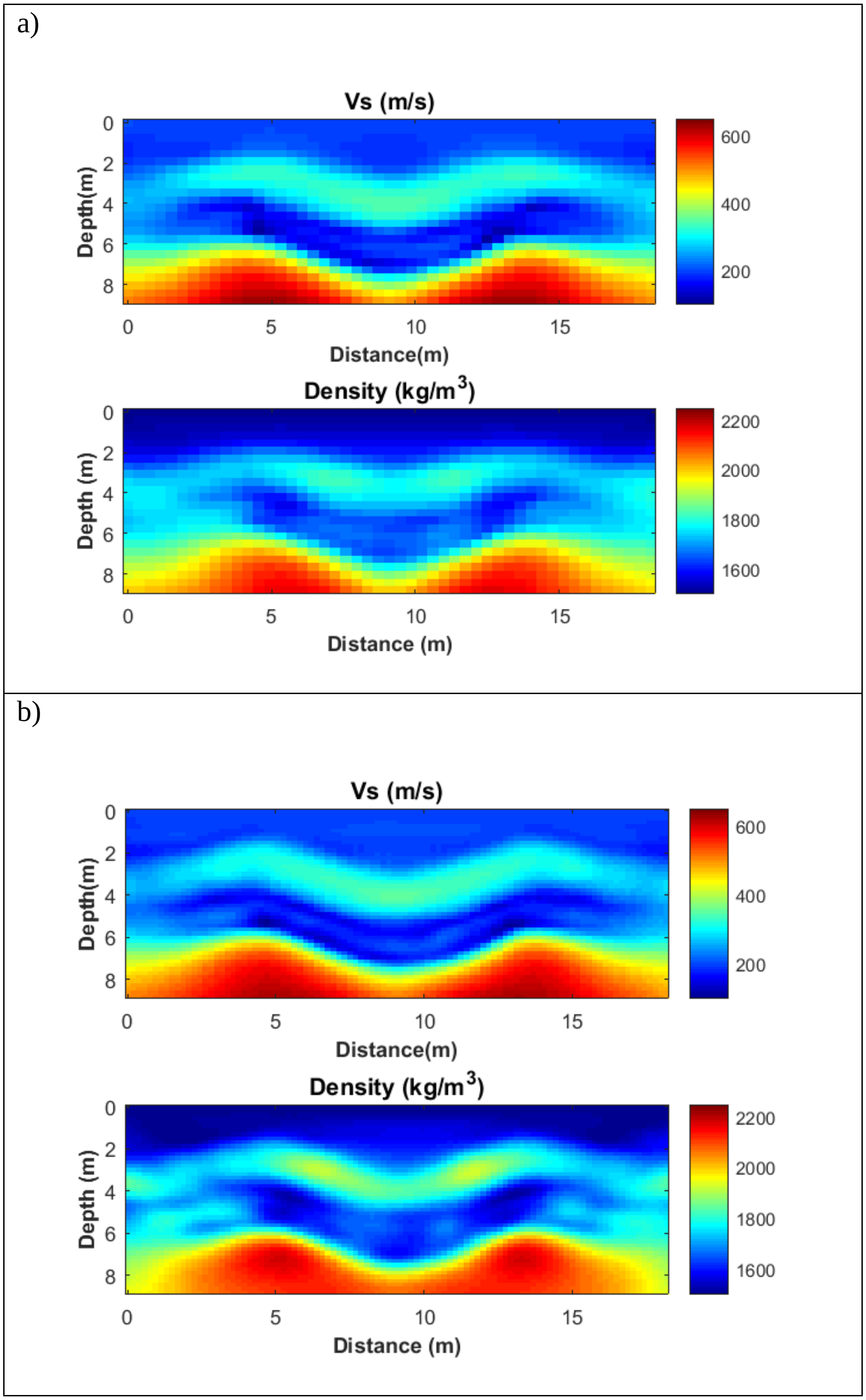

Figure 2.10. Synthetic model: (a) inverted results of the first run, and (b) inverted results of the second run.

Shown in Figure 2.11 provides a detailed comparison of the true, initial, and inverted values of Vs and density at distances of 9 m and 13.5 m. Some discrepancies can be seen again in Vs and density at the bottom of the model, primarily because of limited signal coverage in that area. Furthermore, the Tikhonov regularization used in the inversion process tends to produce smooth inverted models, which can result in mismatches between Vs and density near the layer interfaces. However, the final inverted values for Vs and density show good agreement with the true values.

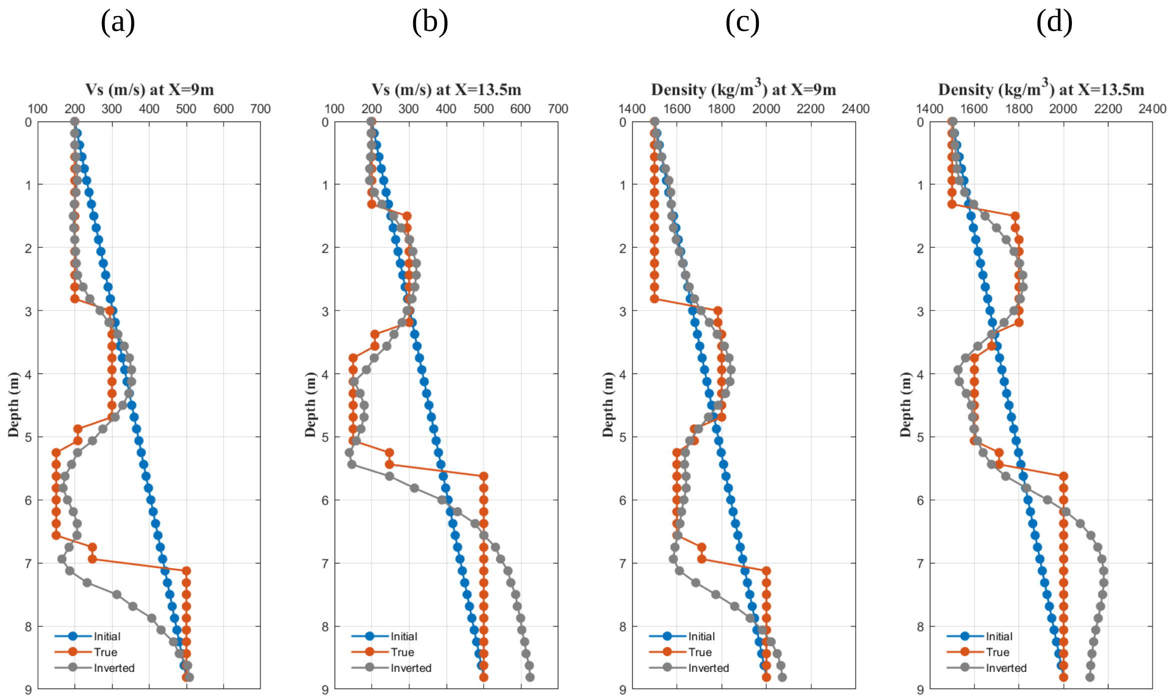

Figure 2.11. Synthetic model: comparison of S-wave velocity at distances of (a) X=9 m and (b) X=13.5 m, and density at distances (c) X=9 m and (d) X=13.5 m.

2.5 Conclusion

In this task, a 2D SH-Love FWI method was developed along with its algorithm to characterize soil and rock properties of near-surface substructures. The main advantage of the method is the sensitivity of SH and Love waves to mass density, enabling its accurate estimation from measured wavefields. For comparison, Rayleigh-wave FWI and dispersion curve inversion methods often fix the density with assumed values during analysis due to its limited sensitivity. In addition, SH-Love wave simulation requires much less computing time (30% of that of P-SV waves), and the 2D SH-Love FWI can be used to obtain quick results in the field (e.g., 20 minutes for the first run).

The method consists of a forward simulation based on 2D elastic SH-wave equations, and the steepest-descent adjoint-state optimization with Tikhonov regularization. Before applying to field experimental data (Task 3), the developed algorithm was tested on two synthetic models in this task to assess its capability. These models include a deep three-layer model with a depth of 60 ft (18 m) and a shallow four-layer model with a depth of 30 ft (9 m). Both models represent the typical Florida geology with soils over highly variable limestone. Results are then compared to the true models for assessment of the algorithm's accuracy.

The results from the two synthetic experiments indicate that the developed 2D SH-Love FWI algorithm can accurately characterize challenging subsurface profiles with variable layers of high and low S-wave velocity and density. Variable layer interfaces, S-wave velocity and density values are well characterized at high resolutions (7.5 in to 30 ft depth and 15 in to 60 ft depth). The algorithm is further optimized to minimize field testing and data analyzing efforts (Task 2) and verified on field experimental data (Task 3), as discussed in the next two chapters.

Chapter 3 – OPTIMIZATION OF TEST CONFIGURATIONS AND WAVE CHARACTERISTICS (TASK 2)

3.1 Introduction

The SH- and Love-wave full-waveform inversion (SH-Love FWI) method and its algorithm were successfully developed in Task 1. The goal of this task is to identify the optimal test configurations (receiver and shot numbers) for detecting layers and interfaces at various depths using the SH-Love FWI algorithm. To achieve this, several parametric studies were performed with synthetic (computational) models. The test configurations identified in this task were then applied for field experiments in Task 3 to streamline the field testing and data analysis efforts.

For parametric studies, two synthetic models (deep and shallow models) were designed to represent the typical geological conditions of Florida, where soils are underlain by variable bedrock. One model includes three variable layers (deep model), while the other includes four layers (shallow model). The steepest-descent adjoint-state optimization technique was employed to minimize errors and update model parameters (density and Vs). In the deep model, survey lines of receivers were studied on the surface at two spacings of 1.5 m (5 ft) and 3.0 m (10 ft) with various source spacings of 1.5 m (5 ft), 3.0 m (10 ft) and 6 m (20 ft). In the shallow model, the tested receiver spacings were 0.75 m (2.5 ft) and 1.5 m (5 ft), while the source spacing was set at 0.75 m (2.5 ft), 1.5 m (5 ft) and 3 m (10 ft). The accuracy and resolution of inverted profiles were compared among the simulations to identify the optimal test configurations.

The frequency range of interest is set to 5-25 Hz (first run) and 5-40 Hz (second run) for the deep model, and 10-50 Hz and 10-80 Hz for shallow model. The inverted density and Vs results are used as the criteria for selecting the test configurations in this task.

3.2 Synthetic experiment on deep model of 18-m depth

3.2.1 Test configuration

The SH-Love FWI algorithm was first tested on a synthetic deep model. The model domain measures 36 m × 18 m (120 ft × 60 ft) in length and depth. It consists of three layers with the following density values: 1,800, 1,600 and 2,000 kg/m^3, and corresponding Vs of 300, 150 and 500 m/s from top to bottom (Figure 3.1a).

To investigate the minimum number of receivers required for successful recovery of subsurface features, four test configurations were analyzed. The test configurations were carried out by decreasing the number of receivers and shots. The test configurations are shown in Figure 3.2 to Figure 3.5. Figure 3.2 shows the densest test configuration with 24 receivers (represented by black triangles) and 25 shots (indicated by white arrows) placed on the surface at 1.5 m (5 ft) spacing. Figure 3.3 depicts a medium dense test configuration with 24 receivers and 16 shots at 1.5 m (5 ft) and 3 m (10 ft) spacing, respectively. Figure 3.4 displays a relatively dense test configuration consisting of 12 receivers and 13 shots at 3 m (10 ft) spacing. Lastly, Figure 3.5 shows the least dense test configuration with 12 receivers and 7 shots spaced at 3 m (10 ft) and 6 m (20 ft), respectively.

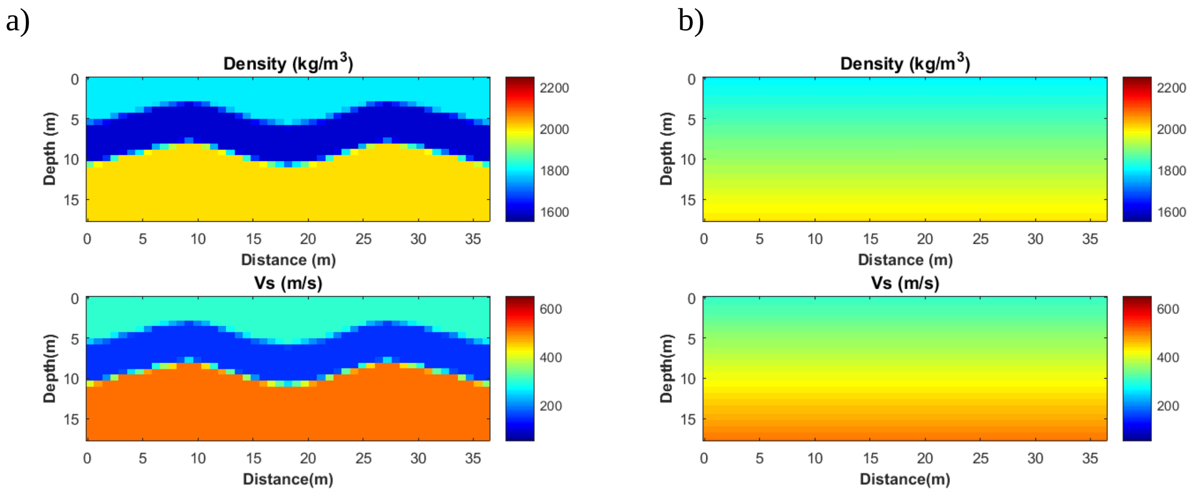

Figure 3.1. Synthetic deep model: (a) true model used for generating synthetic data, (b) initial model at the beginning of iteration.

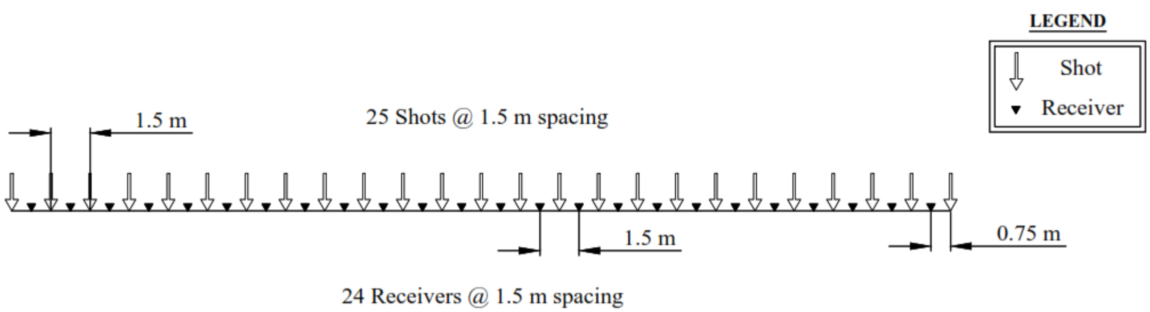

Figure 3.2. Test configuration 1: 24 receivers and 25 shots

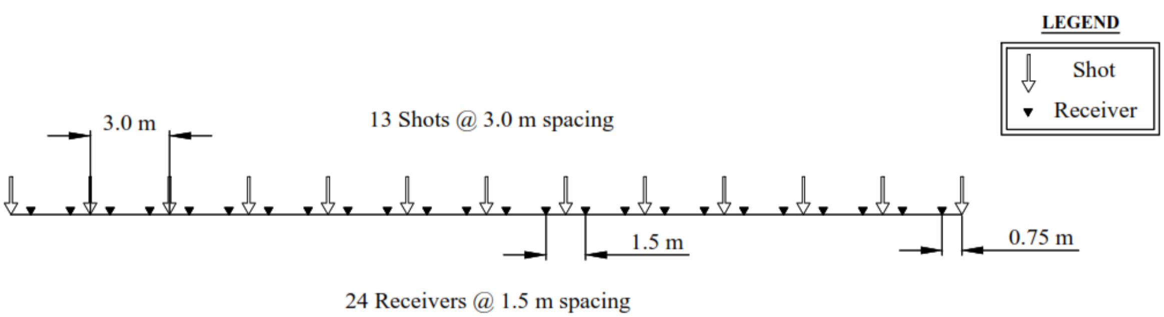

Figure 3.3. Test configuration 2: 24 receivers and 13 shots

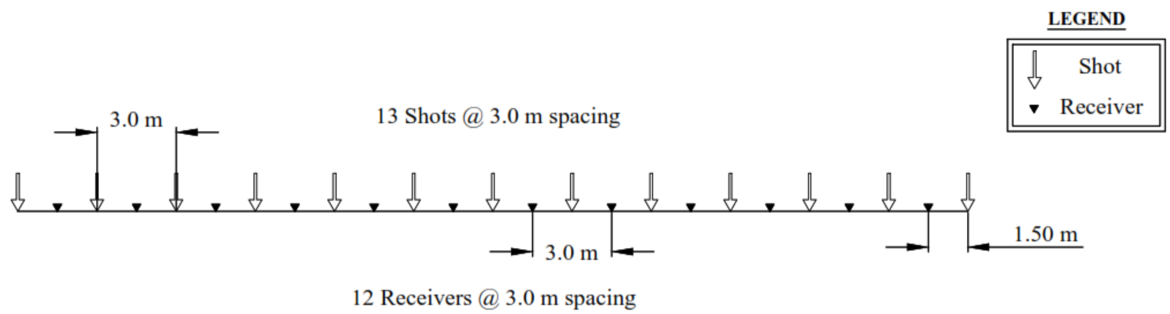

Figure 3.4. Test configuration 3: 12 receivers and 13 shots

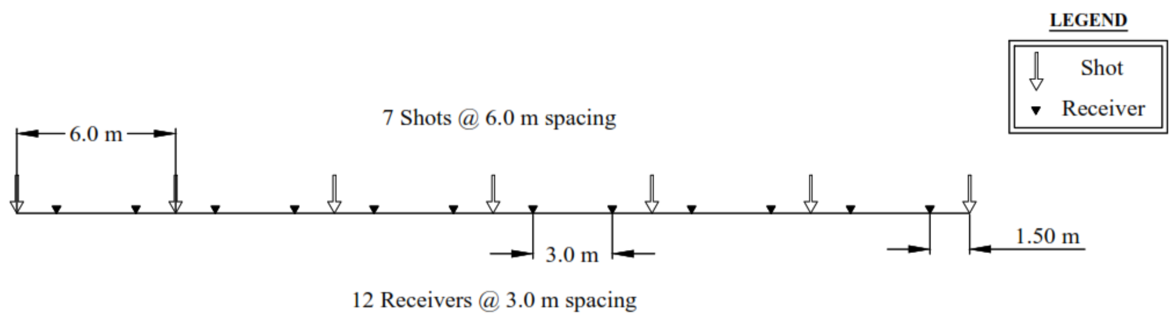

Figure 3.5. Test configuration 4: 12 receivers and 7 shots

3.2.2 Results for test configuration 1 (24 receivers, 25 shots)

The inversion analysis was initially performed for the densest configuration of 24 receivers and 25 shots (Figure 3.2). The analysis utilized 1D density and S-wave velocity profiles as initial models, which show a linear increase in density and Vs with depth. Specifically, the profiles started at free surface with density of 1,800 kg/m^3 and Vs of 300 m/s and gradually reached 2,000 kg/m^3 and 500 m/s at the bottom of the model (Figure 3.6b). Two inversion runs were conducted, with the first run using low-frequency data in the range of 5-25 Hz on the initial model. The second run was performed with the higher-frequency range (5-40 Hz) data using the inverted result from the first run as the input model. Both runs stopped after 50 iterations.

The inverted density and Vs results from the two inversion runs are presented in Figure 3.6. Generally, the true model features, including the layer layout, were successfully recovered in the first run (Figure 3.6a). The second run with higher frequencies at 5-40 Hz improved the inverted model obtained from the first run (Figure 3.6b). A detailed comparison is provided in Figure 3.7, which focuses on two locations within the medium, at distances of 18 m and 27 m from the middle and right, respectively. Compared to the initial values, density and Vs changed significantly during the inversion. The final inverted Vs and density agreed well with their true values at both locations. However, some discrepancies in density and Vs were observed at the bottom of the model. This was mostly due to weak signal coverage in that zone. In addition, the implemented Tikhonov regularization in the SH-Love FWI algorithm always produces a smooth inverted model that led to the mismatch of Vs and density near the layer interfaces. Nevertheless, the presented FWI successfully inverted both Vs and density of the three-layer model with acceptable accuracy.

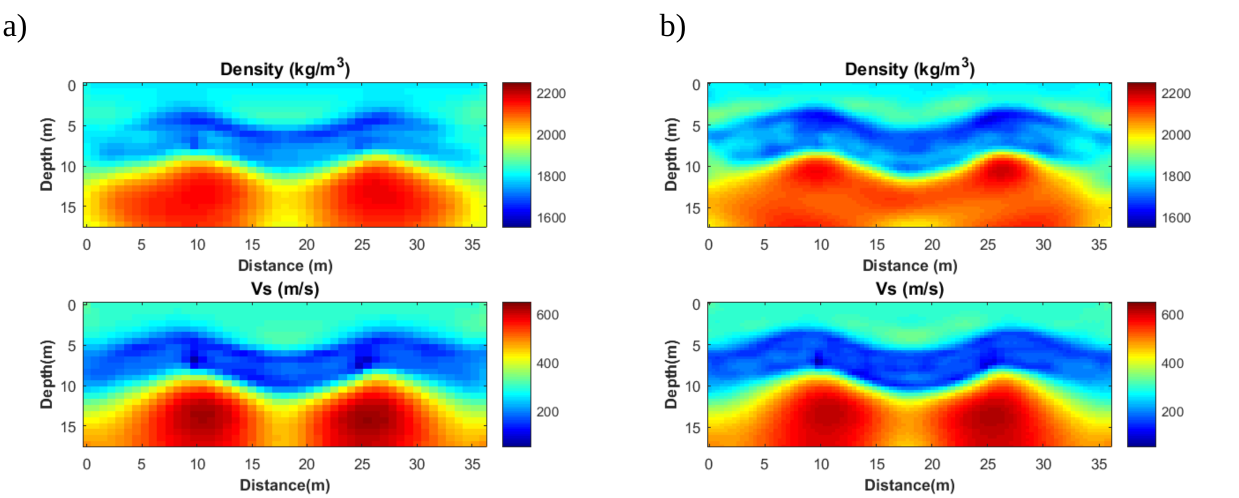

Figure 3.6. Synthetic model of density (kg/m^3) and S-wave velocity (m/s): (a) inverted model at 5-25 Hz and (b) inverted model at 5-40 Hz (deep model, 24 receivers and 25 shots).

Normalized least-squares error for all iterations of the two inversion runs are shown in Figure 3.8, where the error decreased substantially during inversion from 1.0 at the first iteration to less than 0.01 at the final iteration in the second run. In Figure 3.9, the observed waveform data were compared to the estimated waveform data from both the initial and final inverted model for the first shot. The waveform match improved significantly throughout the inversion process. The final residuals for all the receivers were close to zeros, indicating a good fit between the observed and estimated waveform data.

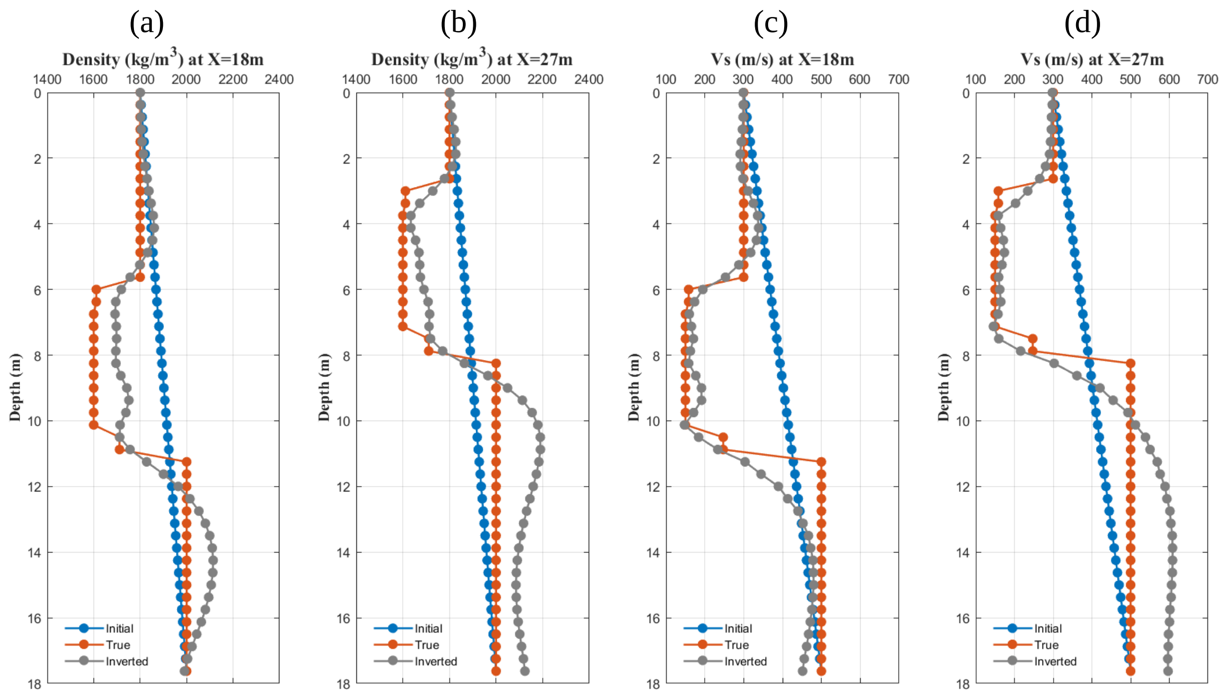

Figure 3.7. Synthetic model (deep model, 24 receivers and 25 shots): comparison of density at distances of (a) X=18 m and (b) X=27 m, and S-wave velocity at distances (c) X=18 m and (d) X=27 m.

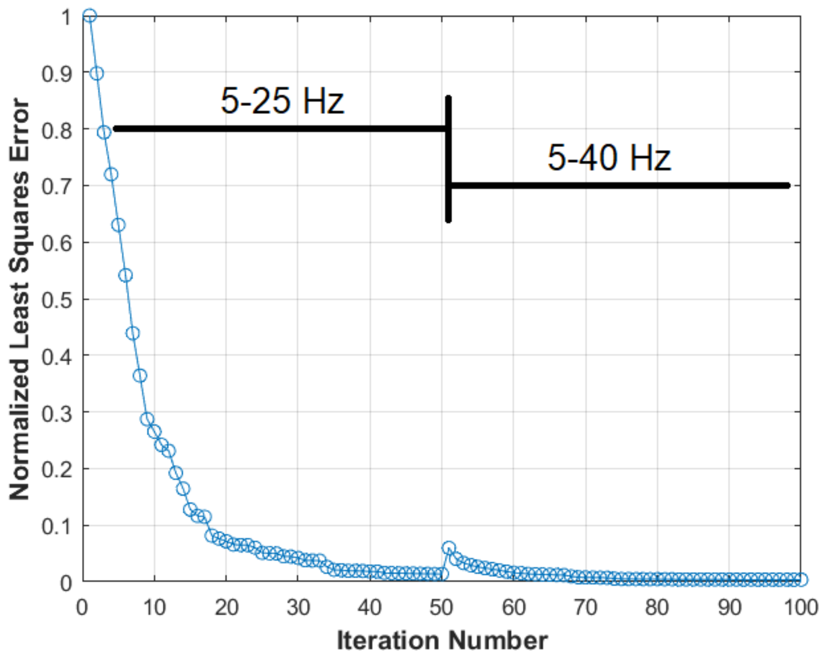

Figure 3.8. Synthetic model: normalized least squares error versus the inversion iteration number (deep model, 24 receivers and 25 shots).

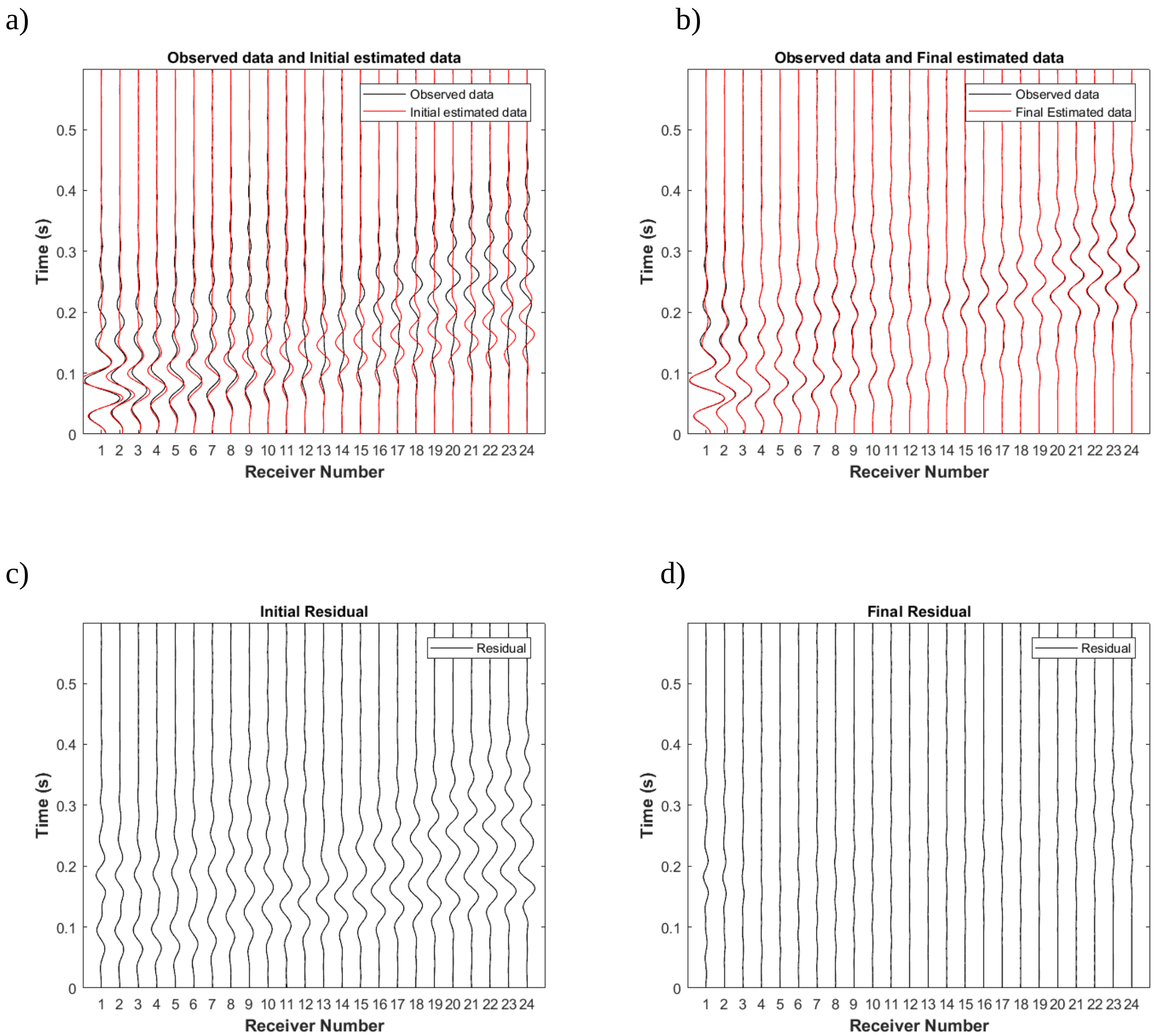

Figure 3.9. Synthetic model (deep model, 24 receivers and 25 shots): waveform comparison for the first shot: (a) observed data and estimated data associated with the initial model, (b) observed data and estimated data associated with the final inverted model, (c) residual associated with the initial model, and (d) residual associated with final inverted model.

3.2.3 Results for test configuration 2 (24 receivers, 13 shots)

The inversion analysis was then carried out using the test configuration of 24 receivers and 13 shots (Figure 3.3) to evaluate the improvement in the results, particularly for density and S-wave velocity. Similar to the analysis of test configuration 1, the inversion began with the same 1D density and Vs profiles that linearly increased with depth. Two inversion runs were conducted with the first run for the lower-frequency (5-25 Hz) data on the initial model, and the second run for higher-frequency (5-40 Hz) data using the result of the first run as input model.

The inverted density and Vs results of the first and second runs are displayed in Figure 3.10. After the first run, the true features, including the layers, are clearly recovered (Figure 3.10a). The second run, incorporating higher-frequency data up to 40 Hz, further improved the inverted model (Figure 3.10b). A detailed comparison is shown in Figure 3.11 for two distances of 18 m and 27 m. Interestingly, reducing the number of shots does not negatively affect results, suggesting that a lot of data redundancy exists with test configuration 1.

The normalized least-squares error of the two inversion runs is shown in Figure 3.12, where the error reduced from 1.0 at the first iteration to about 0.01 at the end of the second run (iteration #100). Waveform and residual comparisons are displayed in Figure 3.13. The inversion process has significantly enhanced the fitting of waveforms, especially for the far-field traces.

a) b)

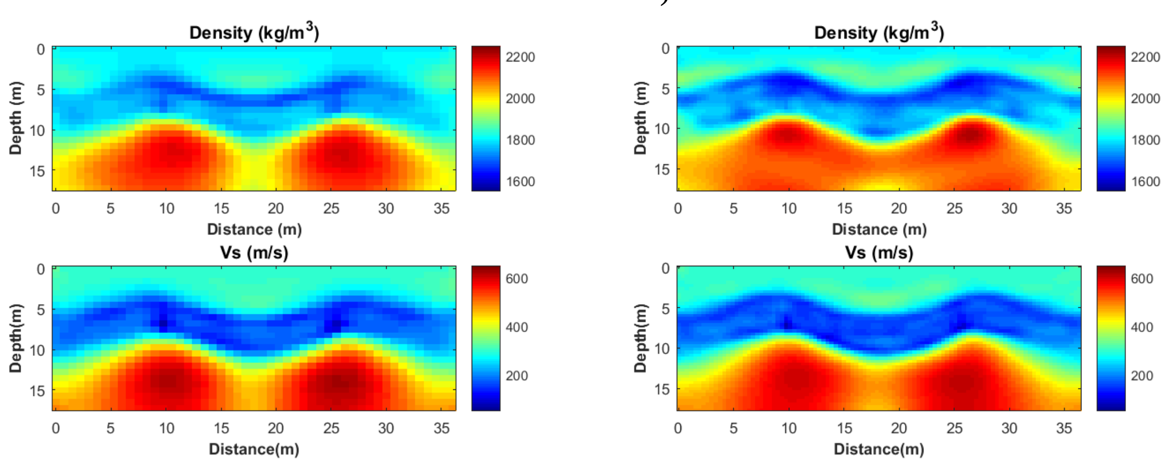

Figure 3.10. Synthetic model of density (kg/m^3) and S-wave velocity (m/s): (a) inverted model at 5-25 Hz and (b) inverted model at 5-40 Hz (deep model, 24 receivers and 13 shots).

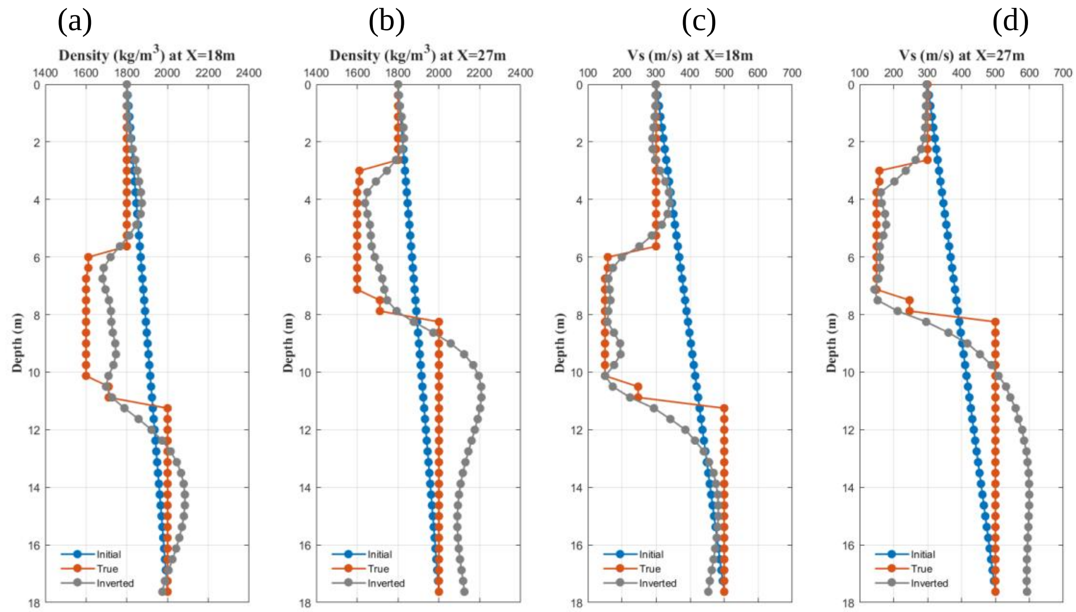

Figure 3.11. Synthetic model (deep model, 24 receivers and 13 shots): comparison of density at distances of (a) X=18 m and (b) X=27 m and S-wave velocity at distances (c) X=18 m and (d) X=27 m.

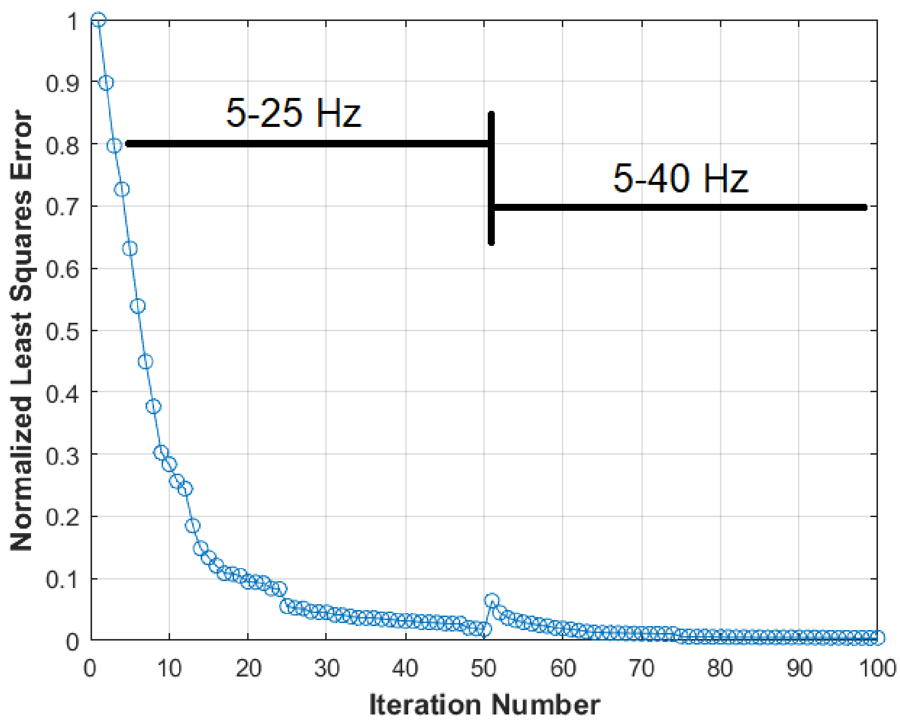

Figure 3.12. Synthetic model: normalized least squares error versus the inversion iteration number (deep model, 24 receivers and 13 shots).

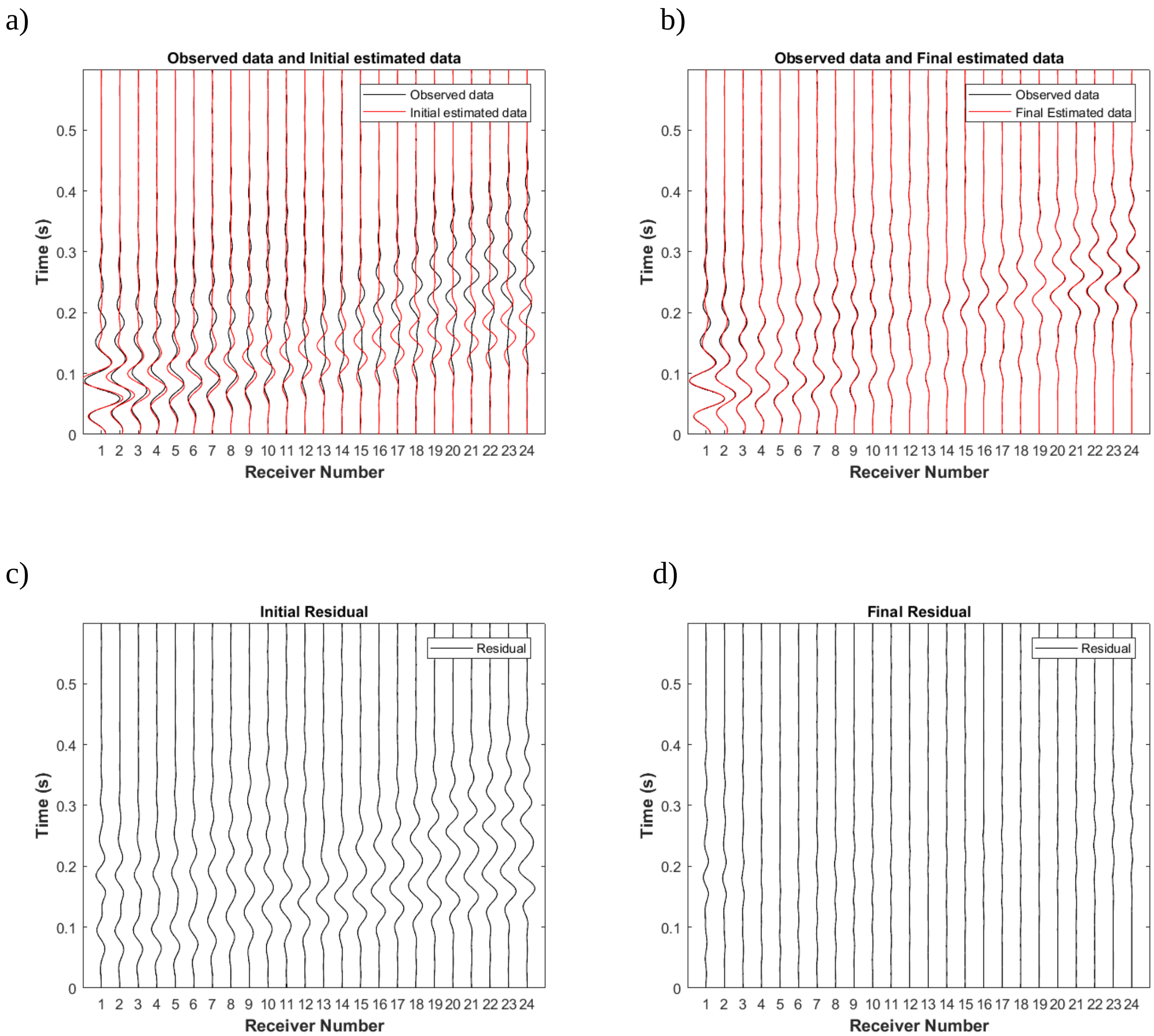

Figure 3.13. Synthetic model (deep model, 24 receivers and 13 shots): waveform comparison for the first shot: (a) observed data and estimated data associated with the initial model, (b) observed data and estimated data associated with the final inverted model, (c) residual associated with the initial model, and (d) residual associated with final inverted model.

3.2.4 Results for test configuration 3 (12 receivers, 13 shots)

Next, the inversion analysis was performed on the relatively dense test configuration, which consisted of 12 receivers and 13 shots (Figure 3.4). The inversion process followed the same procedure as the previous cases, utilizing the initial model and conducting two runs at frequencies of 5-25 Hz and 5-40 Hz. The inverted density and Vs profiles are displayed in Figure 3.14. A detailed comparison is displayed in Figure 3.15 for distances of 18 m and 27 m. Results are similar to those from test configurations 1 and 2, except the overshooting at the middle of top layer in the density image (oval in Figure 3.14b).

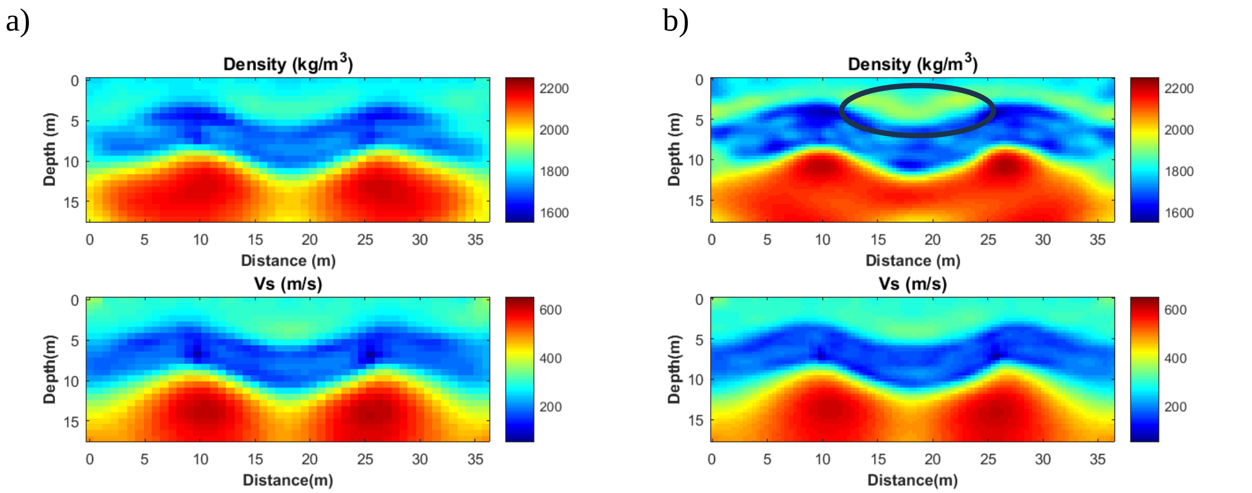

Figure 3.14. Synthetic model of density (kg/m^3) and S-wave velocity (m/s): (a) inverted model at 5-25 Hz and (b) inverted model at 5-40 Hz (deep model, 12 receivers and 13 shots).

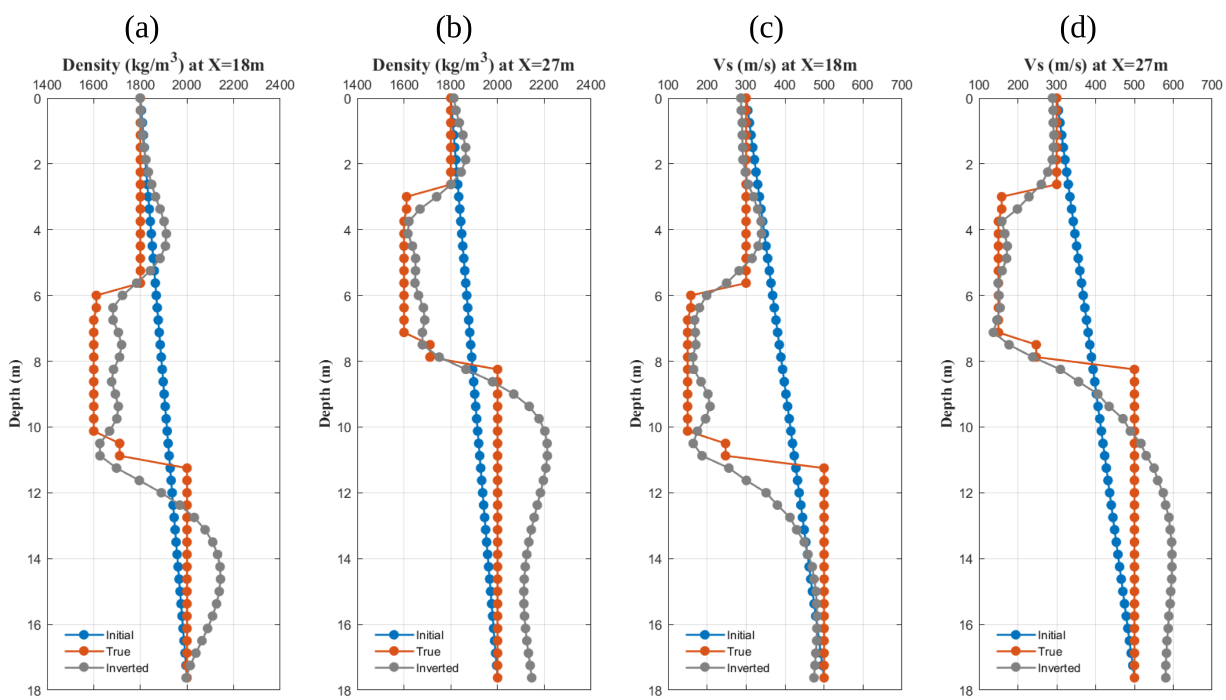

Figure 3.15. Synthetic model (deep model, 12 receivers and 13 shots): comparison of density at distances of (a) X=18 m and (b) X=27 m and S-wave velocity at distances (c) X=18 m and (d) X=27 m.

Figure 3.16 displays the normalized least-squares error for all iterations of the two inversion runs. The error reduced from 1.0 at the beginning of the first iteration to below 0.01 at the end of the inversion process (iteration #100). The waveform and residual comparisons are depicted in Figure 3.17.

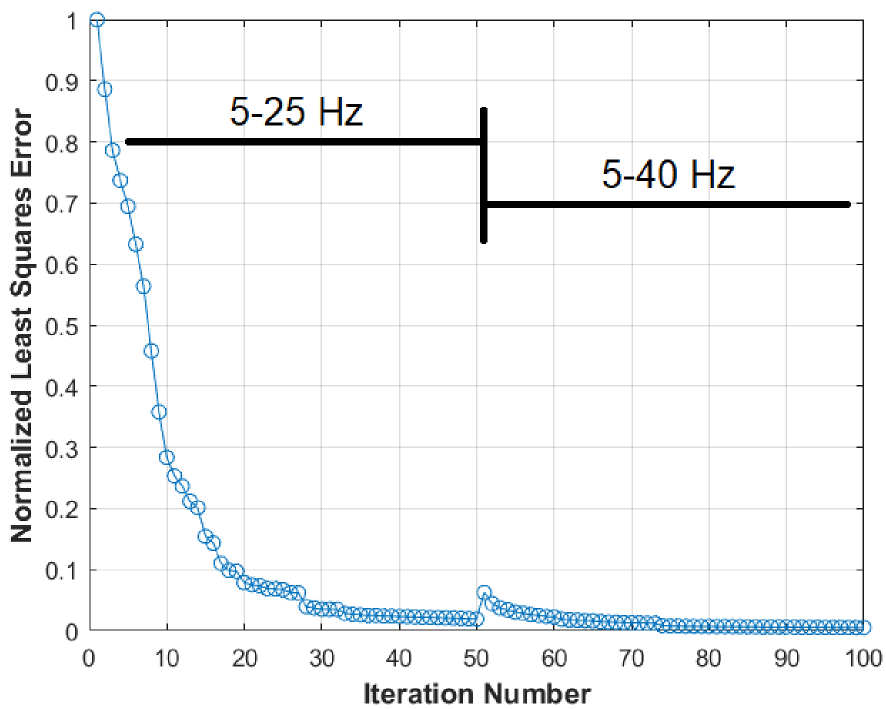

Figure 3.16. Synthetic model: normalized least squares error versus the inversion iteration number (deep model, 12 receivers and 13 shots).

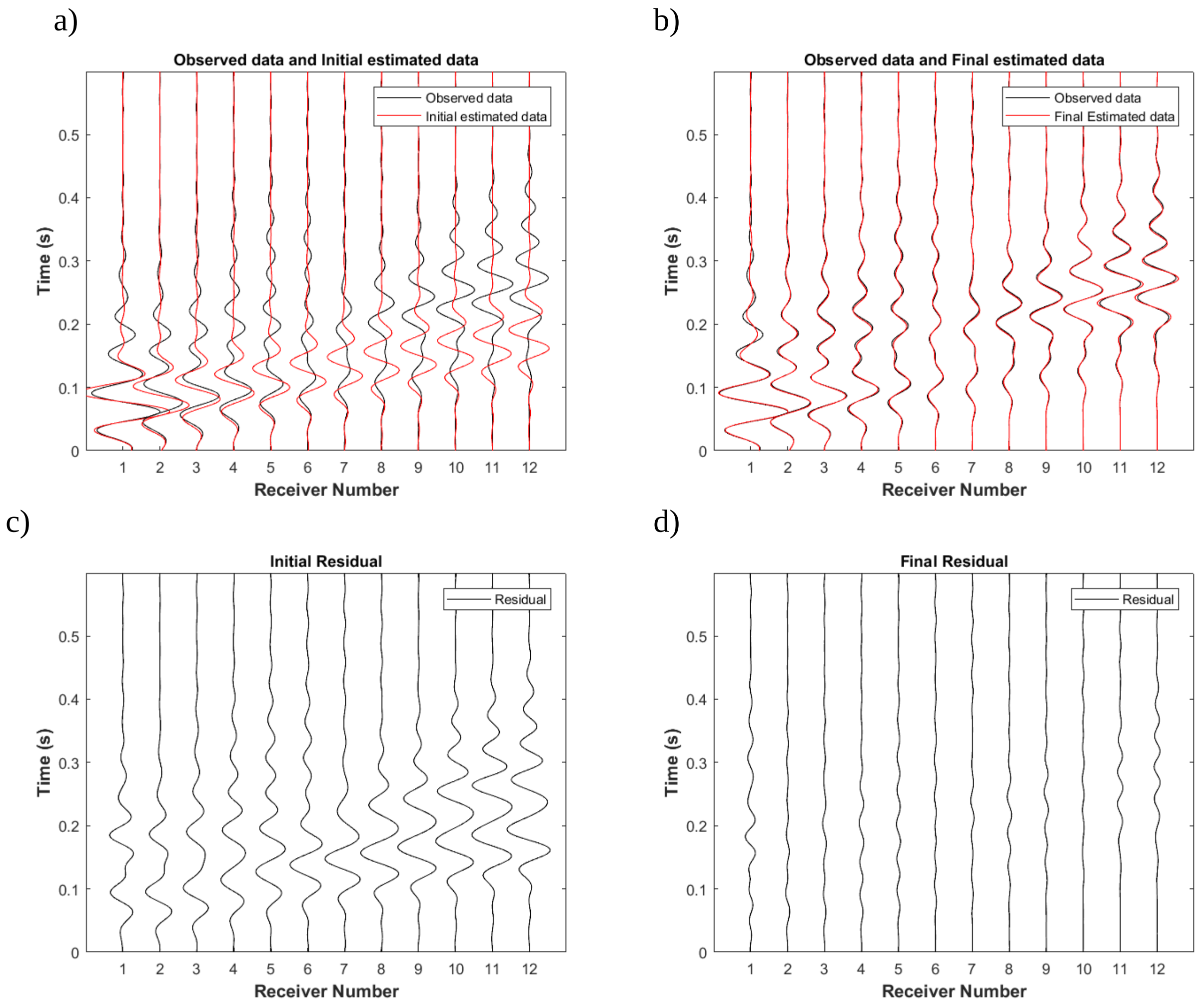

Figure 3.17. Synthetic model (deep model, 12 receivers and 13 shots): waveform comparison for the first shot: (a) observed data and estimated data associated with the initial model, (b) observed data and estimated data associated with the final inverted model, (c) residual associated with the initial model, and (d) residual associated with final inverted model.

3.2.5 Results for test configuration 4 (12 receivers, 7 shots)

Finally, the inversion analysis was performed on the least dense test configuration of 12 receivers and 7 shots (Figure 3.5). Following the same procedure as the previous cases, the inversion began with the same initial model and performed two runs at frequencies of 5-25 Hz and 5-40 Hz. The inverted density and Vs results are displayed in Figure 3.18. The layers were characterized in the first run (Figure 3.18a) and are recovered in the second run (Figure 3.18b). A detailed comparison of two profiles at the distances of 18 m and 27 m are displayed in Figure 3.19 for density and Vs. Again, there is overshooting at the middle of top layer in the density (oval in Figure 3.18b).

Normalized least-squares error for all iterations of the two inversion runs are shown in Figure 3.20. The error reduced from 1.0 at the start of the first iteration to less than 0.01 at the end of second run (iteration #100). Waveform and residual comparisons are shown in Figure 3.21.

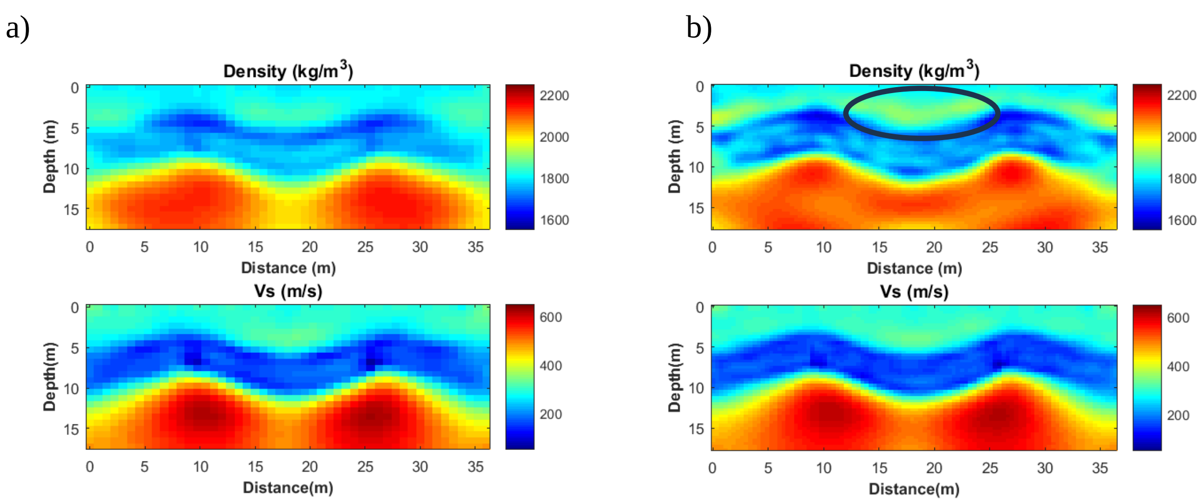

Figure 3.18. Synthetic model of density (kg/m^3) and S-wave velocity (m/s): (a) inverted model at 5-25 Hz and (b) inverted model at 5-40 Hz (deep model, 12 receivers and 7 shots).

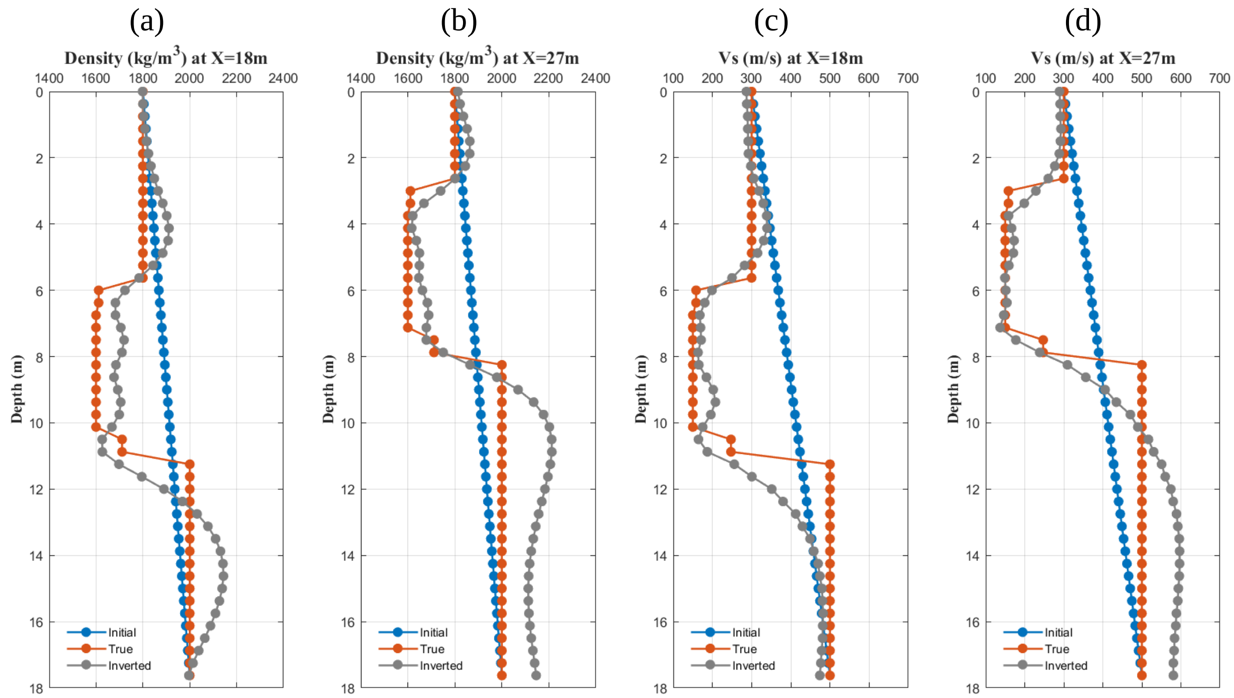

Figure 3.19. Synthetic model (deep model, 12 receivers and 7 shots): comparison of density at distances of (a) X=18 m and (b) X=27 m and S-wave velocity at distances (c) X=18 m and (d) X=27 m.

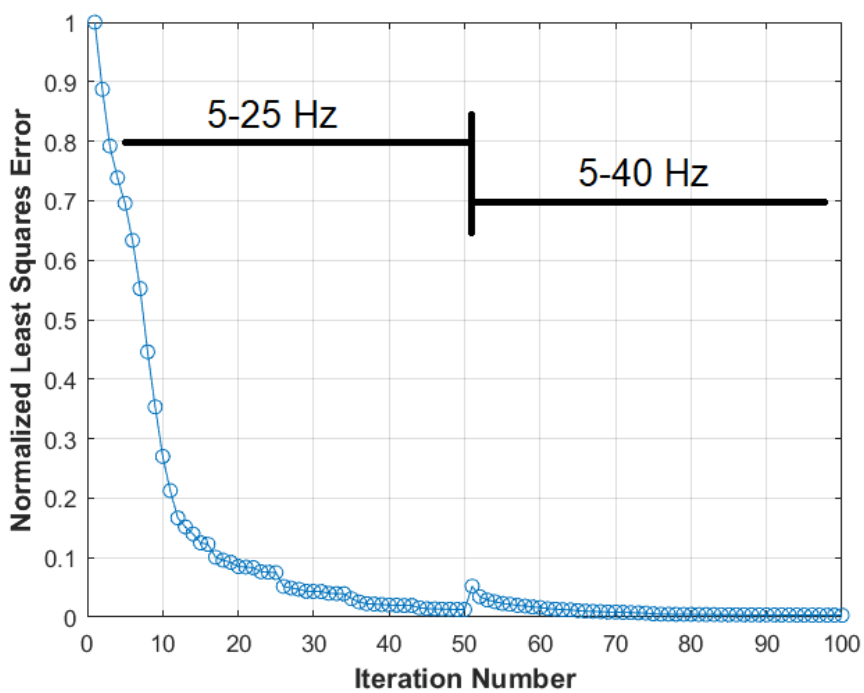

Figure 3.20. Synthetic model: normalized least squares error versus the inversion iteration number (deep model, 12 receivers and 7 shots).

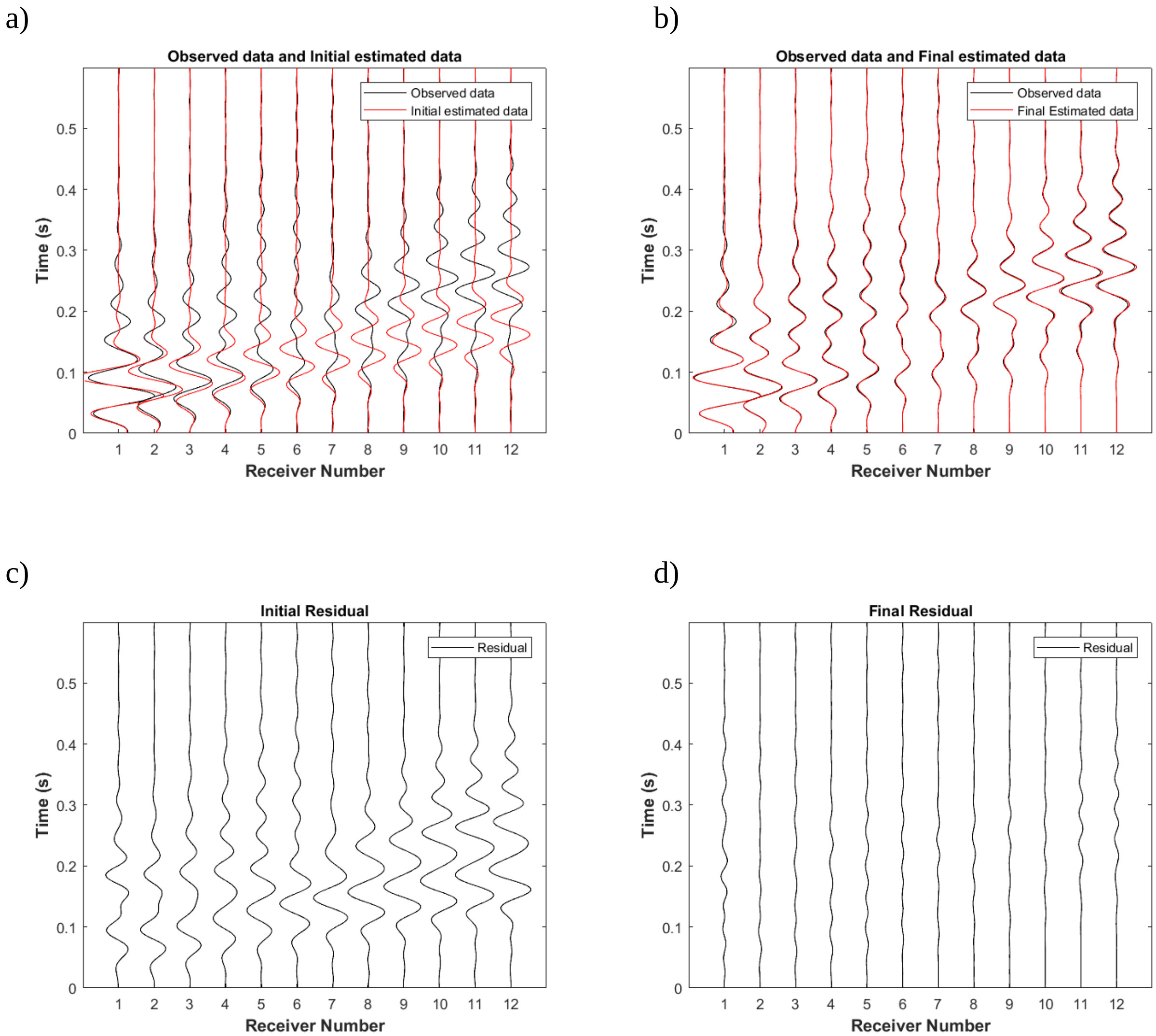

Figure 3.21. Synthetic model (deep model, 12 receivers and 7 shots): waveform comparison for the first shot: (a) observed data and estimated data associated with the initial model, (b) observed data and estimated data associated with the final inverted model, (c) residual associated with the initial model, and (d) residual associated with final inverted model.

In summary, the SH-Love FWI algorithm demonstrated the ability to effectively characterize the deep model (60-ft depth) for all test configurations. The inverted density and Vs profiles (Figure 3.6, Figure 3.10, Figure 3.14, and Figure 3.18) of the four tests were similar. There were some discrepancies in density profiles because of overshooting in the upper layer near the middle of the medium for test configurations 3 and 4. Thus, it is recommended to use a receiver spacing of 1.5 m (5 ft) and a shot spacing as one or two receiver spacings (5 or 10 ft) for field experiments (configuration 1 or 2). These configurations will enable accurate characterization of variable layers to 60-ft depth.

3.3 Synthetic experiment on shallow model of 9-m depth

3.3.1 Test configuration

After successfully recovering the deep model, the SH-Love FWI algorithm was tested on a challenging model consisting of four variable layers with a depth of 9 m (30 ft). The model domain had dimensions of 18 m × 9 m (60 ft × 30 ft) (length × depth) and included four layers with density of 1,500, 1,800, 1,600 and 2,000 kg/m^3 and Vs of 200, 300, 150, and 500 m/s from the top to bottom (Figure 3.22a). This type of profile is of interest for shallow foundation designs, which typically require soil or rock properties with 30 ft from the ground surface.

The initial models used in the analysis were 1D density and S-wave velocity profiles that linearly increased with depth. The S-wave velocity and density ranged from 200 m/s and 1500 kg/m^3 at the free surface to 500 m/s and 2000 kg/m^3 at the bottom of the model (Figure 3.22b), respectively. This model was tested with four configurations:

1. 24 receivers and 25 shots at 0.75 m (2.5 ft) spacing (Figure 3.23).

2. 24 receivers at 0.75 m (2.5 ft) and 13 shots 1.5 m (5 ft) spacing (Figure 3.24).

3. 12 receivers and 13 shots at 1.5 m (5 ft) spacing (Figure 3.25).

4. and 12 receivers at 1.5 m (5 ft) and 7 shots at 3 m (10 ft) spacing (Figure 3.26).

Similar to the previous deep model, each configuration was tested with two inversion runs with frequency ranges of 10-50 Hz and 10-80 Hz, respectively. Each run stopped after 50 iterations. It is noted that higher frequency data (up to 80 Hz) is needed for characterization at sub-foot pixel resolutions.

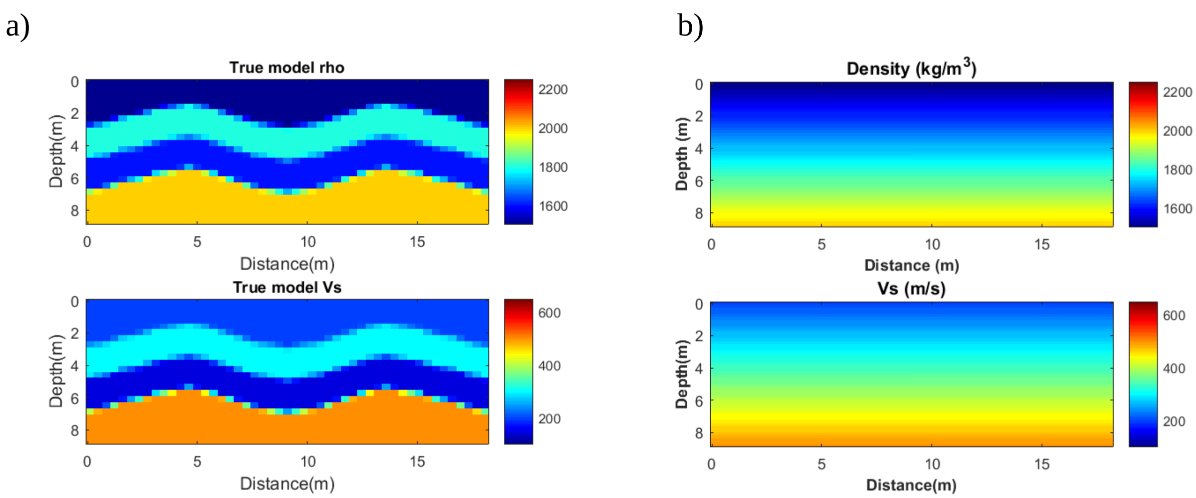

Figure 3.22. Synthetic shallow model: (a) true model used for generating synthetic data and (b) initial model at the beginning of iteration.

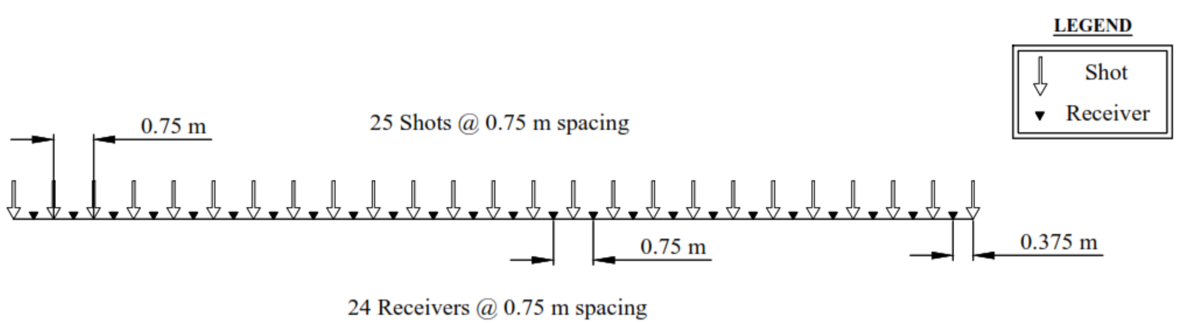

Figure 3.23. Test configuration 1: 24 receivers and 25 shots

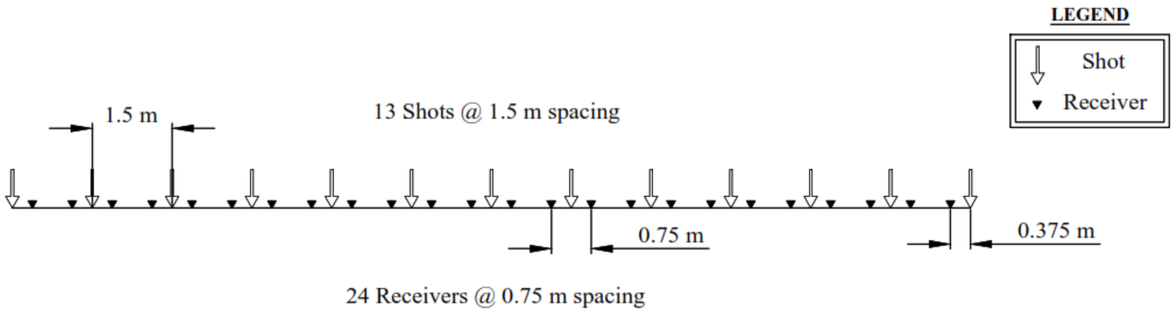

Figure 3.24. Test configuration 2: 24 receivers and 13 shots

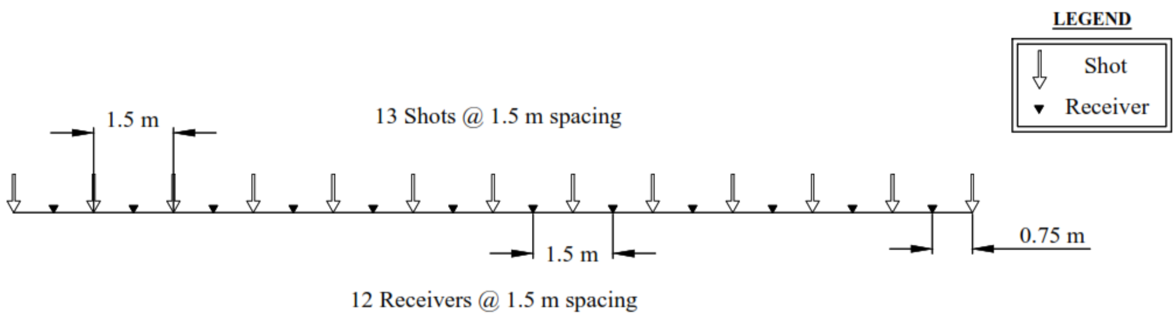

Figure 3.25. Test configuration 3: 12 receivers and 13 shots

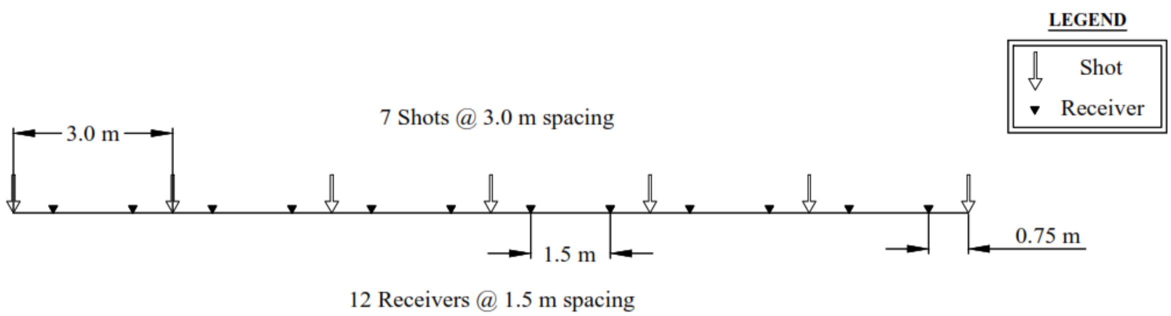

Figure 3.26. Test configuration 4: 12 receivers and 7 shots

3.3.2 Results for test configuration 1 (24 receivers, 25 shots)

The inversion analysis was first carried out for the densest configuration of 24 receivers and 25 shots (Figure 3.23). Two inversion runs were again conducted with the first run for the low frequency range (10-50 Hz) data on the initial model, and the second run for higher frequency range (10-80 Hz) data using the result of the first run as input. The inverted density and Vs results of the two runs are displayed in Figure 3.27. A detailed comparison among the true, initial, and inverted values of density and Vs at distances of 9 m and 13.5 m is displayed in Figure 3.28. Some discrepancies can be seen in Vs and density at the bottom of the model, primarily because of limited signal coverage in that area.

The normalized least-squares error for all iterations of the two inversion runs are shown in Figure 3.29, where the error reduced from 1.0 at the onset of the first iteration to about 0.01 at the final iteration (iteration #100) of the second run. Waveform and residual comparisons are displayed in Figure 3.30.

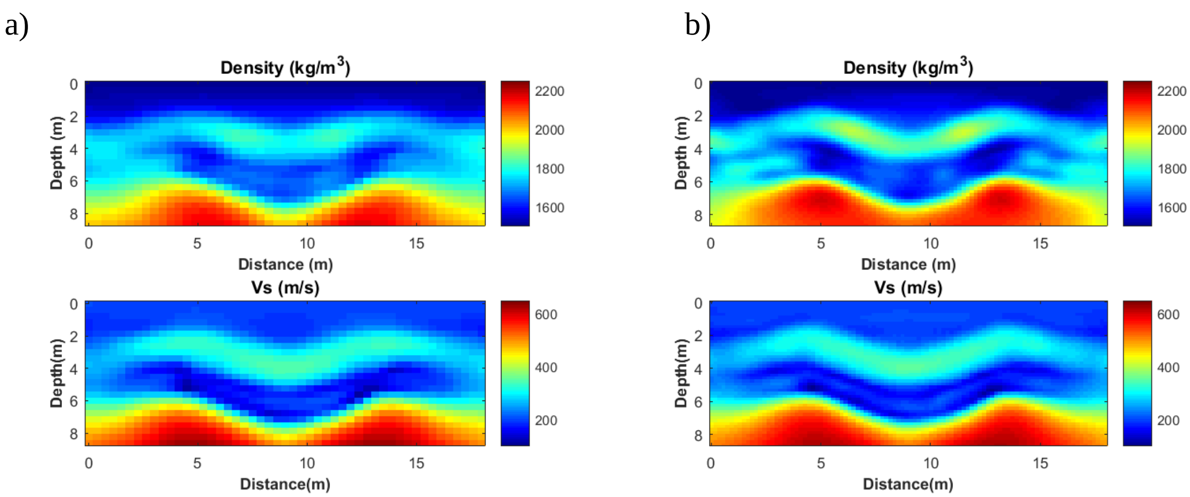

Figure 3.27. Synthetic model of density (kg/m^3) and S-wave velocity (m/s): (a) inverted model at 10-50 Hz and (b) inverted model at 10-80 Hz (shallow model, 24 receivers and 25 shots).

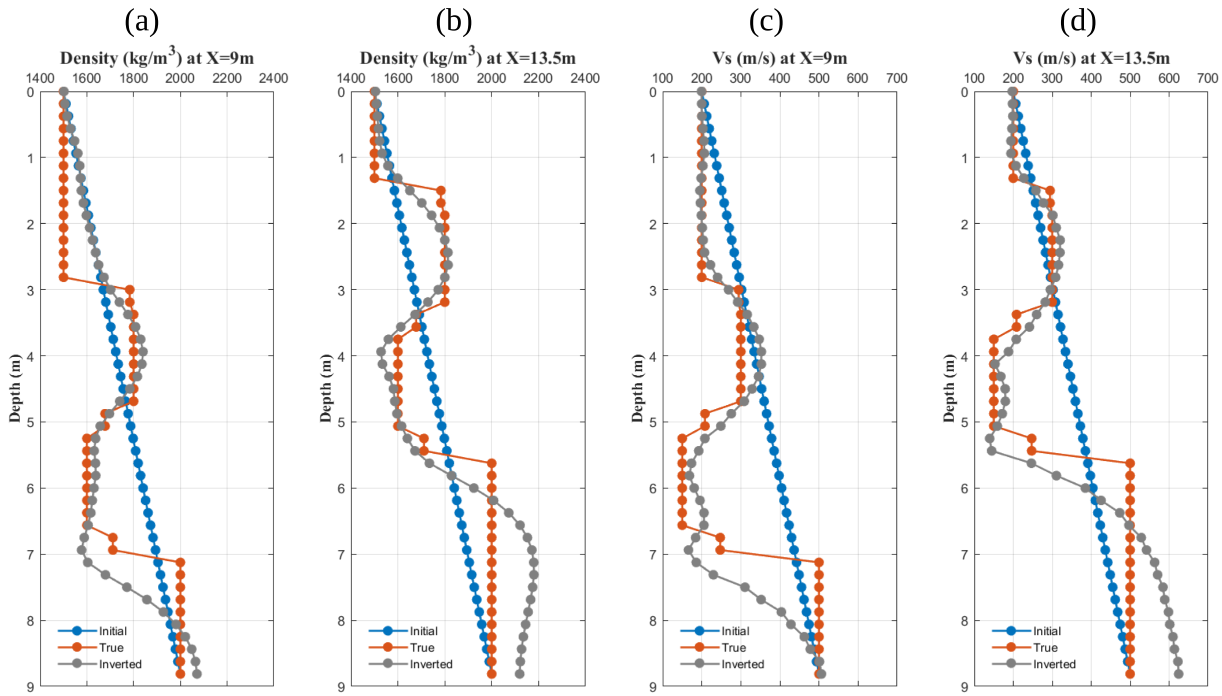

Figure 3.28. Synthetic model (shallow model, 24 receivers and 25 shots): comparison of density at distances of (a) X=9 m and (b) X=13.5 m and S-wave velocity at distances (c) X=9 m and (d) X=13.5 m.

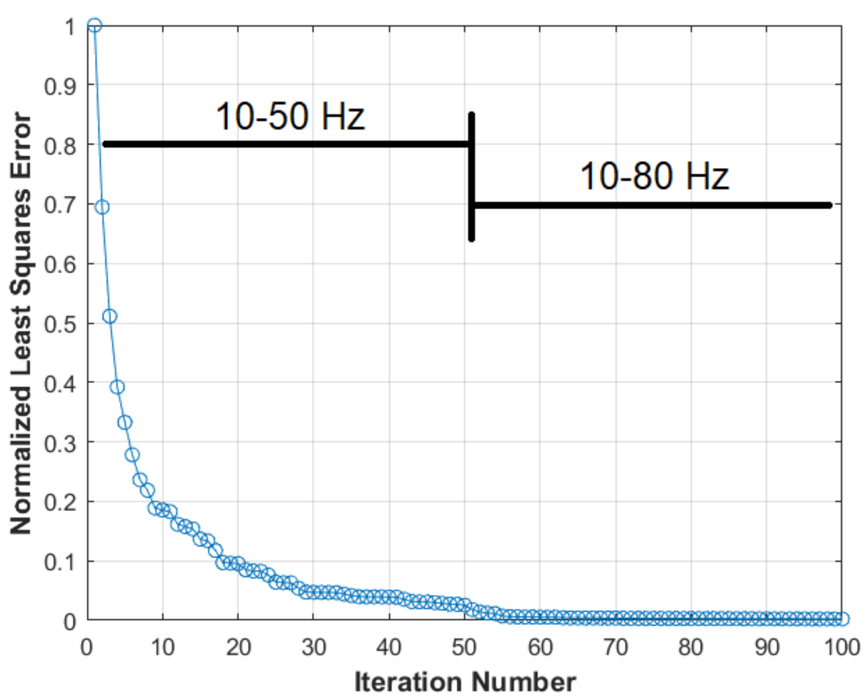

Figure 3.29. Synthetic model: normalized least squares error versus the inversion iteration number (shallow model, 24 receivers and 25 shots).

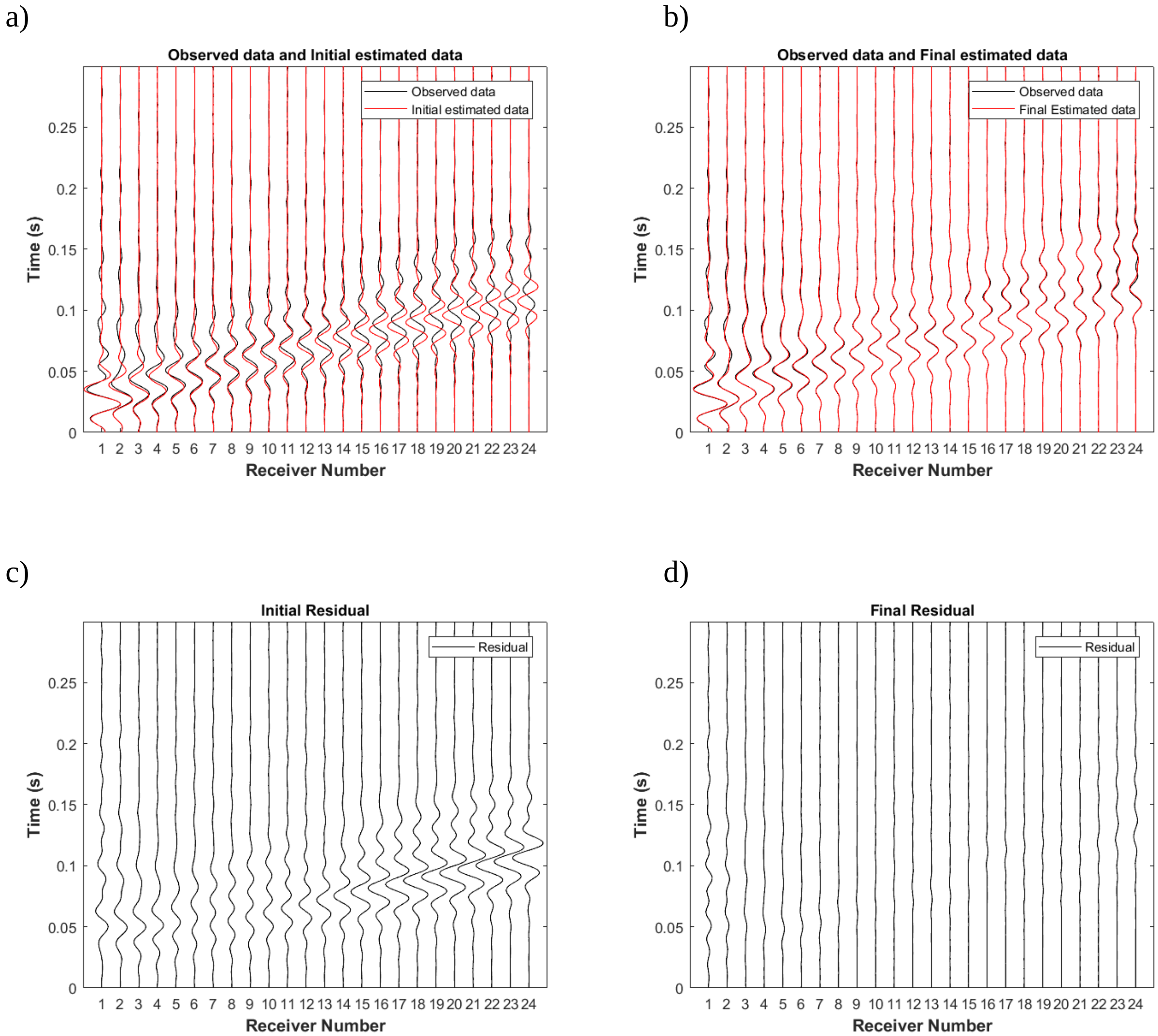

Figure 3.30. Synthetic model (shallow model, 24 receivers and 25 shots): waveform comparison for the first shot: (a) observed data and estimated data associated with the initial model, (b) observed data and estimated data associated with the final inverted model, (c) residual associated with the initial model, and (d) residual associated with final inverted model.

3.3.3 Results for test configuration 2 (24 receivers, 13 shots)

We then tried with a test configuration of 24 receivers and 12 shots (Figure 3.24) to assess result improvement, particularly for density result. The inverted density and Vs obtained at iteration #50 are displayed in Figure 3.31. Similar to the previous case with 24 receivers and 25 shots, the true model features, including layers, were generally recovered after the first run (Figure 3.31a). The second run with higher frequency data up to 80 Hz improved the inverted model from the first run (Figure 3.31b). A detailed comparison is displayed in Figure 3.32 for two distances of 9 m and 13.5 m.

Normalized least-squares error for all iterations of the two inversion runs are shown in Figure 3.33, where the error was reduced from 1.0 at the onset of the first iteration to about 0.02 at the final iteration (iteration #50) of the first run and 0.01 on the second run. The waveform and residual comparisons are displayed in Figure 3.34, illustrating the improvement in waveform fitting throughout the inversion process.

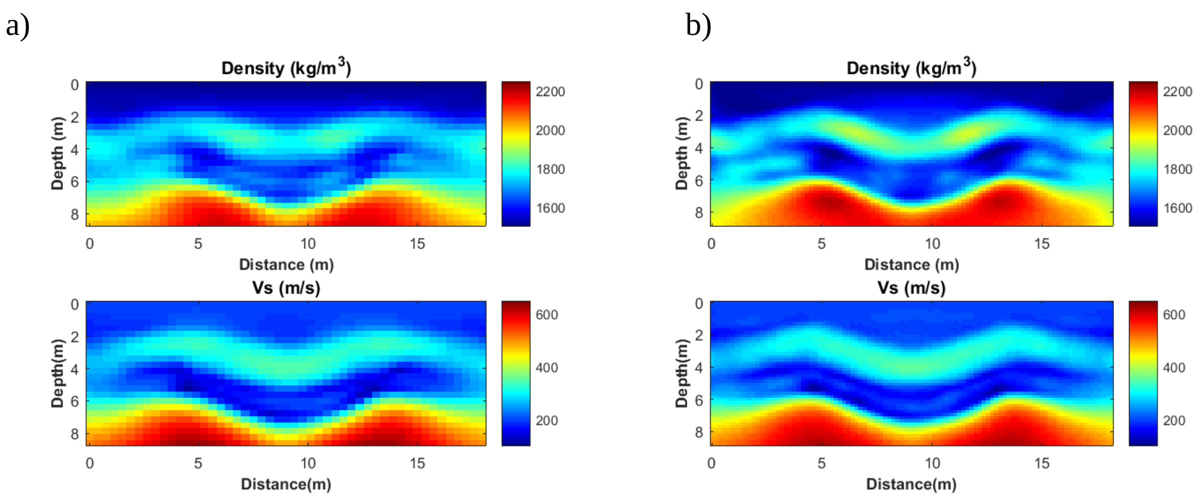

Figure 3.31. Synthetic model of density (kg/m^3) and S-wave velocity (m/s): (a) inverted model at 10-50 Hz and (b) inverted model at 10-80 Hz (shallow model, 24 receivers and 13 shots).

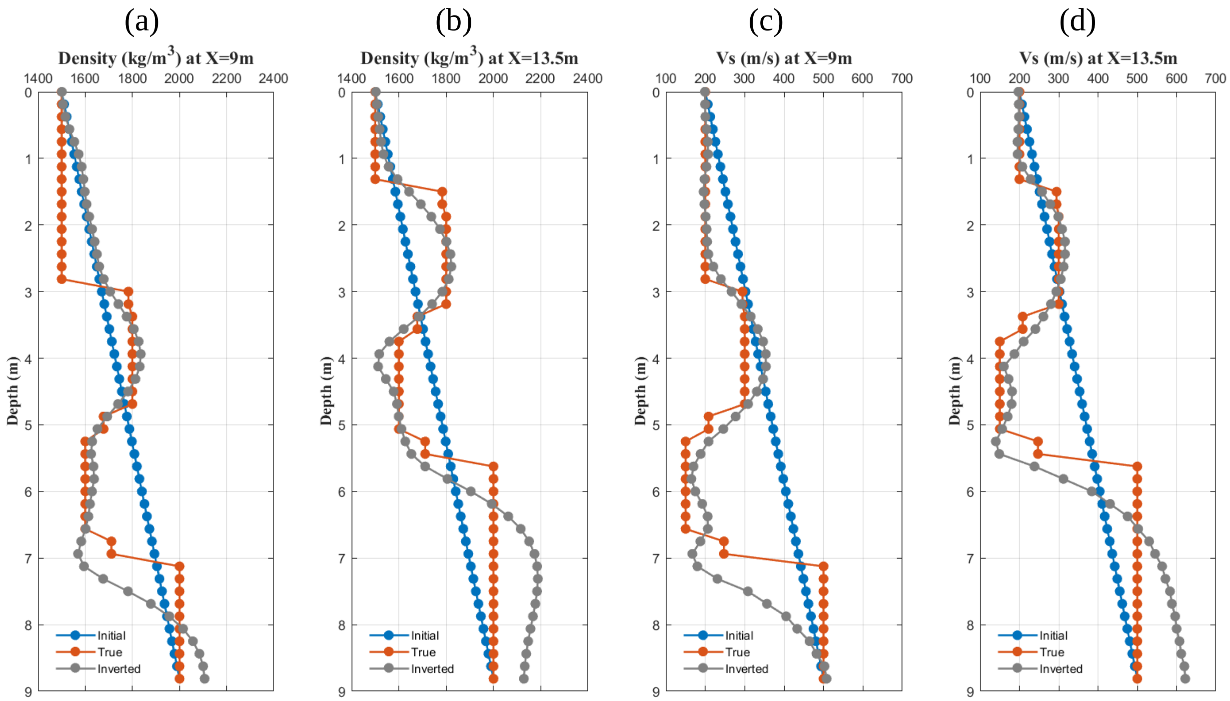

Figure 3.32. Synthetic model (shallow model, 24 receivers and 13 shots): comparison of density at distances of (a) X=9 m and (b) X=13.5 m and S-wave velocity at distances (c) X=9 m and (d) X=13.5 m.

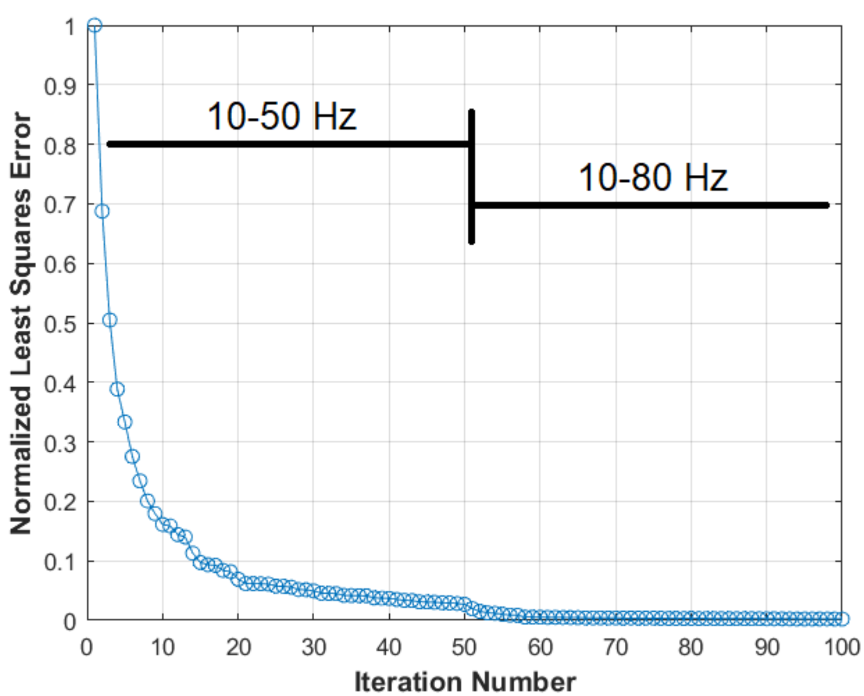

Figure 3.33. Synthetic model: normalized least squares error versus the inversion iteration number (shallow model, 24 receivers and 13 shots).

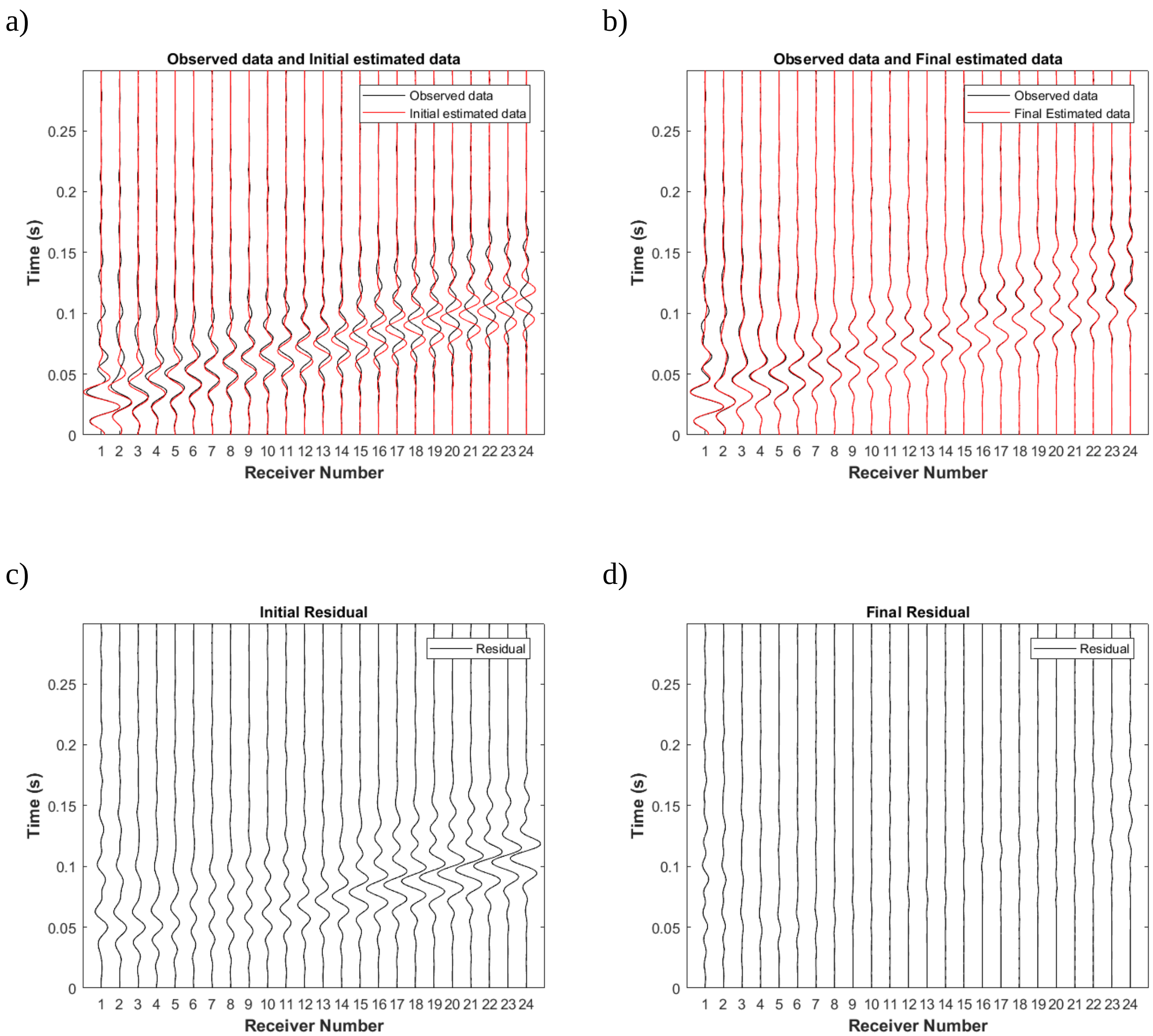

Figure 3.34. Synthetic model (shallow model, 24 receivers and 13 shots): waveform comparison for the first shot: (a) observed data and estimated data associated with the initial model, (b) observed data and estimated data associated with the final inverted model, (c) residual associated with the initial model, and (d) residual associated with final inverted model.

3.3.4 Results for test configuration 3 (12 receivers, 13 shots)

Next, the inversion was conducted on a relatively dense test configuration of 12 receiver and 13 source stations (Figure 3.25) to identify any possible improvement over the previous two test configurations. The inverted density and Vs obtained at iteration #50 are displayed in Figure

3.35. A detailed comparison is presented in Figure 3.36 for distances of 9 m and 13.5 m. It is evident that density and Vs values were not accurately represented after the initial run. This lack of accurate layer characterization is attributed to the limited precision resulting from the coarse configuration of shots and receivers.

The normalized least-squares error for all iterations of the two inversion runs are shown in Figure 3.37. The error reduced from 1.0 at the start of the first iteration to about 0.01 at the end of the analysis (iteration #100). Waveform and residual comparisons are displayed in Figure 3.38.

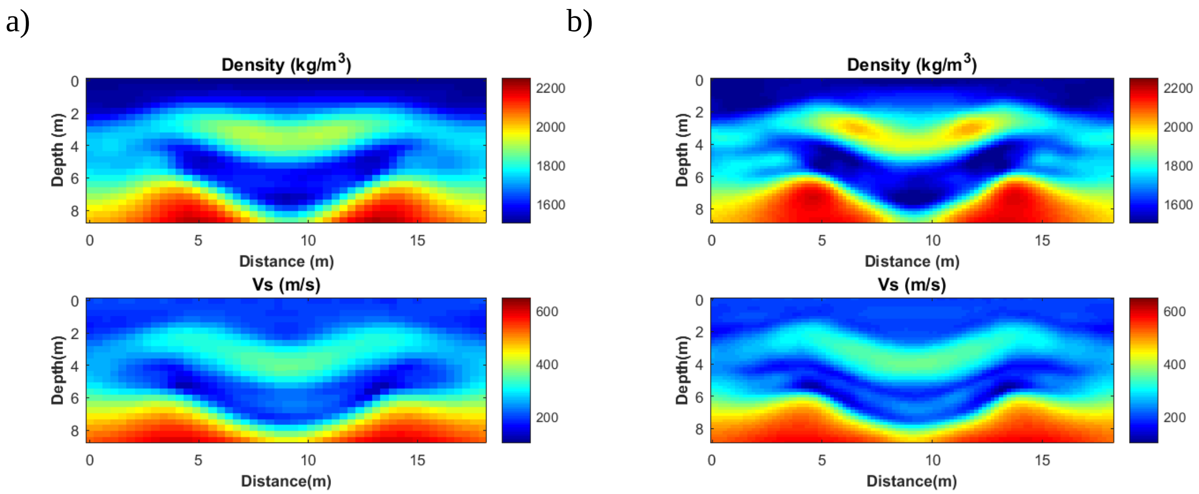

Figure 3.35. Synthetic model of density (kg/m^3) and S-wave velocity (m/s): (a) inverted model at 10-50 Hz and (b) inverted model at 10-80 Hz (shallow model, 12 receivers and 13 shots).

(a) (b) (c) (d)

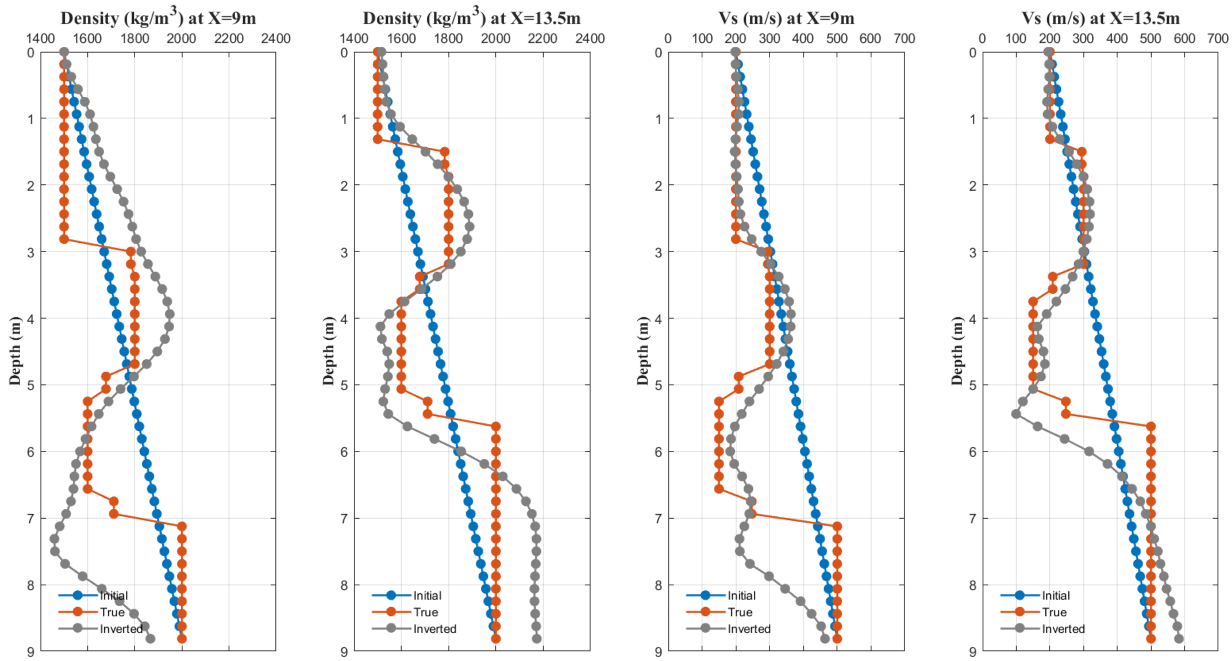

Figure 3.36. Synthetic model (shallow model, 12 receivers and 13 shots): comparison of density at distances of (a) X=9 m and (b) X=13.5 m and S-wave velocity at distances (c) X=9 m and (d) X=13.5 m.

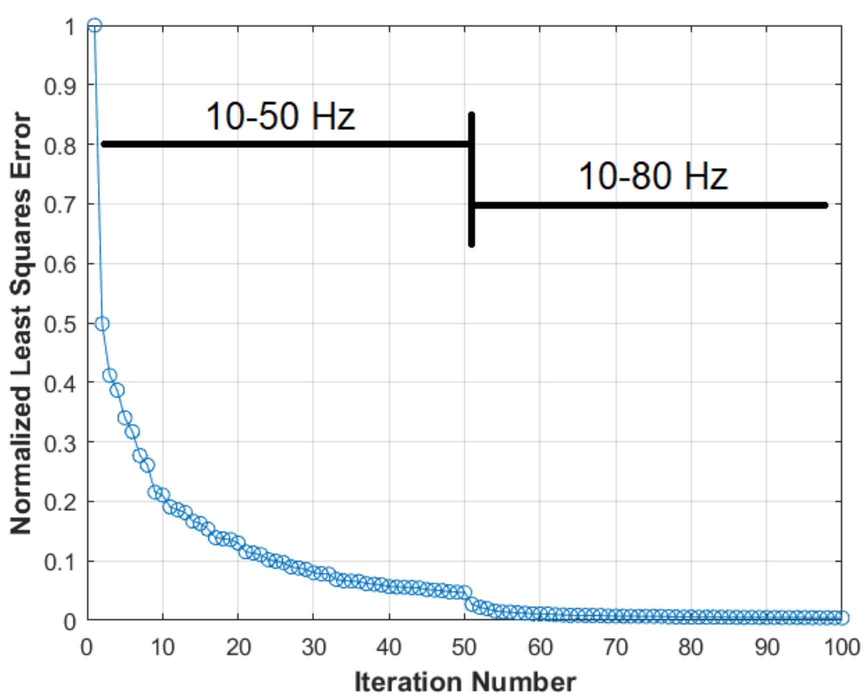

Figure 3.37. Synthetic model: normalized least squares error versus the inversion iteration number (shallow model, 12 receivers and 13 shots).

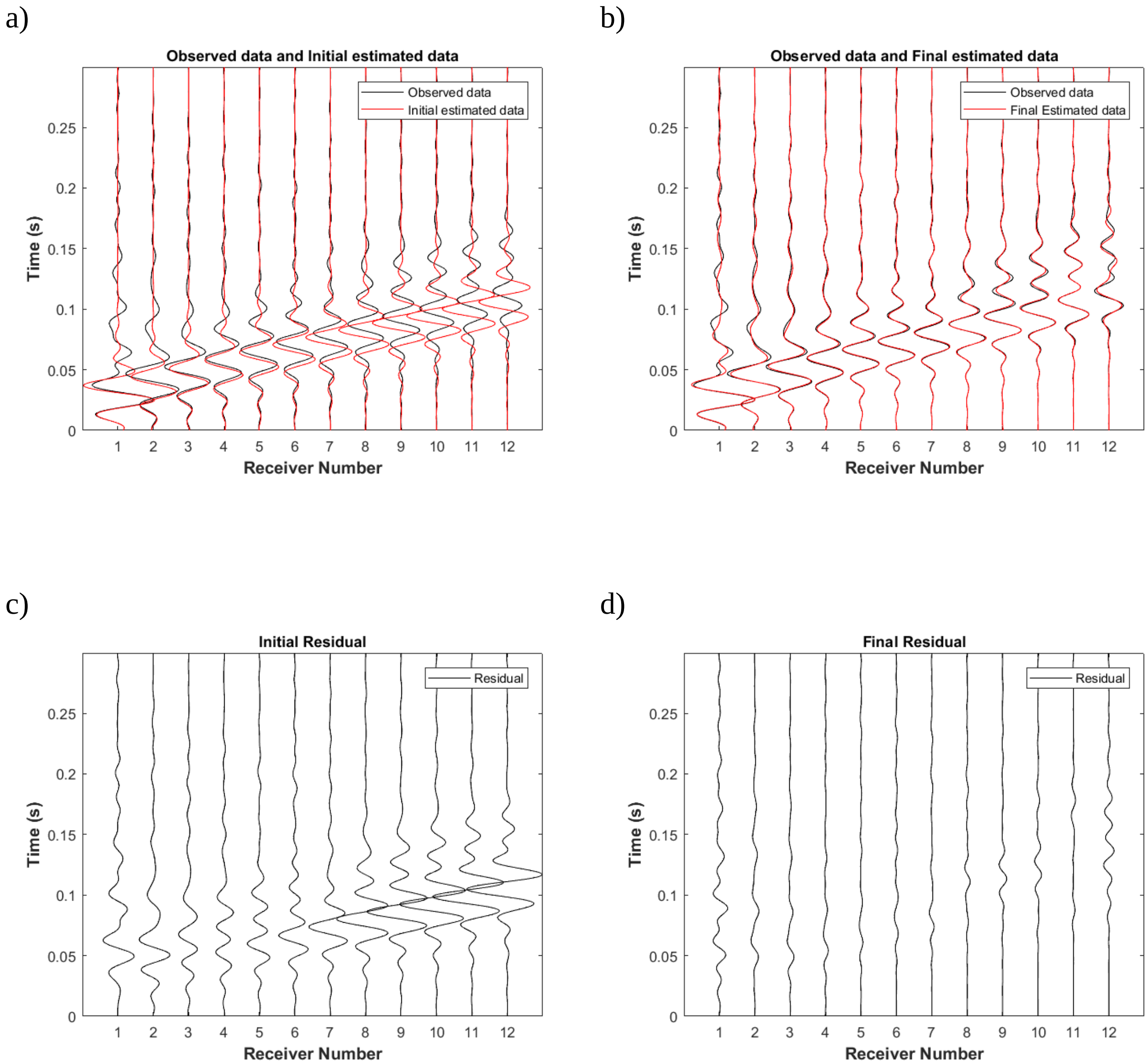

Figure 3.38. Synthetic model (shallow model, 12 receivers and 13 shots): waveform comparison for the first shot: (a) observed data and estimated data associated with the initial model, (b) observed data and estimated data associated with the final inverted model, (c) residual associated with the initial model, and (d) residual associated with final inverted model.

3.3.5 Results for test configuration 4 (12 receivers, 7 shots)

Finally, the inversion was done on the least dense test configuration of 12 receiver and 7 source stations (Figure 3.26). Using the same inversion parameter settings and initial model, the inverted density and Vs obtained at iteration #50 and #100 are displayed in Figure 3.39. It is evident that after the first run, the density and Vs values were not accurately characterized, as shown in Figure 3.39b. A detailed comparison of two profiles at distances of 9 m and 13.5 m is presented in Figure 3.40 for density and Vs.

Normalized least-squares error for all iterations of the two inversion runs are shown in Figure 3.41. The error reduced from 1.0 at the start of the first iteration to less than 0.01 at the end of the analysis (iteration #100). Waveform and residual comparisons are displayed in Figure 3.42.

a) b)

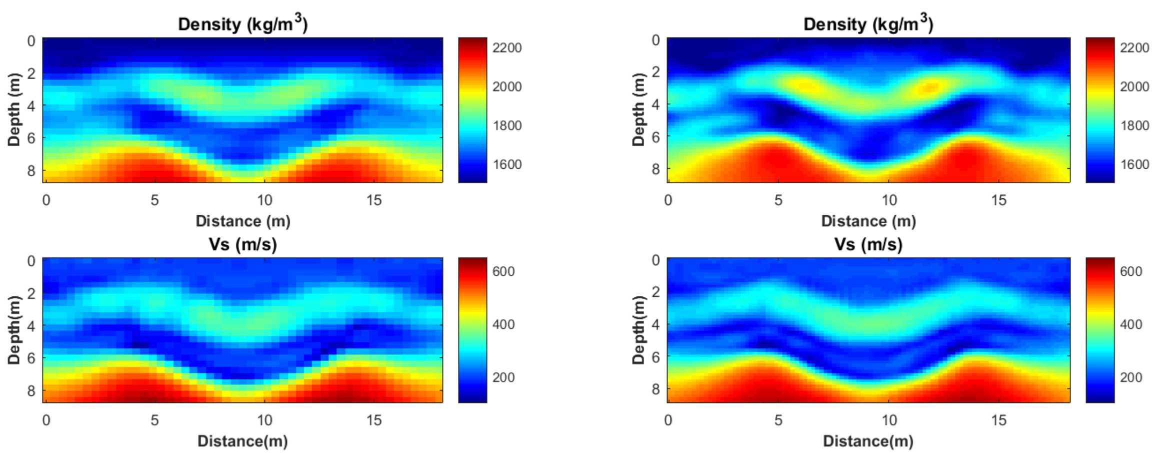

Figure 3.39. Synthetic model of density (kg/m^3) and S-wave velocity (m/s): (a) Inverted model at 10-50 Hz and (b) Inverted model at 10-80 Hz (shallow model, 12 receivers and 7 shots).

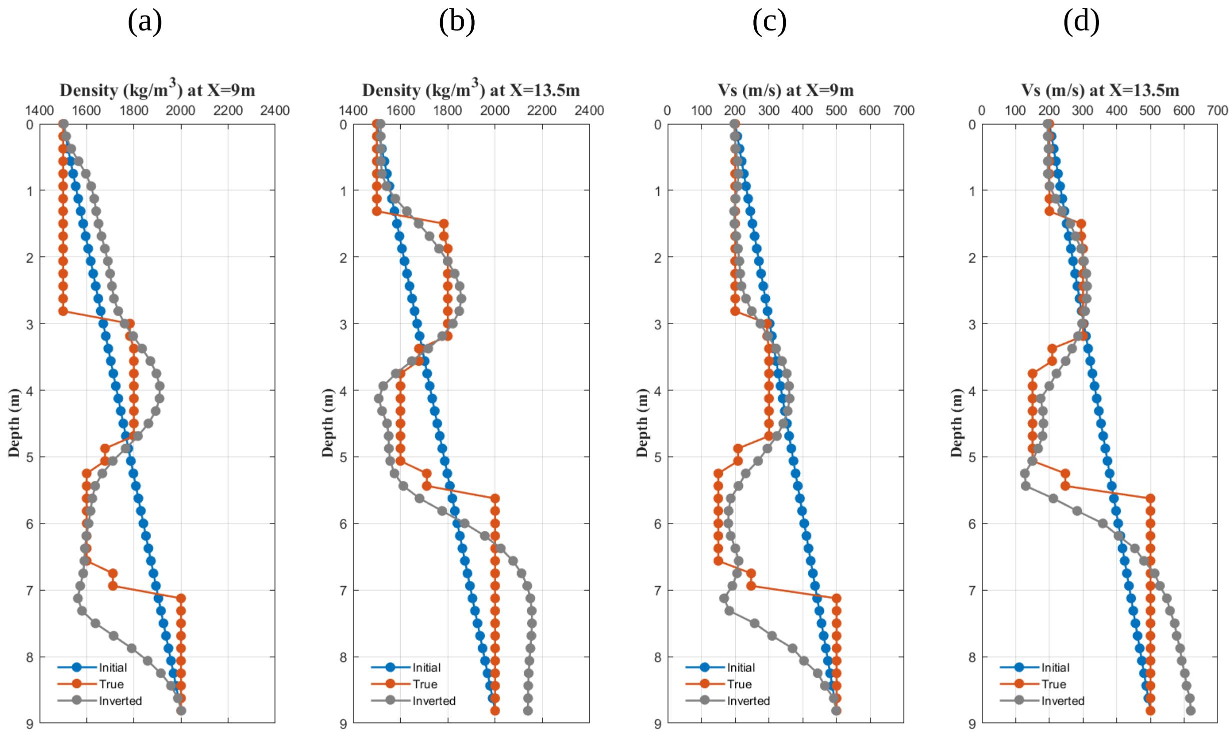

Figure 3.40. Synthetic model (shallow model, 12 receivers and 7 shots): comparison of density at distances of (a) X=9 m and (b) X=13.5 m and S-wave velocity at distances (c) X=9 m and (d) X=13.5 m.

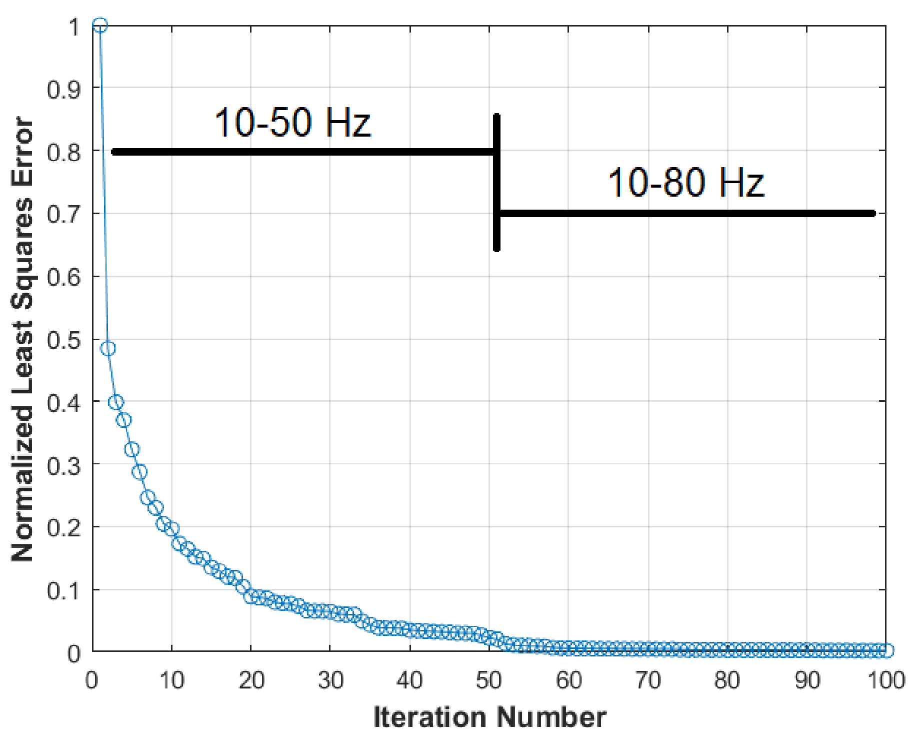

Figure 3.41. Synthetic model: normalized least squares error versus the inversion iteration number (shallow model, 12 receivers and 7 shots).

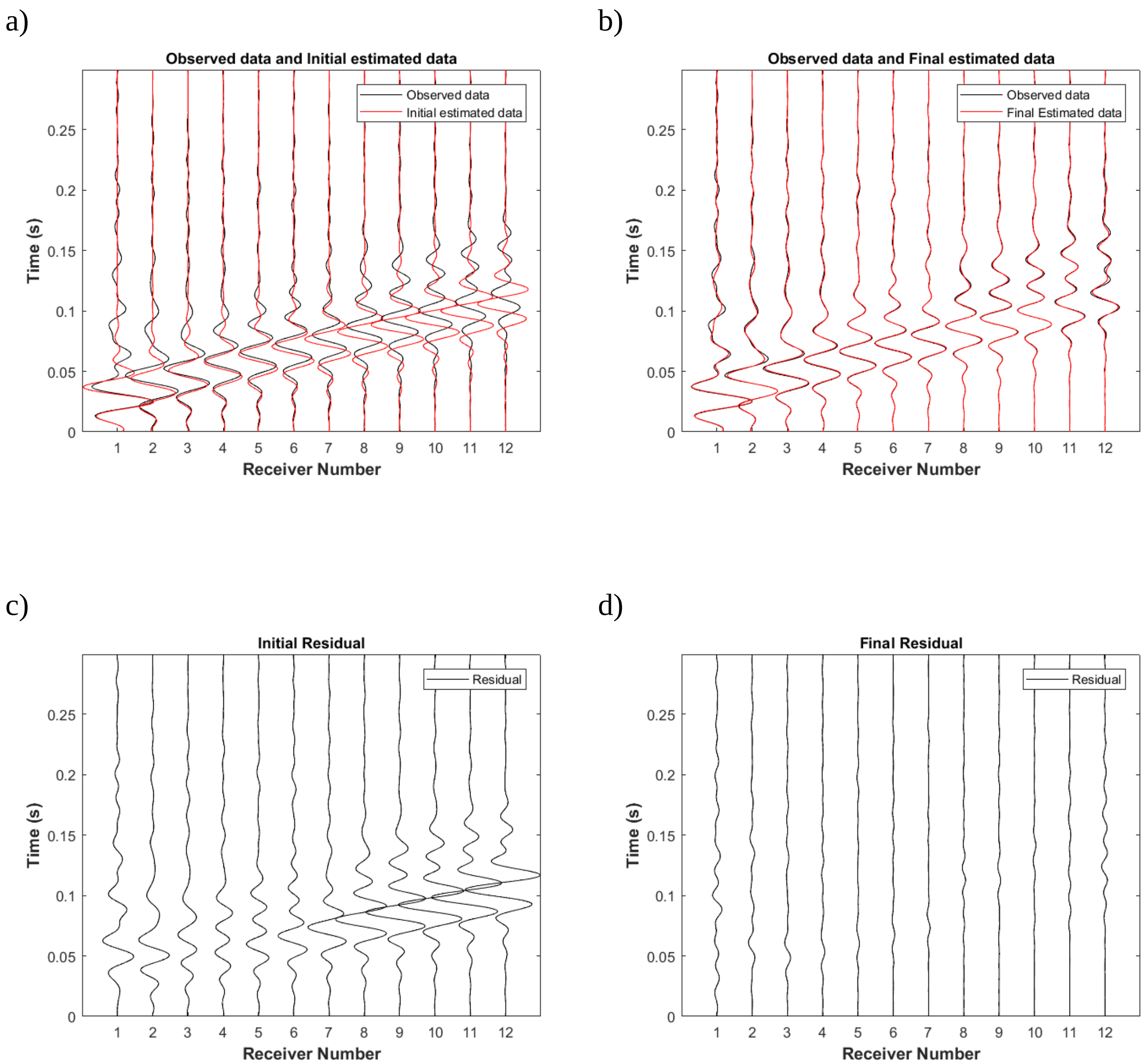

Figure 3.42. Synthetic model (shallow model, 12 receivers and 7 shots): waveform comparison for the first shot: (a) observed data and estimated data associated with the initial model, (b) observed data and estimated data associated with the final inverted model, (c) residual associated with the initial model, and (d) residual associated with final inverted model.

In summary, tested on shallow four-layer model, the algorithm can match the observed and simulated waveforms for all test configurations. From the inverted density and Vs (Figure 3.27, Figure 3.31, Figure 3.35, and Figure 3.39) of the four tests, the increasing of receiver density has improved the accuracy and resolution of the inverted results. Significant discrepancies arise in the density and Vs profiles due to overshooting for test configurations 3 and 4. Based on these findings, it is suggested that a receiver spacing of 0.75 m (2.5 ft) and a shot spacing of one or two receiver spacings (2.5 or 5 ft) (configuration 1 and 2) should be used for field experiments to characterize subsurface layers down to a depth of 30 ft.

3.4 Conclusion

An optimization of test configurations (receiver and shot number and location) has been performed using the SH-Love FWI algorithm developed in Task 1. The goal was to find the minimum number of receivers and shots (maximum spacing) that enabled a successful characterization of variable layers. Several test configurations of receivers and shots placed at 1.5-m to 6-m (5 ft to 20 ft) spacing for three-layer model and at 0.75-m to 3-m (2.5 ft to 10 ft) spacing for challenging four-layer model were analyzed. Accuracy and resolution of inverted density and Vs results were compared between simulations to identify the optimal test configuration.

The analyses were first performed on a deep model of 18-m depth (60 ft). Analyses of all four test configurations (24 receivers and 25 shots, 24 receivers and 13 shots, 12 receivers and 13 shots, 12 receivers and 7 shots) were shown to successfully recover three variable layers. However, there were some discrepancies in both density and Vs due to overshooting in upper layer near the middle of the medium for test configurations 3 and 4. The results suggested that the geophone spacing of 1.5 m (5 ft) and source spacing of 1.5 m or 3 m (5 ft or 10 ft) were the optimal configurations for deep model imaging.

Next, the inversion analyses were performed on a shallow model of 9-m depth (30 ft). The density and Vs results showed that all the receiver and source configurations could produce successful recovery of variable four layers. However, only configurations with geophone spacing of 0.75 m (2.5 ft) and source spacing of 0.75 m or 1.5 m (2.5 ft or 5 ft) were able to accurately recover density and Vs values of four layers. There were discrepancies in both density and Vs because of overshooting if using a larger geophone spacing of 1.5 m (5 ft). The results suggested that geophone spacings of 0.75 m (2.5 ft) and source spacing of 0.75 m or 1.5 m (2.5 ft or 5 ft) were acceptable.

From the results of the analyses performed in this task, the length of geophone array should be at least twice the targeted depth of investigation. For deep characterization up to 60-ft depth, requirements include geophone spacing of 5 ft, source spacing of 5 or 10 ft, and data from 5 to 40 Hz. For shallow characterization up to 30-ft depth, requirements include geophone spacing of 2.5 ft, source spacing of 2.5 or 5 ft, and data from 10 to 80 Hz. It is recommended that the geophone spacing should be from 2 to 5 ft, and the source spacing should be one or twice of the geophone spacing (e.g., striking at every one or two geophones). These optimal test configurations were applied, and proper seismic sources were used to generate seismic data at the required frequencies on field experiments in Task 3 (next chapter).

Chapter 4 – VERIFICATION OF SH-LOVE FWI ALGORITHM WITH FIELD EXPERIMENTS (TASK 3)

4.1 Introduction

The SH- and Love-wave full-waveform inversion (SH-Love FWI) method and its algorithm were developed in Task 1. The method leverages the high sensitivity of SH- and Love-waves to material density and simultaneously provides density and S-wave velocity (Vs) for direct computation of shear modulus, which can be used for foundation design. The optimal test configurations (geophone/source number and spacing) have been identified in Task 2, for characterizing subsurface profiles up to 60 ft. Validation through synthetic modeling has demonstrated the algorithm's capability to resolve complex subsurface profiles of multiple variable layers (Task 2). This task is to validate the algorithm on field experiments.

The field experiments with shear-wave seismic testing and rock coring were conducted at three Florida sites (Bell, CR 250 and Kanapaha). At each site, seismic testing was conducted for multiple test lines up to 120 ft in length, and rock coring samples were collected. Seismic data were analyzed by the algorithm and densities from seismic data were compared to those from rock cores to assess the method's capabilities. The details of experiments and results are documented in the following sections.

4.2 Bell site

The seismic testing was first performed at Bell site (Figure 4.1). The site is located at 301-399 SW 50th Ave in Bell, Florida. As an effort to image subsurface soil or rock at high resolution (submeter pixel), two lines of SH-wave data were collected at high frequencies (10-60 Hz) for the targeted resolution. Details regarding the testing setup, analysis, and results of SH-wave testing are elaborated below.

Figure 4.1. Bell site: test setup with a line of geophones

Two test lines were conducted as shown in Figure 4.2. Line 1 is along the east-west direction, and line 2 is along the north-south direction. The acquisition geometry of each test line (Figure 4.3) includes 25 shots (source impacts) and 24 receivers on the ground surface. Both shots and receiver were uniformly placed at a spacing interval of 1.5 m (5 ft). Seismic wavefields were generated by horizontally striking a sledgehammer on a steel shear-beam (Figure 4.4). A vehicle wheel was on top of the shear-beam to couple it with soil. For each shot, a wavefield was generated by striking one end of the beam and recorded by 24 4.5-Hz horizontal geophones for a recording time of one second with a sampling rate of 0.5 milliseconds.

Figure 4.2. Bell site: two test lines and boring location.

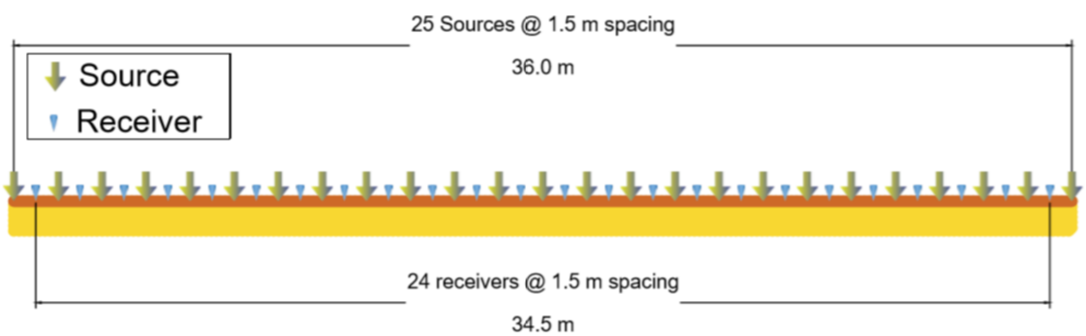

Figure 4.3. Bell site: data acquisition geometry.

Figure 4.4. Bell site: wave excitation by striking sledgehammer to shear-beam pressed by a vehicle-wheel.

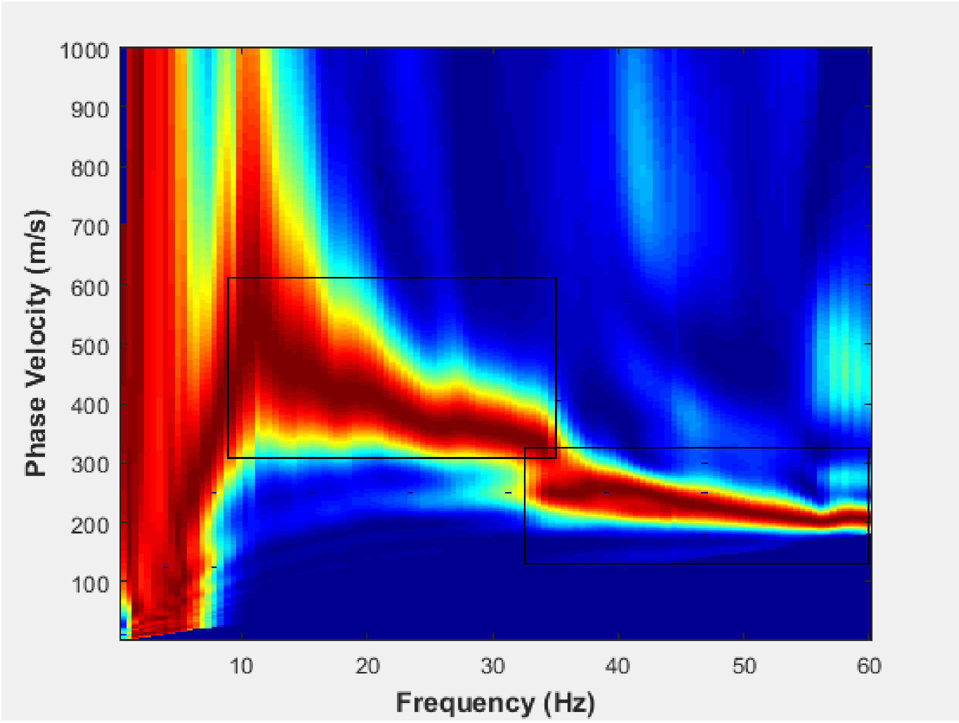

Figure 4.5. Bell site: spectral image of measured data.

An analyzed domain of 36 × 18 m (120 × 60 ft) (length × depth) was used and discretized into a 96 × 48 grid of 0.375 m (1.25 ft) for wave simulation and inversion. This grid spacing was chosen for convenient placement of source and receiver positions on the numerical nodes. The depth of the analyzed domain was selected as half of the testing length for good signal coverage.

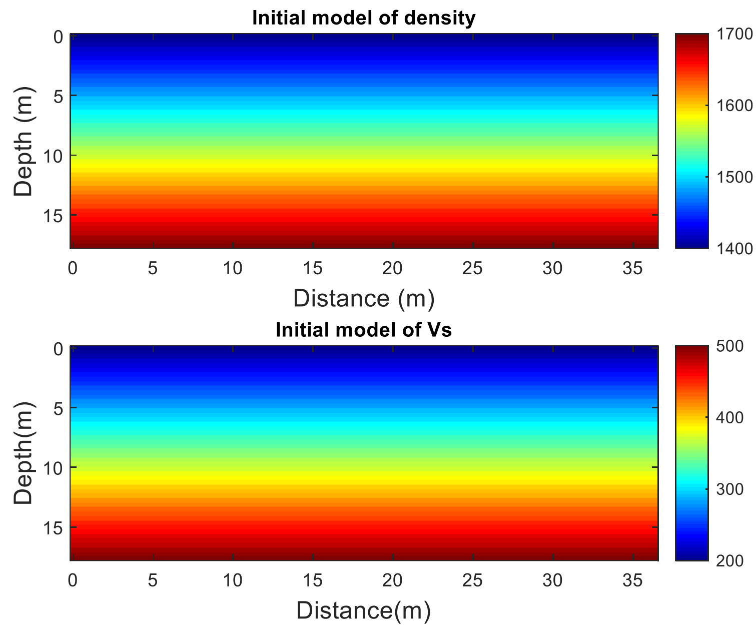

Figure 4.6. Bell site: initial models of density and Vs used for both test lines.

Based on the spectral analysis of surface waves (Figure 4.5), the wave velocity varies from about 200 m/s to 500 m/s at the frequency range of 10 to 60 Hz. Thus, the initial Vs (Figure 4.6, bottom) was estimated from 200 m/s at the ground surface to 500 m/s at the bottom of the model (18 m depth). The initial density (Figure 4.6, top) was taken as the typical value of 1,400 kg/m^3 for shallow soils to 1,700 kg/m^3 for limestone.

For the analysis, the recorded data was filtered through the frequency bandwidth of 10-60 Hz and utilized for one inversion run for each test line. The termination criterion of inversion was determined when the analysis reached a predefined maximum number (40) of iterations, or the least-squares error decreased less than 1% (or increased) for ten iterations. The computation time for each test line was about 25 minutes on a desktop computer (8 cores with 3.70 GHz each, 64GB RAM).

The entire medium was updated cell by cell during the inversion process, and the waveform match improved. Shown in Figure 4.7 are waveform comparisons at the end of the inversion run for line 1 and line 2. It is noted that channels close to the source were removed to reduce the effect of source-receiver coupling on the inversion process. Apparently, the estimated and observed data agrees for most of the channels. The waveform match shows that the choice of the initial velocity was sufficient.

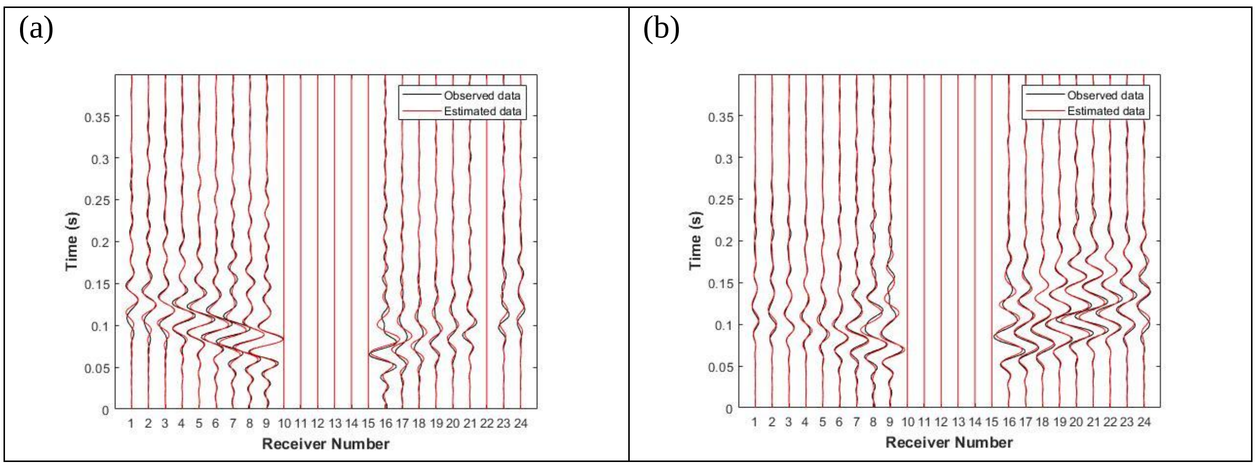

Figure 4.7. Bell site: waveform comparison of observed and estimated data from the final inverted model: (a) line 1 and (b) line 2.

The inverted results are shown in Figure 4.8 for the two test lines. Both results show similar profiles. They consist of four layers: 1) a soft soil layer from the surface to about 1.5 m depth (5 ft) with density of about 1,400 kg/m^3 (87 pcf), 2) a stiff rock layer at 1.5-4.0 m (5 to 13 ft) depth with density of about 1,600 kg/m^3 (100 pcf), 3) another soft soil layer 4-6 m (13 to 20 ft) with density of about 1,400 kg/m^3 (87 pcf), and 4) a limestone layer from about 6 m (20 ft) to the bottom of the model, with the density of about 1,600 kg/m^3 (100 pcf).

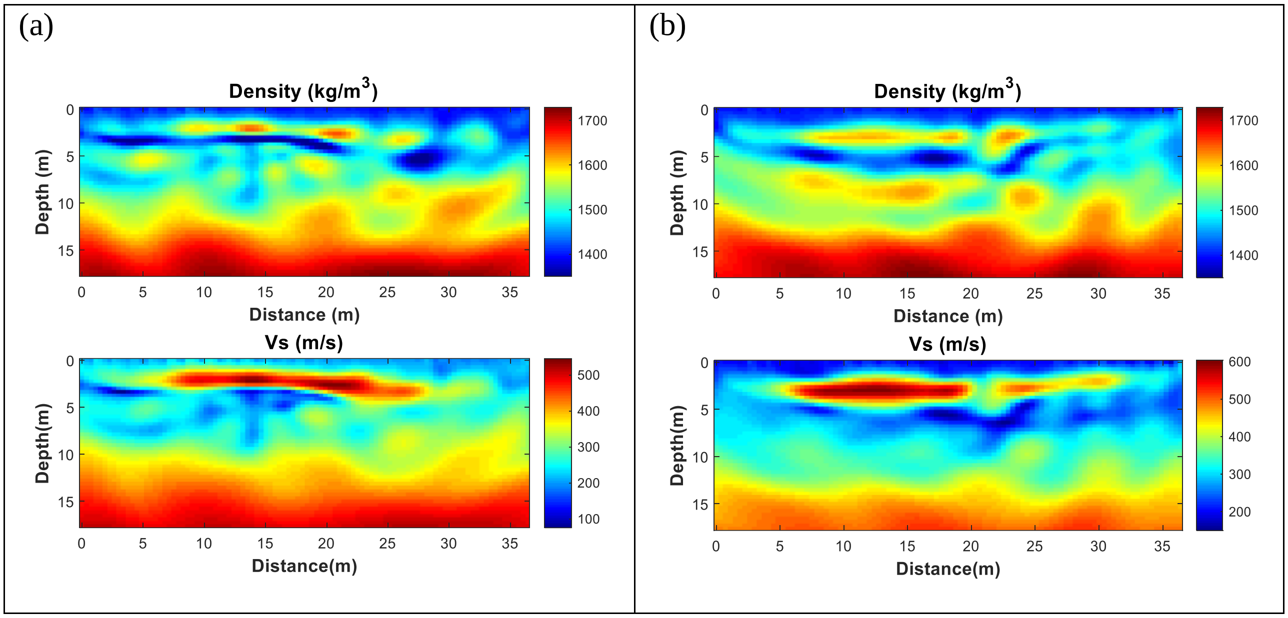

Figure 4.8. Bell site: density and Vs profile for (a) line 1 and (b) line 2

Because both mass density (ρ) and S-wave velocity (Vs) are characterized, shear (G) and Young (E) moduli can be computed by Equations 1 and 2. These moduli can be used for determination of shallow foundation's settlement and bearing capacity and other geotechnical analyses. It is noted that the mass properties (density or unit weight, Young's modulus) are required for both bearing and settlement estimates of a footing. Poisson's ratio can be assumed to be 0.1 as a typical value for Florida limestone or measured from laboratory testing of intact specimens from boring cores.

Shown in Figure 4.9 are the calculated shear modulus (top) and Young's modulus (bottom). For instance, the shear and Young's moduli of line 1 (Figure 4.9a) are calculated from the inverted Vs and density from Figure 4.8a. The variations in the shear and Young's moduli of both lines closely resemble that of Vs and show the existence of four distinct layers.

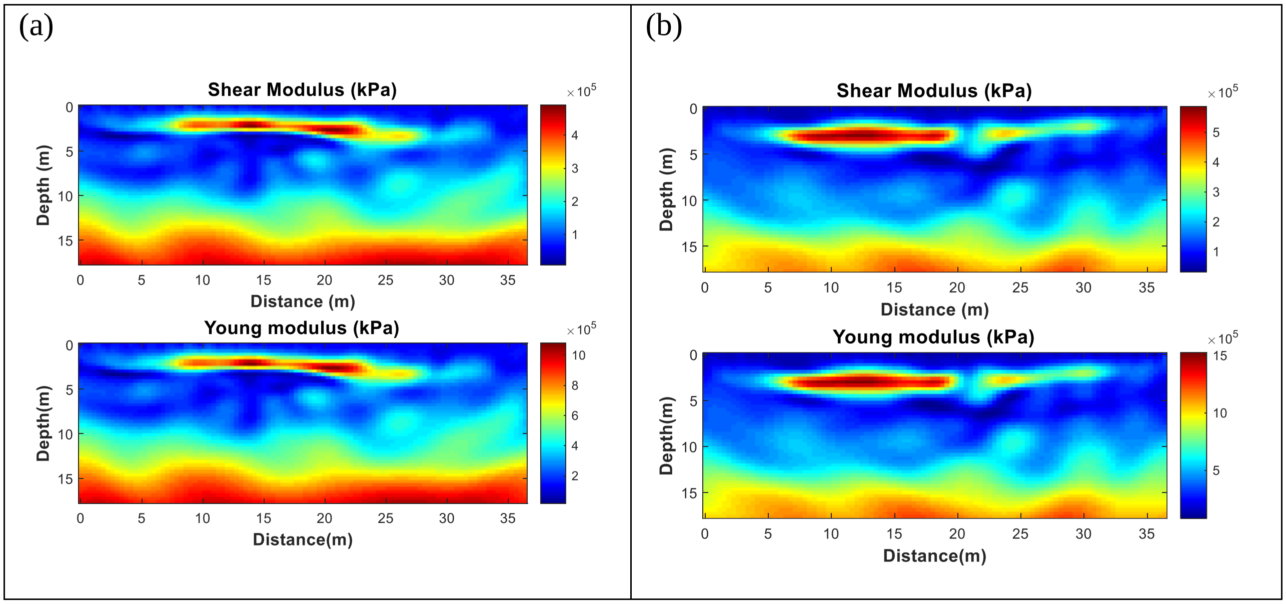

Figure 4.9. Bell site: shear and Young's modulus calculated from inverted results for (a) line 1 and (b) line 2

For verification of the seismic results, rock coring samples were collected at the intersection of the two seismic test lines. Shown in Figure 4.10 are the density profiles at the center of each test line (same coring location) and that of rock coring samples. The density values from seismic testing agree well with those from rock coring samples. Both seismic and rock coring results consist of 1) a stiff rock layer at 2-4 m (6.5-13 ft) depth with density of about 1,600 kg/m^3 (100 pcf), 2) soft soil layer at about 4-6 m (13-20 ft) depth with density of about 1,400 kg/m^3 (87 pcf), and 3) a limestone layer below 6 m (20 ft) depth, with the density of about 1,600 kg/m^3 (100 pcf). It is noted that the density values from the coring samples are more erratic than those of seismic results. This is due to the fact that the seismic results are averaged over larger volumes (1.25 ft pixel) than coring samples. Nevertheless, these results show the proof of concept that the mass density can be obtained from seismic testing with good accuracy.

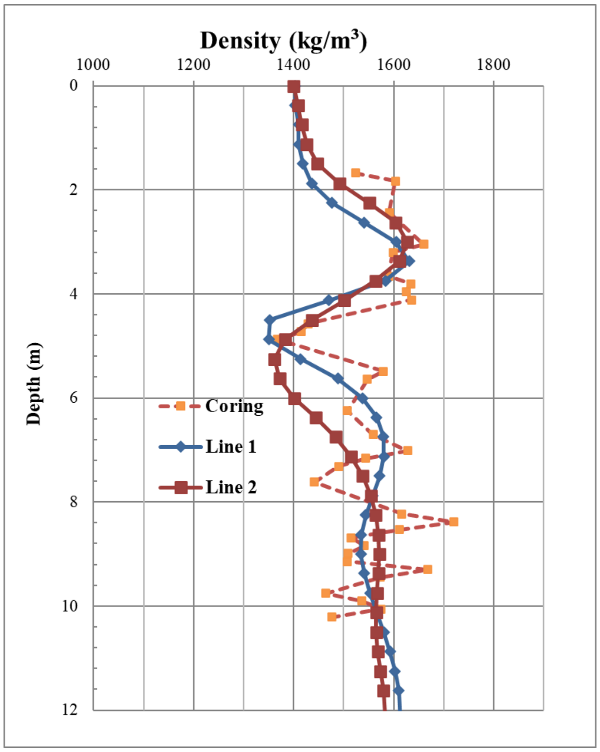

Figure 4.10. Bell site: comparison of density from seismic testing with that of rock coring samples.

4.3 CR 250 site

The second test site is at CR 250 in Suwannee County, and next to Suwannee River. To improve data consistency, a new seismic shear source (Figure 4.11a) was developed in this Task and used for this test site. This system includes a seismic shear box (for generating shear waves), two steel tubes for raising and lowering the box, two air bags that apply downward force for ground coupling, and two coil springs that lift the box once the air bags are deactivated. The shear box is connected to the steel tubes using two 12 mm pins, each covered with 4 mm of rubber to isolate shear wave energy from traveling into the truck frame.

This portable seismic shear device is mounted to the truck via the trailer hitch located at the rear of the vehicle. The shear box (Figure 4.11b) enables control over both the frequency content and energy of the generated wavefields, which depend on the mass of the hammer and the impact speed. The hammer speed is regulated by adjusting the air (nitrogen) flow rate, measured in standard cubic feet per minute (SCFM), through nylon tubes and by tuning the solenoid valve's CV (flow coefficient) value.

a)

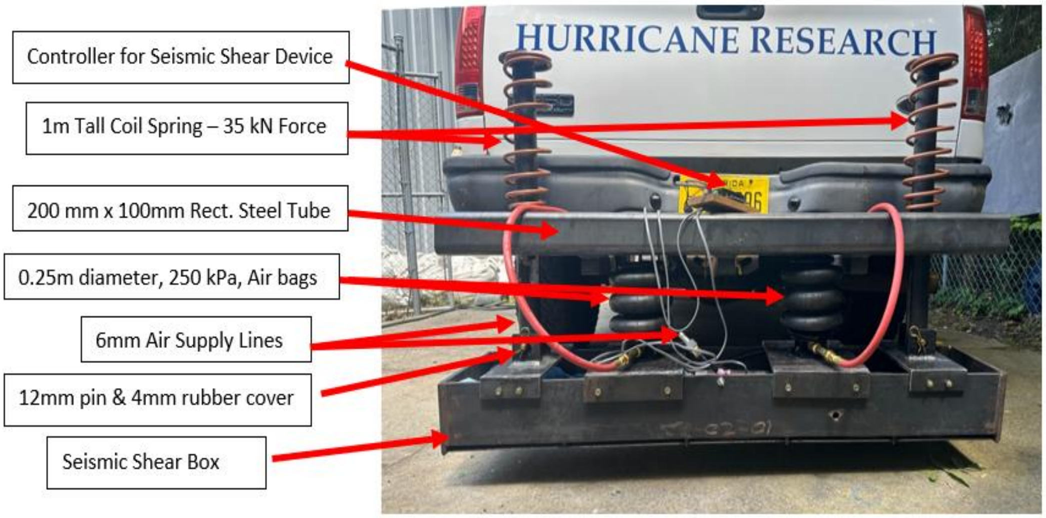

b)

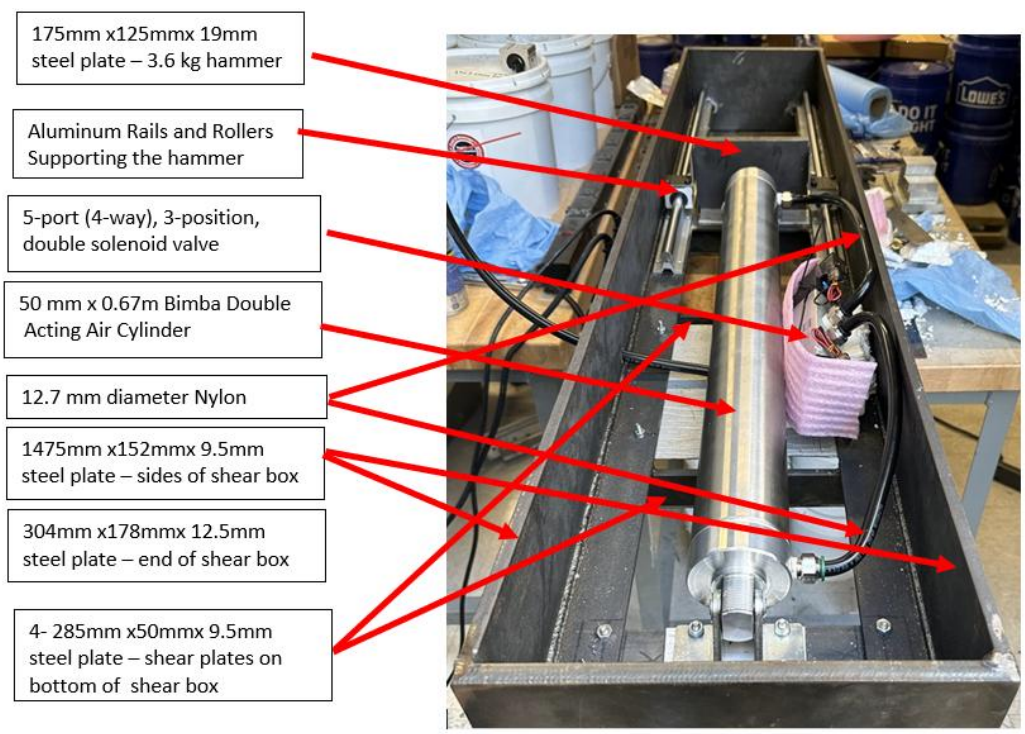

Figure 4.11. (a) New seismic shear source and (b) zoom-in shear box

The source parameters were optimized to generate wavefields in the 10–100 Hz frequency range, with sufficient energy to propagate across the entire 36-meter test length. Seismic wavefields were produced by striking the hammer against one end of the shear box. Consistent wave energy was maintained across all source locations by using the same air pressure and hammer stroke settings.

For data acquisition, two test lines were deployed on the ground (

Figure 4.12a), each with a total length of 28.8 meters (96 ft). They are parallel and 6 meters apart (20 ft). Test configurations for both test lines are presented in

Figure 4.12b. Each test line comprises 13 sources (shots) and 24 geophones, with a source spacing of 2.4 meters (8 ft) and a geophone spacing of 1.2 meters (4 ft). The same wave energy was induced at all source locations (same pressure and hammer stroke). The generated wavefields were recorded by 24 horizontal 4.5 Hz geophones, for a recording duration of one second with a sampling rate of 0.5 milliseconds.

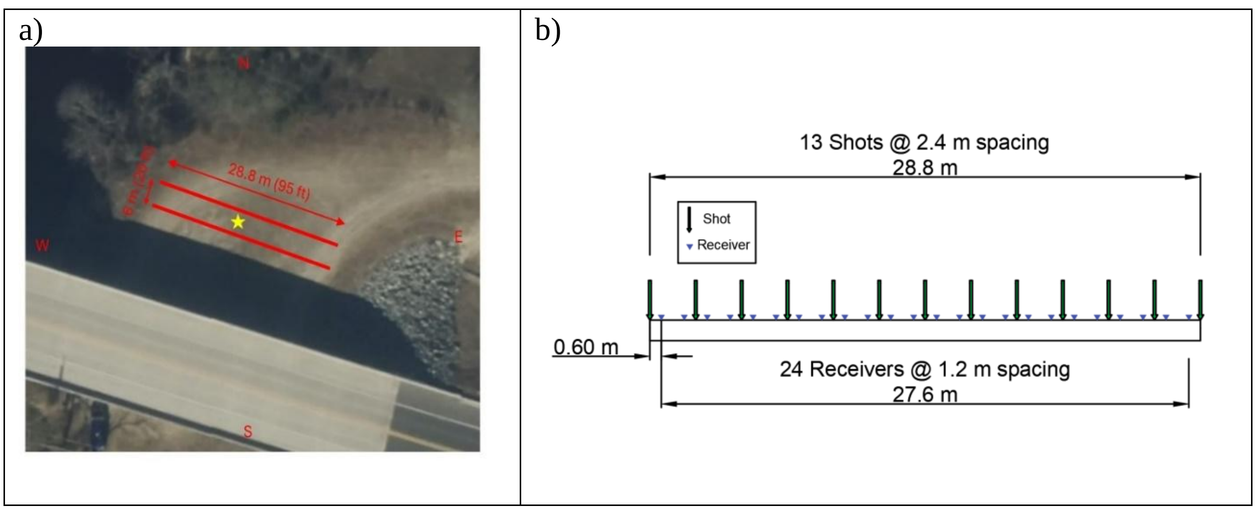

Figure 4.12. CR 250 site: (a) site map with locations of two test lines and coring (yellow star) and (b) acquisition geometry used for both test lines.

The inversion analysis was conducted in the same fashion as discussed in Bell site experiment. The analyzed domain of 28.8 × 18 meters (96 × 60 ft, length × depth) was used and discretized into cells of 0.3 × 0.3 m (1 × 1 ft) for both forward modeling and inversion. The analysis covered a frequency range of 10 to 60 Hz. The initial Vs model was determined through spectral analysis (Figure 4.13a). As shown in Figure 4.13b, wave velocity increases from 200 m/s to 500 m/s within this frequency range. Consequently, the initial Vs model was defined as a gradient model, increasing from 200 m/s at the surface to 500 m/s at the bottom, as illustrated in Figure 4.13b (bottom). The density model (Figure 4.13b, top) ranged from 1,400 kg/m^3 for shallow soils to 1,700 kg/m^3 for deeper limestone.

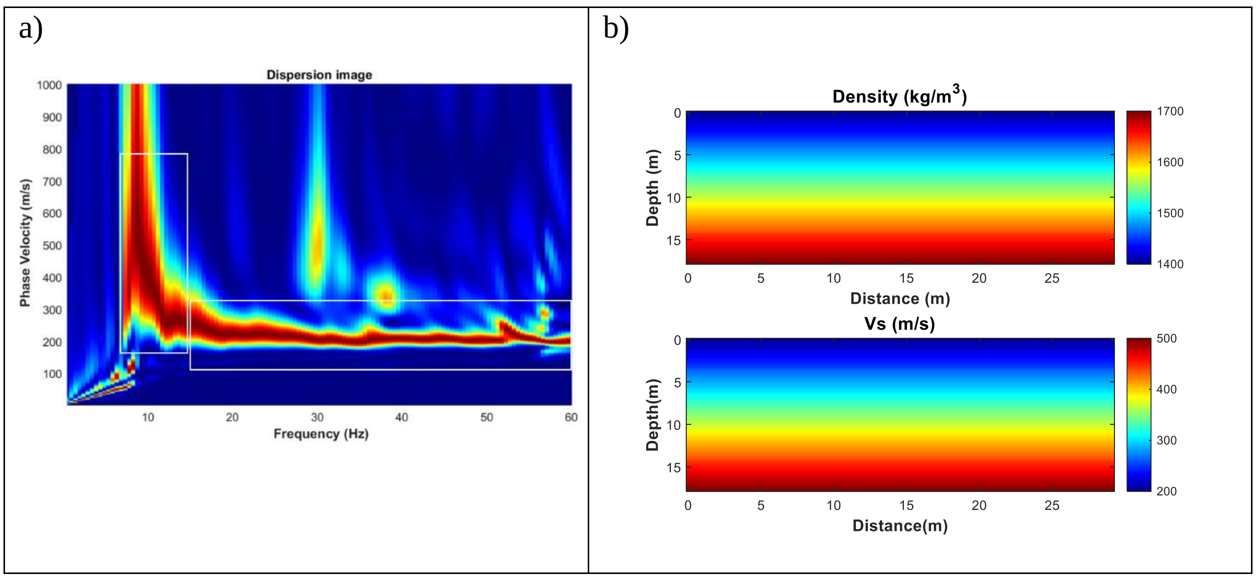

Figure 4.13. CR 250 site: (a) spectral image and (b) initial models of density and Vs used for both test lines.

For analysis, the inversion process was run for about 30 iterations to achieve the predefined convergence criteria. It took approximately 20 minutes for each line. Shown in Figure 4.14 is the comparison of waveform data for the first shot of each line. The final estimated and observed data agree well for all channels, suggesting that the algorithm performed well.

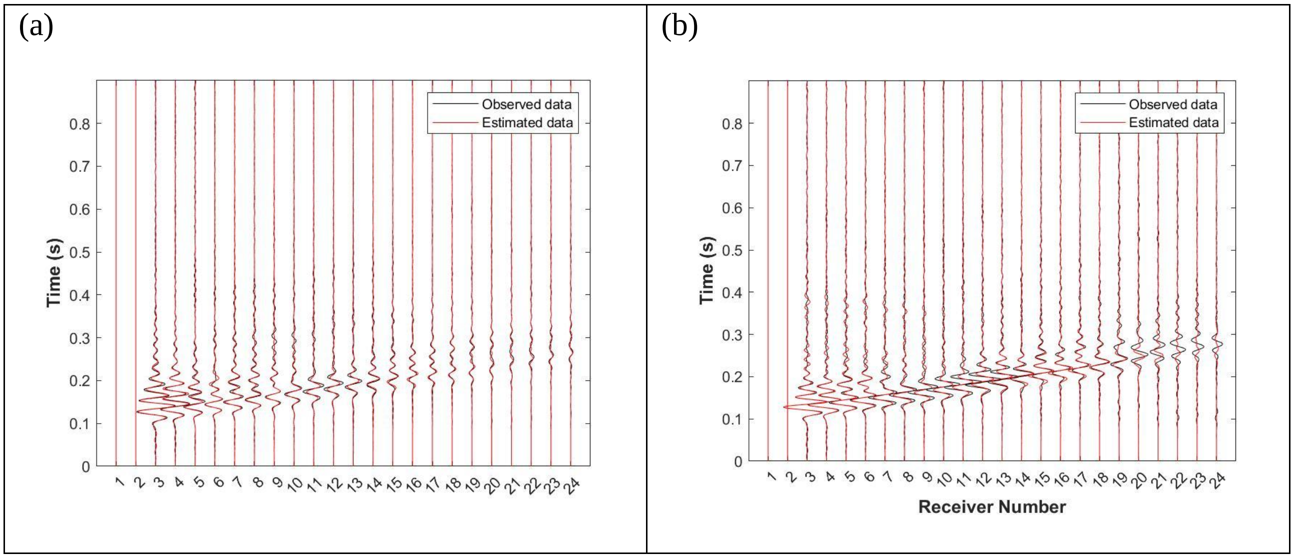

Figure 4.14. CR 250 site: waveform comparison of observed and estimated data from the final inverted model for the first shot: (a) line 1 and (b) line 2.

The inversion results for two lines are presented in Figure 4.15. The results of two lines are similar, consisting of a soil layer from the surface to about 6-m depth (20 ft) with density of approximately 1,400 kg/m³ (87 pcf), and a limestone layer below 6-m depth with density of 1,600 to 1,800 kg/m³ (100 to 112 pcf). Line 2 has softer materials from 6- to 10- m depth than that of line 1. This could be due to the fact that line 2 is closer to the Suwannee River, leading to a more rock weathering process.

The shear modulus and Young's modulus are also calculated and shown in Figure 4.16 for both lines, with Poisson's ratio (μ) assumed to be 0.1. They clearly show three layers of soil, weathered limestone and strong limestone.

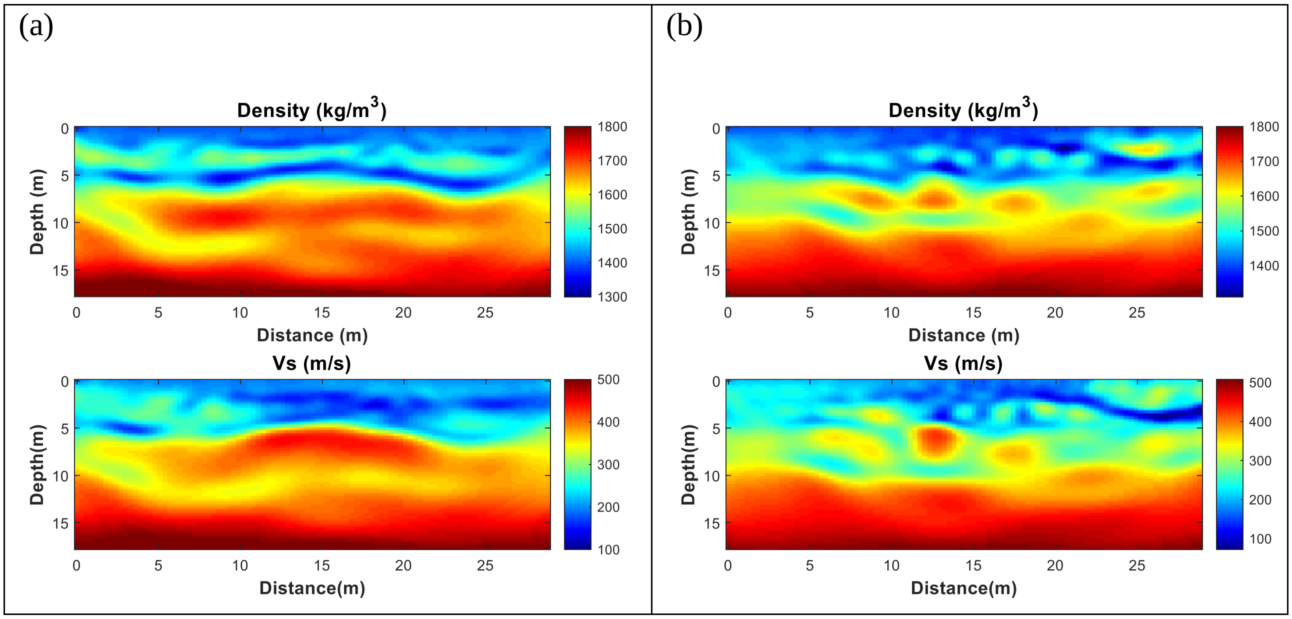

Figure 4.15. CR 250 site: density and Vs profile for (a) line 1 and (b) line 2.

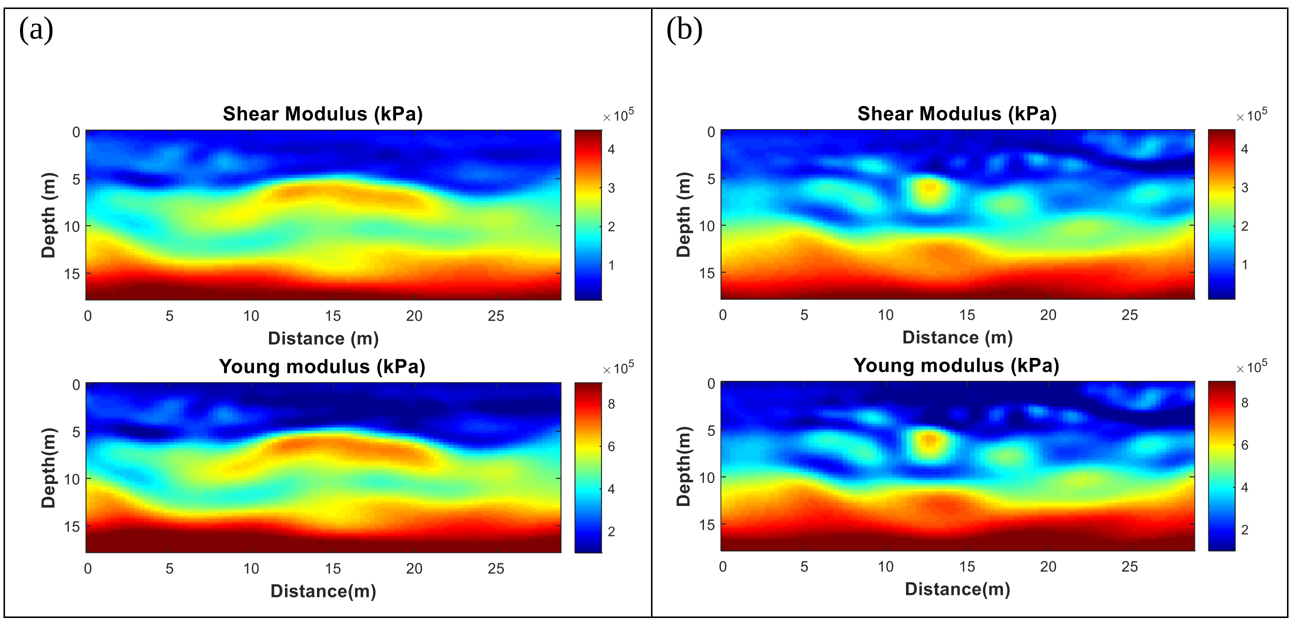

Figure 4.16. CR 250 site: shear and Young's modulus for (a) line 1 and (b) line 2.

To verify the seismic results, rock coring samples were collected for direct measurement of density. The coring location was between the two seismic lines, or 3 meters (10 ft) from each line (yellow star in

Figure 4.12a). Based on the boring log, the site consisted of sandy soils from the ground surface to 6.4-m depth (21 ft), underlain by limestone. It agrees well with the seismic results (Figure 4.15 &Figure 4.16), which showed a soft layer (blue) from the surface to about 6- m depth, underlain by a stiff layer (red). The rock samples were taken at depths from 6.4 m to 16.6 m (21 to 55 ft), and there were no coring samples for shallow soils.

Shown in Figure 4.17 are the density profile from rock samples, together with seismic-derived density profiles at the center of each test line (10 ft away from coring location). The seismic results, particularly test line 2, were consistent with the coring results. Both indicated a weathered limestone layer from 6- to 10- m depth (20 to 33 ft) with density of 1,500 to 1,600 kg/m^3 (94-100 pcf) and a strong limestone layer from 10- to 16.6-m depth (33 to 55 ft) with density of 1,600 to 1,800 kg/m^3 (100 to 112 pcf). The discrepancy between the seismic and coring results were mostly due to 1) coring samples and seismic cells were not at the same locations (10 ft apart), and 2) seismic results were averaged over larger volumes (one-foot pixel) and smoothed by regularization. Nevertheless, the trend of seismic-derived density matches that of the coring samples, demonstrating the accuracy of seismic results.

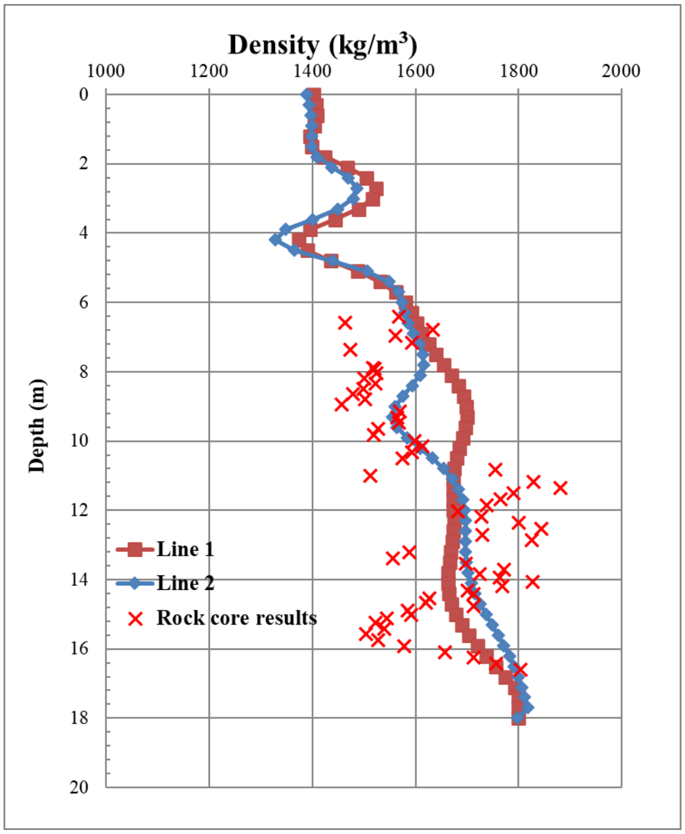

Figure 4.17. CR 250 site: comparison of density from seismic testing with that of rock coring samples. The coring location is 10 ft away from each of the two test lines.

4.4 Kanapaha site

The final field testing was at Kanapaha site (Figure 4.18). For data acquisition, three test lines were deployed on the ground (Figure 4.19), each with a total length of 36 meters (120 ft). Lines 1 and 2 are parallel and 10 ft apart. Line 3 is perpendicular to lines 1 and 2 and intersects with these lines at the middle of each line.

The same test configuration (Figure 4.20) was used for three lines. Each test line comprises 13 sources and 24 geophones, with a source spacing of 3 meters (10 ft) and a geophone spacing of 1.5 meters (5 ft). The new seismic shear source (Figure 4.18) was used to generate consistent wave energy at all source locations (same pressure and hammer stroke). Generated seismic waves were recorded by 24 horizontal 4.5 Hz geophones, for a recording duration of one second with the sampling rate of 0.5 milliseconds.

Figure 4.18. Kanapaha site: field experiment

Figure 4.19. Kanapaha site: locations of three test lines and two borings B21 and B22.

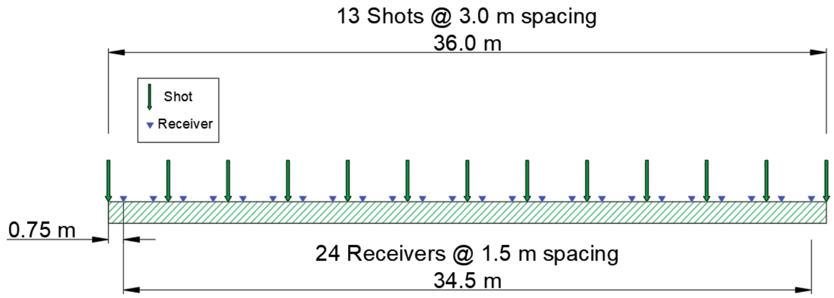

Figure 4.20. Kanapaha site: data acquisition geometry.

The inversion analysis was done the same in previous sites. The analyzed domain of 36 × 18 meters (120 × 60 ft, length × depth) was used and discretized into cells of 0.375 × 0.375 m (1.25 × 1.25 ft) for both forward modeling and inversion. The analysis covered a frequency range of 10 to 60 Hz. The computation time for each test line was about 25 minutes on the same desktop computer (8 cores with 3.70 GHz each, 64GB RAM).

Figure 4.21 illustrates waveform comparisons between the estimated data from forward simulations and the observed data from the field experiment for line 1 (a), line 2 (b), and line 3 (c). For all three test lines, the observed and estimated data agree well, suggesting that the analyses converge to the global solutions.

The inverted results are displayed in Figure 4.22 for all three test lines. The results of the three lines are similar, and consist of 1) a soft soil layer at 0-5 m (0-16.5 ft) depth with density of about 1,400 kg/m^3 (88 pcf), 2) a stiff soil layer mixed with weathered limestone at about 5-13 m (16.5-40 ft) depth with density of about 1,500 kg/m^3 (93.6 pcf), and 3) a limestone layer below 12 m (40 ft) depth with density of over 1,600 kg/m^3 (100 pcf). Shear modulus and Young's modulus are computed via Equations 1 and 2 and shown in Figure 4.23. They reveal 3-layer profiles, resembling the density and Vs profiles.

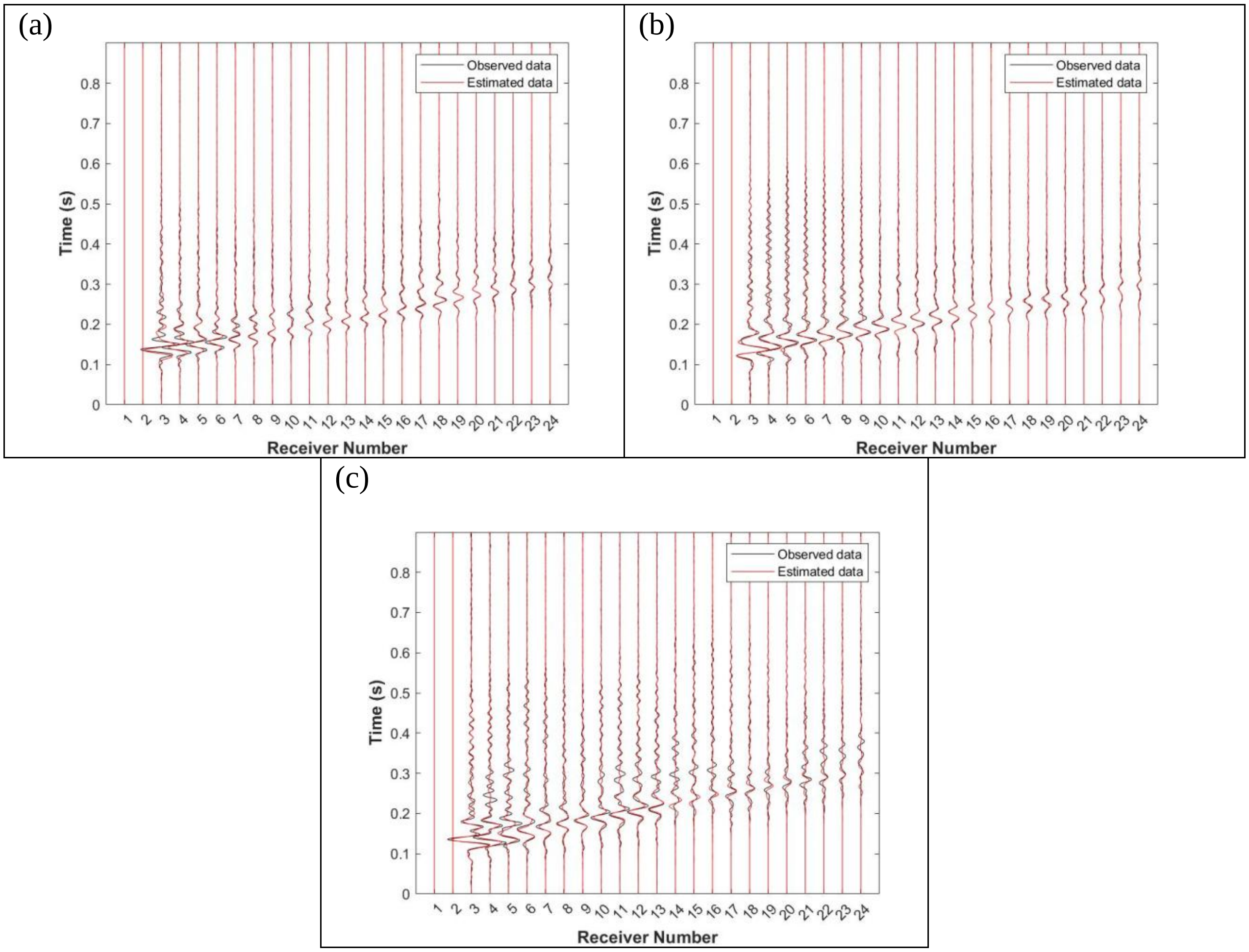

Figure 4.21. Kanapaha site: waveform comparison of observed and estimated data for the first shot: (a) line 1, (b) line 2, and (c) line 3.

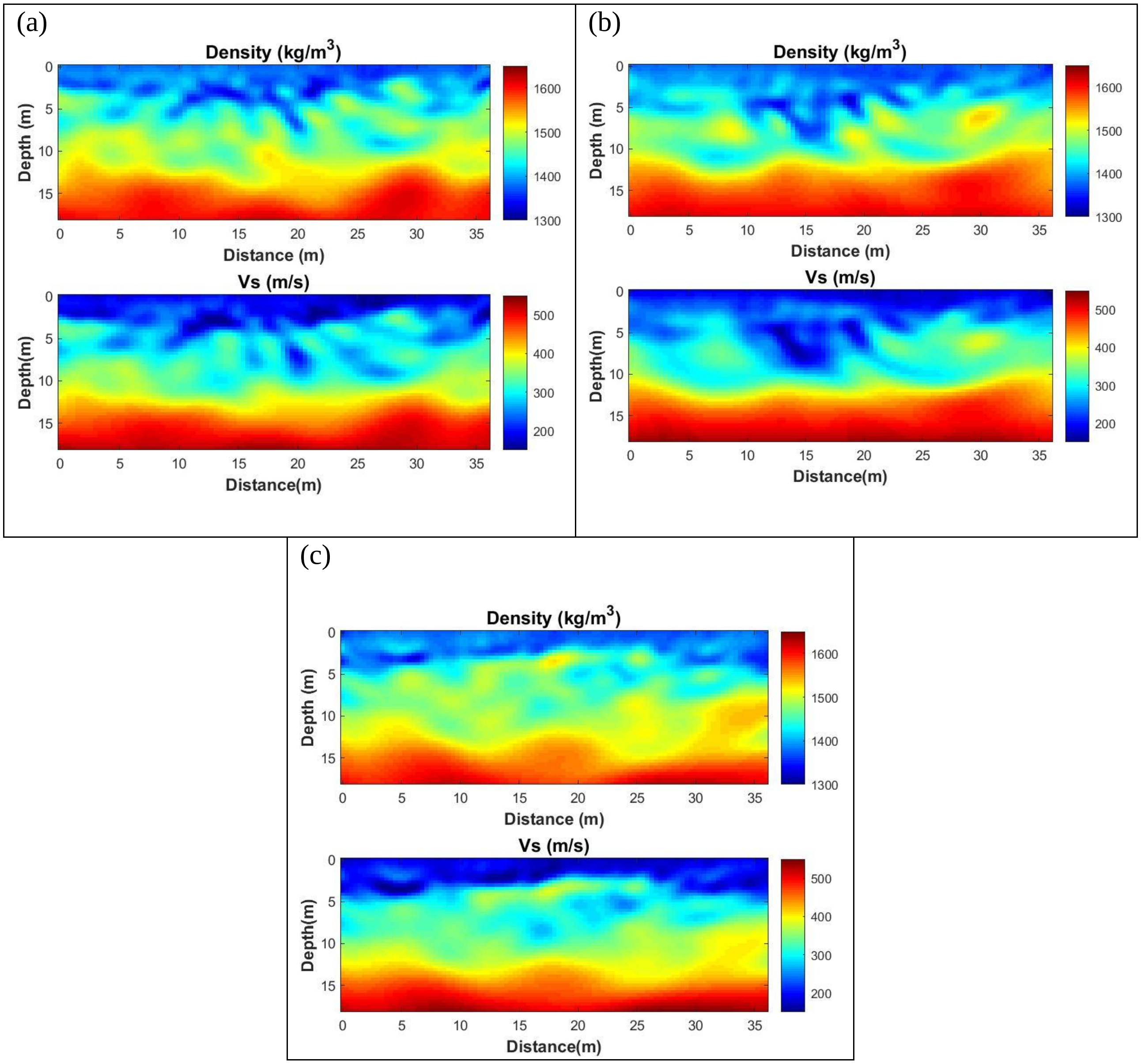

Figure 4.22. Kanapaha site: density and Vs profiles for (a) line 1, (b) line 2, and (c) line 3.

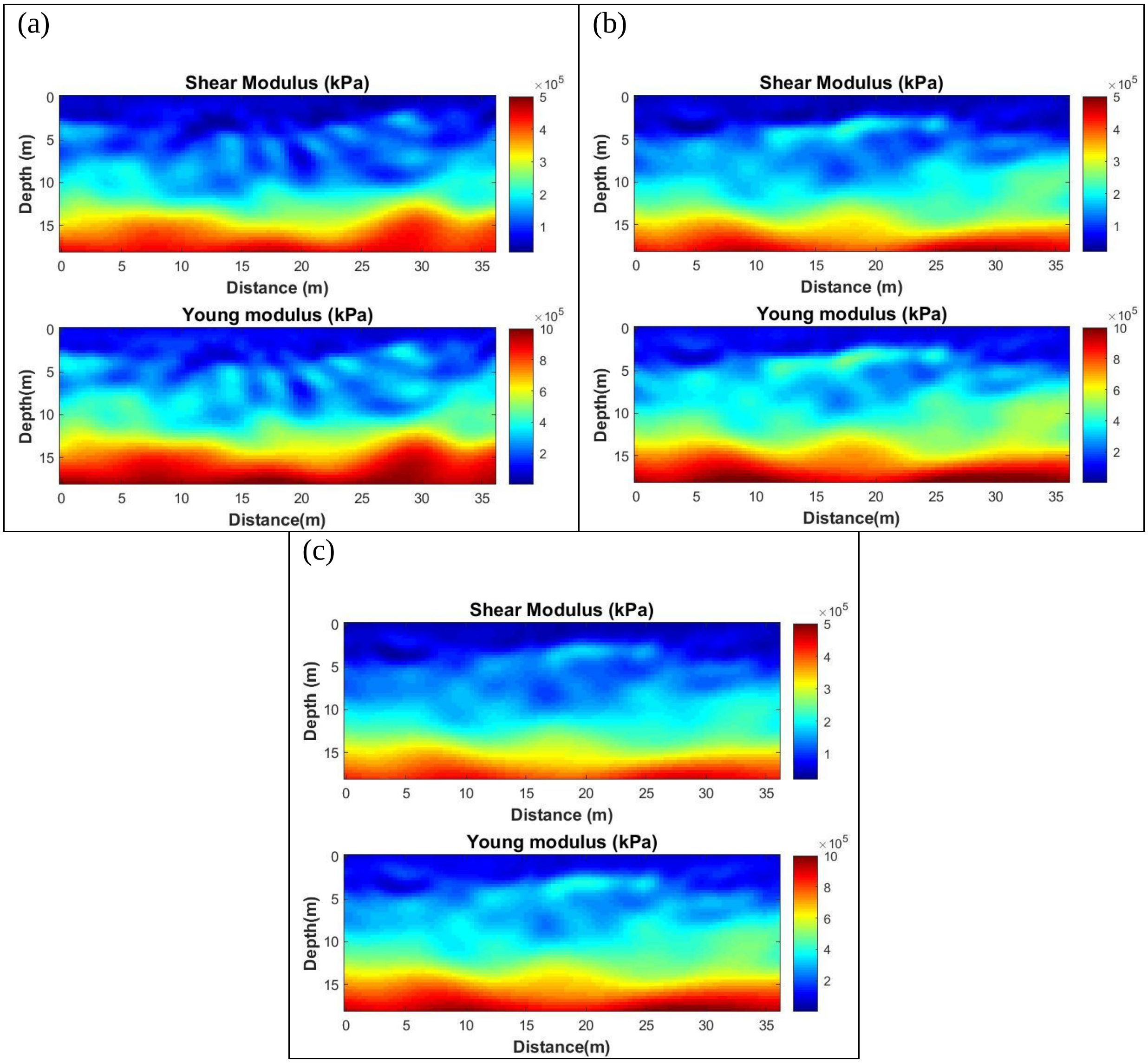

Figure 4.23. Kanapaha site: Shear and Young's modulus calculated from inverted results for (a) line 1, (b) line 2, and (c) line 3.

Based on boring logs, the top of limestone is around 40 ft (12 m) in depth, which agrees well with the seismic results (Figure 4.22). The rock samples were taken below 40 ft depth (12 m), and there were no coring samples for soils above 40 ft depth.

Figure 4.24 compares density profiles from seismic testing and rock cores. As seen in Figure 4.24a, the seismic results at the intersection of lines 1 and 3 are similar, showing consistency of the algorithm. The seismic-derived densities generally agree with those of rock cores, showing average values of about 1,600 kg/m^3 (100 pcf) at both Borings 21 and 22. However, there are discrepancies between the seismic and coring results, because the seismic results are averaged over larger volumes than those of coring samples. Furthermore, the resolution of seismic results is limited at deeper depths (> 40 ft) due to wave attenuation, resulting in smoother variations compared to those from coring samples. Nevertheless, seismic testing is able to characterize complex subsurface profiles of three variable layers and estimate the average density of limestone.

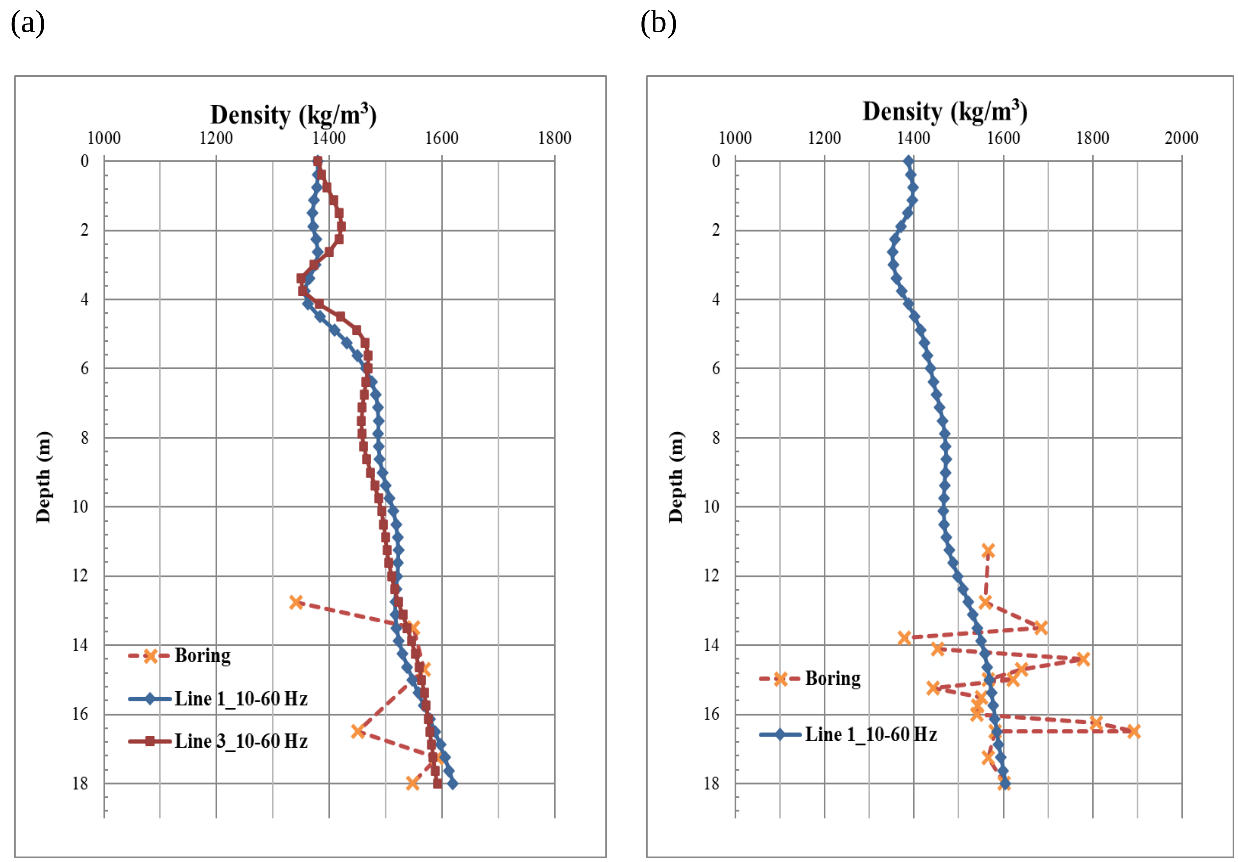

Figure 4.24. Comparison of density from seismic testing with that of rock coring samples, (a) Boring 22 and (b) Boring 21.

Three seismic test lines were conducted at Kanapaha site. Seismic results from the three lines are similar and consistently show three distinct layers (soft and stiff soils, limestone). Soil and rock properties are characterized at submeter pixels to 18 m depth (60 ft). The seismic-derived densities generally agree with those of rock cores, showing an average value of about 1,600 kg/m^3 (100 pcf) for limestone.

4.5 Conclusion

The SH-Love FWI method and its algorithm have been verified in field conditions. Field experiments with seismic testing and rock coring were conducted at three test sites (Bell, CR 250, and Kanapaha) to evaluate the method's capability. The results demonstrate that the seismic SH-Love FWI method effectively characterizes both density and S-wave velocity (Vs) at foot pixels up to 60 ft depth. For Bell site, the seismic results reveal four distinct layers of soil and rock extending from the surface to 60 ft depth, with mass density ranging from 1,400 to 1,600 kg/m^3 (87-100 pcf). For CR 250 site, the results identify three layers of soil, weathered limestone, and strong limestone with progressively increasing densities, ranging from 1,400 to 1,800 kg/m^3 (87-112 pcf). Lastly, for Kanapaha site, the method is able to characterize three subsurface layers (soft soil, stiff soil mixed with weathered limestone, and limestone) and estimate the average density of limestone. The agreement between density values from seismic testing and rock coring samples suggested that the material density could be obtained from the developed SH-Love FWI method with good accuracy.

Finally, all field results presented in this report were obtained within 25 minutes on a standard desktop computer for each test line (120 ft length, 60 ft depth). This suggests that the developed algorithm is computationally practical. It was subsequently implemented into a GUI software package (Task 4) and transferred to FDOT for future uses.

Chapter 5 – DEVELOPMENT OF DATA REDUCTION AND INTERPRETATION MODULE (TASK 4)

5.1 Introduction

Task 4 is to develop Graphical User Interface (GUI) software and user manual for the SH-Love FWI. The effort focuses on creating software that facilitates graphical input, preprocess data, analysis, and output. The GUI is designed for technician-level personnel to operate in the field after basic training, without requiring any programming skills. The software performs the SH-Love FWI analysis developed in Task 1 and generates subsurface profiles of S-wave velocity (Vs) and density, displayed directly on the GUI.

Users graphically input the spacing/number of geophones and sources and raw collected seismic data from computers. Then, users can then condition the input data (i.e., filtering, windowing, removing poor channels) and check the quality of conditioned data before analyzing. After inversion, users can save input parameters, conditioned data, Vs and density profiles, and additional results (e.g., shear modulus, Young's modulus, waveforms comparison, errors, estimated source, and mean-2D-to-1D Vs) for further analysis or sharing via GUI. This report includes a detailed user manual on how to operate the software. A summary of the software development process is provided in the following sections.

5.2 Summary of software development and validation

The GUI aims to enable users to input domains, import data, preprocess and analyze them, obtain subsurface density and S-wave velocity profiles, and save results. To accomplish this, the GUI has been developed using MATLAB, which is the same programming language as the original code developed in Tasks 1 to 3. The GUI's accuracy and robustness were validated by comparing its results with the original code using field data from three test sites (Bell, CR 250, and Kanapaha). The GUI closely generates the original results, confirming its correct implementation and reliability across various site conditions.

5.3 Conclusion

A user-friendly GUI software of the SH-Love FWI analysis has been developed. It was written in MATLAB and compiled to an executable file that can be run on computers without MATLAB. The required computer time is approximately 20-30 minutes for analysis of each test lines (24 geophones), depending on amount of recorded data.

The software allows users to define domains, import and preprocess data, and analyze data to obtain density and S-wave velocity profiles. The software also provides the shear modulus, Young's modulus, waveform comparison, source estimation, error, and mean-2D-to-1D Vs profile. Furthermore, the inversion results and input parameters can be saved and opened in the program, allowing for future analysis and transfer of analysis files. A user manual for the SH-Love FWI software is included in the Appendix.

Chapter 6 – SUMMARY

6.1 General

A novel 2D SH-Love full-waveform inversion (FWI) method has been developed for geotechnical site characterization of soil or rock properties. The method utilizes a time-domain finite-difference scheme for forward wavefield simulation. Moreover, an adjoint-state approach to iteratively invert model parameters (Vs and density) by minimizing the misfit between observed and simulated waveforms. Field experiments at three sites in Florida validated the method, with inverted profiles closely matching rock core sample densities and resolving subsurface structures up to 60 ft depth. A standalone GUI software of the 2D SH-Love FWI analysis has also been developed and transferred to FDOT for future uses. A discussion of each main aspect of this study follows.

6.2 Development of SH-Love FWI algorithm

The 2D SH-Love FWI method and its computing algorithm was developed to accurately characterize soil and rock properties. It includes forward simulation using 2D SH-wave equations and adjoint-state optimization with Tikhonov regularization. The method leverages the sensitivity of SH- and Love-waves to mass density, enabling its estimation directly from wavefields—unlike Rayleigh-wave FWI, which often assumes fixed density values due to limited sensitivity. SH-Love wave simulation is also computationally efficient, requiring only 30% of the time needed for P-SV wave inversion, making it suitable for quick field applications.

The algorithm's accuracy was tested on two synthetic models representing Florida geology: a deep three-layer model (60 ft depth) and a shallow four-layer model (30 ft depth). Both models showed the algorithm's ability to resolve variable layer interfaces, S-wave velocities, and densities with high resolution. Results confirm that 2D SH-Love FWI can accurately characterize complex subsurface profiles.

6.3 Optimization of field test configurations and wavefield characteristics

Parametric studies have been performed to optimize test configurations (source and geophone locations) and wavefield characteristics to minimize efforts on field testing and data analysis. Based on analyzed results, the length of geophone array should be at least twice the targeted depth of investigation. For deep characterization up to 60 ft depth, requirements include geophone spacing of 5 ft, source spacing of 5 or 10 ft, and data from 5 to 40 Hz. For shallow characterization up to 30 ft depth, requirements include geophone spacing of 2.5 ft, source spacing of 2.5 or 5 ft, and data from 10 to 80 Hz. It is recommended that the geophone spacing should be from 2 to 5 ft, and the source spacing should be one or twice of the geophone spacing (e.g., striking at every one or two geophones). These optimal test configurations were applied, and proper seismic sources were used to generate seismic data at the required frequencies on field experiments for verification of the SH-Love FWI method.

6.4 Verification of SH-Love FWI algorithm with field experiments

The SH-Love FWI method and its algorithm have been validated through field experiments at three sites in Florida: Bell, CR 250, and Kanapaha. These experiments consisted of seismic testing and rock coring to assess the method's ability to characterize subsurface density and S--wave velocity (Vs) to depths of up to 60 ft.

At the Bell site, seismic results identified four distinct soil and rock layers with densities ranging from 1,400 to 1,600 kg/m³ (87–100 pcf). At the CR 250 site, three layers—soil, weathered limestone, and strong limestone—were characterized, with densities increasing from 1,400 to

1,800 kg/m³ (87–112 pcf). At CR 250 site, the seismic results revealed three layers of soil, weathered limestone, and strong limestone with progressively increasing densities, ranging from 1,400 to 1,800 kg/m³ (87-112 pcf). At the Kanapaha site, three subsurface layers (soft soil, stiff soil mixed with weathered limestone, and strong limestone) were identified, and the average density of limestone was estimated. The seismic-derived densities agree well with those from rock core samples for all three sites, confirming the accuracy of the SH-Love FWI method.

In addition, with density and S-wave velocity obtained from the SH-Love FWI method, the shear and Young's moduli can be directly computed for analysis of foundation bearing capacity and settlement. The ability to determine rock density, elastic moduli, and variability over large volumes without the need for extensive borings represents a significant advancement in the field of geotechnical engineering. The method offers a powerful tool for engineers, providing detailed and accurate subsurface models that can enhance the design and safety of shallow foundations.

6.5 Development of data reduction and interpretation module

A user-friendly GUI software of the SH-Love FWI analysis has been developed. It was written in MATLAB and compiled to an executable file that can be run on computers without MATLAB. The required computer time is approximately 20-30 minutes for analysis of each test lines (24 geophones), depending on amount of recorded data. The software allows users to define domains, import and preprocess data, and analyze data to obtain density, S-wave velocity, shear and Young's moduli. Input parameters and results can be saved for future use. The software manual is included in the Appendix of this report.

REFERENCES

Aki, K., & Richards, P. G. (1980). *Quantitative Seismology*. W.H. Free-man and Company.

Chen, R., & Tran, K. T. (2021). 2D Gauss-Newton full waveform inversion of SH- and Love-waves in the time domain. *Journal of Applied Geophysics*, *191*, 104363.

Chen, R., Tran, K. T., & Wang, Y. (2021). 2D time-domain full-waveform inversion of SH- and Love-waves for geotechnical site characterization. *Near Surface Geophysics*, *19*(3), 283–295.

Dokter, E., Köhn, D., Wilken, D., De Nil, D., & Rabbel, W. (2017). Full waveform inversion of SH- and Love-wave data in near-surface prospecting. *Geophysical Prospecting*, *65*(S1), 216–236.

Fathi, A., Poursartip, B., & Kallivokas, L. F. (2015). Time-domain hybrid formulations for wave simulations in three-dimensional PML-truncated heterogeneous media. *International Journal for Numerical Methods in Engineering*, *101*(3), 165–198.

Groos, L., Schäfer, M., Forbriger, T., & Bohlen, T. (2017). Application of a complete workflow for 2D elastic full-waveform inversion to recorded shallow-seismic Rayleigh waves. *Geophysics*, *82*(2), R109–R117.

Köhn, D., Wilken, D., De Nil, D., Wunderlich, T., Rabbel, W., Werther, L., Schmidt, J., Zielhofer, C., & Linzen, S. (2019). Comparison of time-domain SH waveform inversion strategies based on sequential low and bandpass filtered data for improved resolution in near-surface prospecting. *Journal of Applied Geophysics*, *160*, 69–83.

Komatitsch, D., & Martin, R. (2007). An unsplit convolutional perfectly matched layer improved at grazing incidence for the seismic wave equation. *Geophysics*, *72*(5), SM155–SM167.

Levander, A. R. (1988). Fourth-order finite-difference *P-SV* seismograms. *Geophysics*, *53*(11), 1425–1436.

McVay, M., Song, X., Wasman, S., Nguyen, T., & Wang, K. (2019). Strength Envelopes for Florida Rock and Intermediate Geomaterials. *Florida. Department of Transportation*.

Mirzanejad, M., Tran, K. T., McVay, M., Horhota, D., & Wasman, S. J. (2020). Sinkhole detection with 3D full seismic waveform tomography. *Geophysics*, *85*(5), B169–B179.

Mirzanejad, M., Tran, K. T., McVay, M., Horhota, D., & Wasman, S. J. (2021). Deep void detection with 3D full waveform inversion of surface-based and in-depth source seismic wavefields. *Engineering Geology*, *294*, 106407.

Nguyen, T., McVay, M., Song, X., Herrera, R., Wasman, S., & Wang, K. (2019). Strength Envelopes of Florida Carbonate Rocks near Ground Surface. *Journal of Geotechnical and Geoenvironmental Engineering*, *145*(8), 04019034.

Nguyen, & Tran, K. T. (2018). Site characterization with 3D elastic full-waveform tomography. *Geophysics*, *83*(5), R389–R400.

Nocedal, J., & Wright, S. J. (2006). *Numerical optimization* (2nd ed). Springer.

Pan, Y., Gao, L., & Bohlen, T. (2018). Time-domain full-waveform inversion of Rayleigh and Love waves in presence of free-surface topography. *Journal of Applied Geophysics*, *152*, 77–85.

Pan, Y., Xia, J., Xu, Y., Gao, L., & Xu, Z. (2016). Love-wave waveform inversion in time domain for shallow shear-wave velocity. *Geophysics*, *81*(1), R1–R14.

Plessix, R.-E. (2006). A review of the adjoint-state method for computing the gradient of a functional with geophysical applications. *Geophysical Journal International*, *167*(2), 495–503.

Smith, J. A., Borisov, D., Cudney, H., Miller, R. D., Modrak, R., Moran, M., Peterie, S. L., Sloan, S. D., Tromp, J., & Wang, Y. (2019). Tunnel detection at Yuma Proving Ground, Arizona, USA — Part 2: 3D full-waveform inversion experiments. *Geophysics*, *84*(1), B107–B120.

Tikhonov, A. N., & Arsenin, V. Y. (1977). *Solutions of Ill-Posed Problems*. Washington, D.C.: John Wiley & Sons, New York.

Tran, K. T., McVay, M., Faraone, M., & Horhota, D. (2013). Sinkhole detection using 2D full seismic waveform tomography. *Geophysics*, *78*(5), R175–R183.

Tran, K. T., Mirzanejad, M., McVay, M., & Horhota, D. (2019). 3-D time-domain Gauss–Newton full waveform inversion for near-surface site characterization. *Geophysical Journal International*, *217*(1), 206–218.

Tran, K. T., Nguyen, T. D., Dennis R. Hiltunen, Stokoe, K., & Menq, F. (2020). 3D full-waveform inversion in time-frequency domain: Field data application. *Journal of Applied Geophysics*, *178*, 104078.

Tran, K. T., & Sperry, J. (2018). Application of 2D full-waveform tomography on land-streamer data for assessment of roadway subsidence. *Geophysics*, *83*(3), EN1–EN11.

Virieux, J. (1984). *SH* -wave propagation in heterogeneous media: Velocity-stress finite-difference method. *Geophysics*, *49*(11), 1933–1942.

Virieux, J., & Operto, S. (2009). An overview of full-waveform inversion in exploration geophysics. *Geophysics*, *74*(6), WCC1–WCC26.

Wittkamp, F., Athanasopoulos, N., & Bohlen, T. (2019). Individual and joint 2-D elastic full-waveform inversion of Rayleigh and Love waves. *Geophysical Journal International*, *216*(1), 350–364.

Zhang, Z., Huang, L., & Lin, Y. (2012). Double-Difference Elastic-Waveform Inversion with Weighted Gradients for Monitoring EGS Reservoirs. *In Thirty-Seventh Workshop on Geothermal Reservoir Engineering. California: Stanford University*.

Appendix: Software Manual

1. Introduction

Welcome to the SH-Love full-waveform inversion (FWI) software. This tool analyzes SH- and Love-waves to determine 2D subsurface profiles of S-wave velocity, density, shear modulus, and Young's modulus. Its main applications are for characterization of soil or rock properties and imaging of buried anomalies (voids, soft soils). Key features include:

- Modifiable parameters
- Simple data import and processing
- Analysis and exporting results

The SH-Love FWI process involves six required steps:

1. Geometry (Step 1)
2. Input Data (Step 2)
3. Preprocessing (Step 3)
4. Spectral Analysis (Step 4)
5. Initial Model (Step 5)
6. Inversion (Step 6)

2. Input parameters

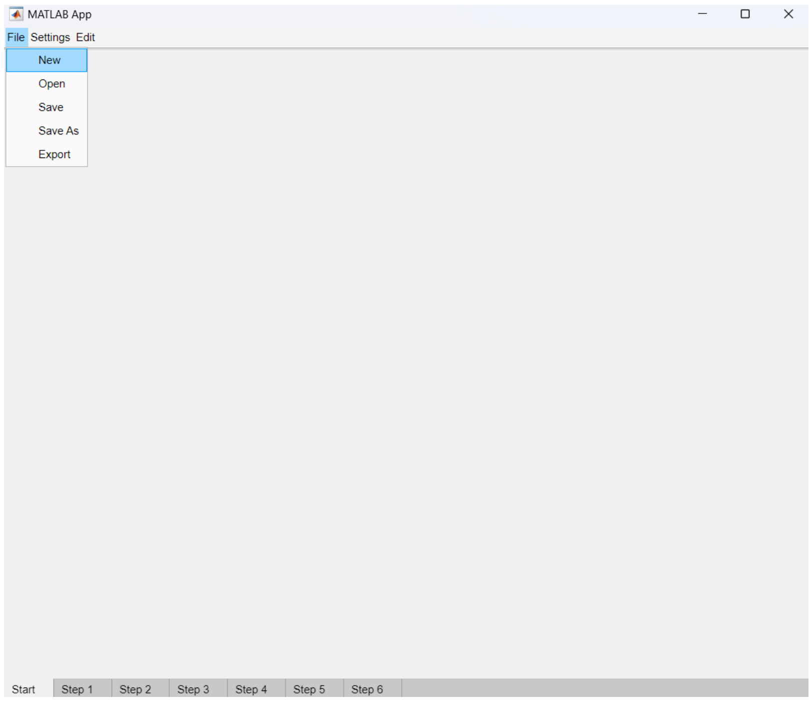

Figure 1. Start page

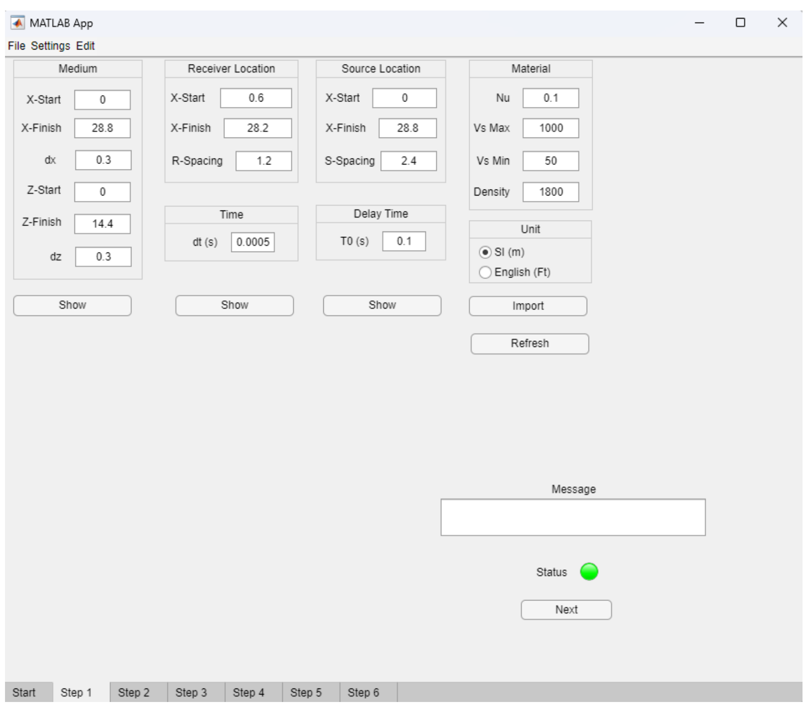

Figure 2. Geometry page

Table 1. Geometry setting

Medium		
X/Z-Start	-	Starting location of the analyzed domain [m, ft]
X/Z-Finish	-	Ending location of the analyzed domain [m, ft]
dx/dz	-	Spacing of grid points in x/z direction [m, ft]
Receiver Location		
X -Start	-	Physical start location of receivers [m, ft]
X -Finish	-	Physical end location of receivers [m, ft]
R-Spacing	-	Spacing between receivers [m, ft]
Source Location		
X -Start	-	Physical start location of shots [m, ft]
X -Finish	-	Physical end location of shots [m, ft m]
S-Spacing	-	Spacing between sources [m, ft]
Material		
Nu	-	Poisson ratio of material
Vs Max	-	Maximum shear wave velocity of material [m/s, ft/s]
Vs Min	-	Minimum shear wave velocity of material [m/s, ft/s]
Density	-	Density of the medium [kg/m^3, pcf]
Time		
T0	-	Delay Time [s]
dt	-	Time interval or sampling rate [s]
Unit		
SI	-	m
English	-	ft

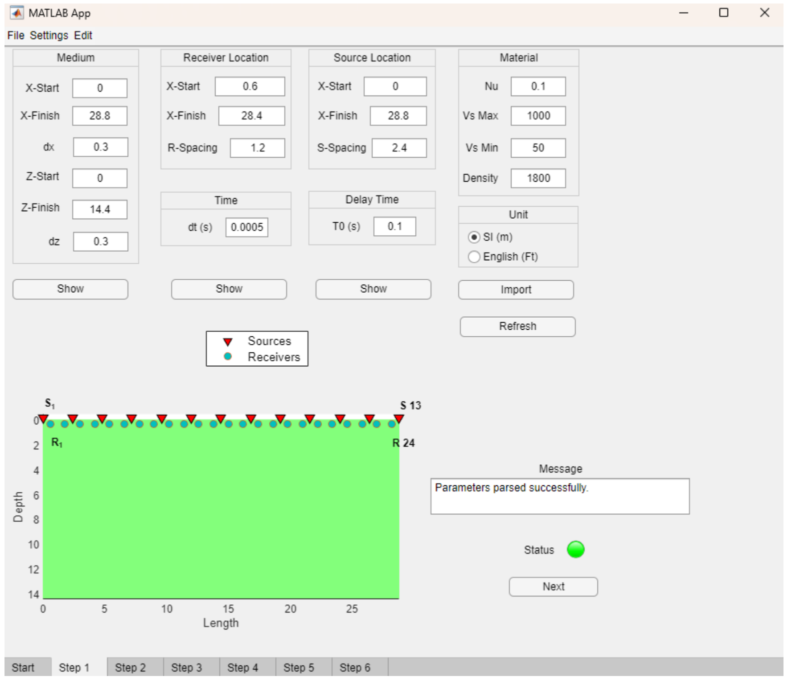

Figure 3. Import geometry parameters.

3. Input data

Step 2 of the SH-Love FWI process is to input data. For this purpose, choose either:

1. Settings > Input Data.
2. Click the “Next” button in the “Step 1” tab.
3. Click the “Step 2” at the bottom of the app.

To import raw data from a file recorded in the field, click the “**Open**” button in the upper left, then select the path that contains the file (As shown in Figure 4).

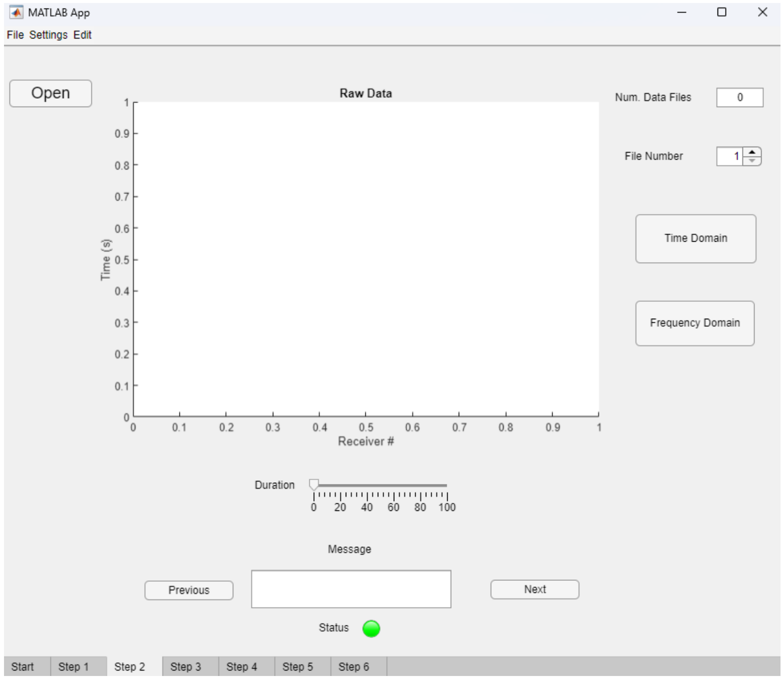

Figure 4. Open raw data.

This action will open a window entitled “Select File to Open” (Figure 5). Users can select data files and click “Open”.

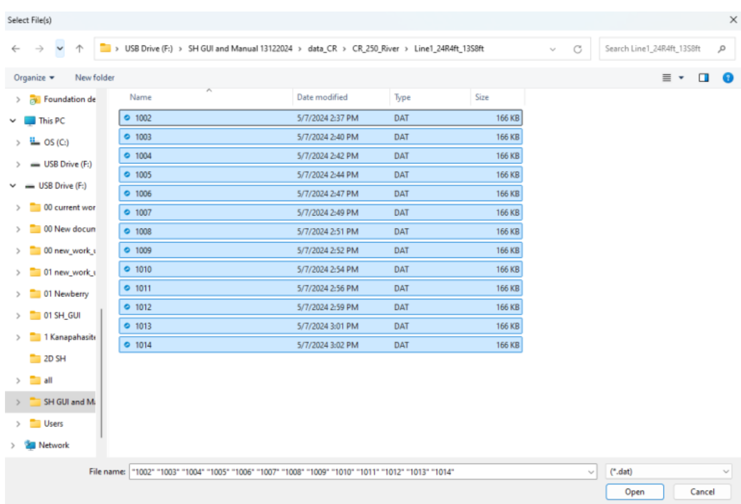

Figure 5. Data selection.

The loaded data will be shown as seen in Figure 6. Users also can click the spinner up button to view the next source file.

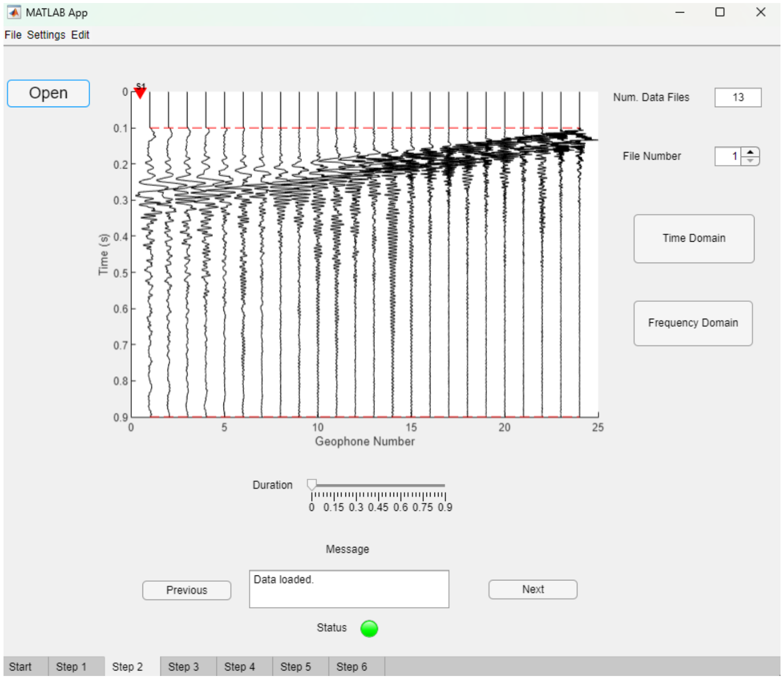

Figure 6. Display of loaded data in time domain

If users want to view the data in frequency domain, click the “Frequency Domain” button or click the “Time Domain” button to return to time domain (as shown in Figure 7).

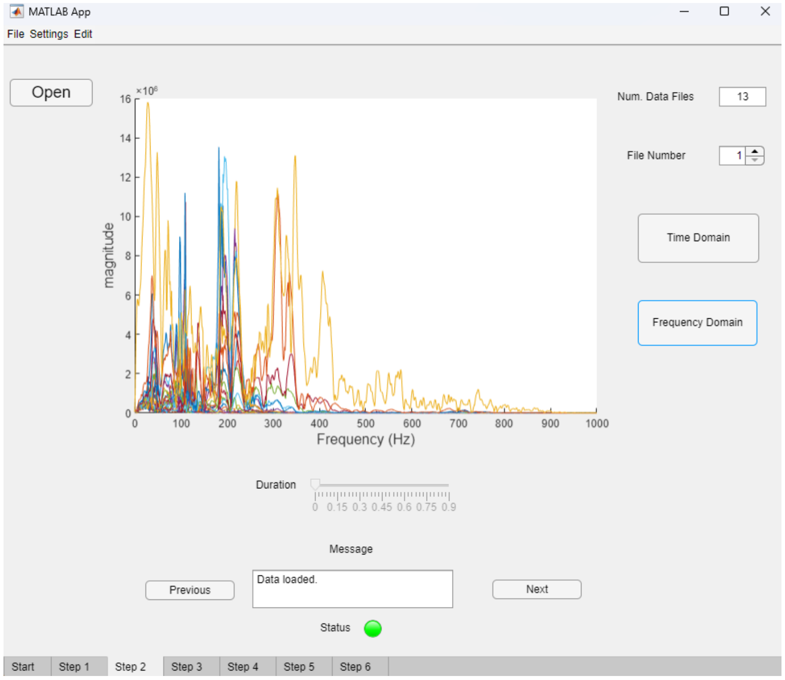

Figure 7. Display of loaded data in frequency domain

4. Preprocessing

Step 3 of the SH-Love FWI process is to preprocess the imported data, which must be done carefully. Select one of the following options:

1. Settings > Preprocessing
2. Click the “Next” button in the “Step 2” tab to move to “Step 3”.
3. Click “Step 3” at the bottom of the app.

to open the corresponding window as seen in Figure 8.

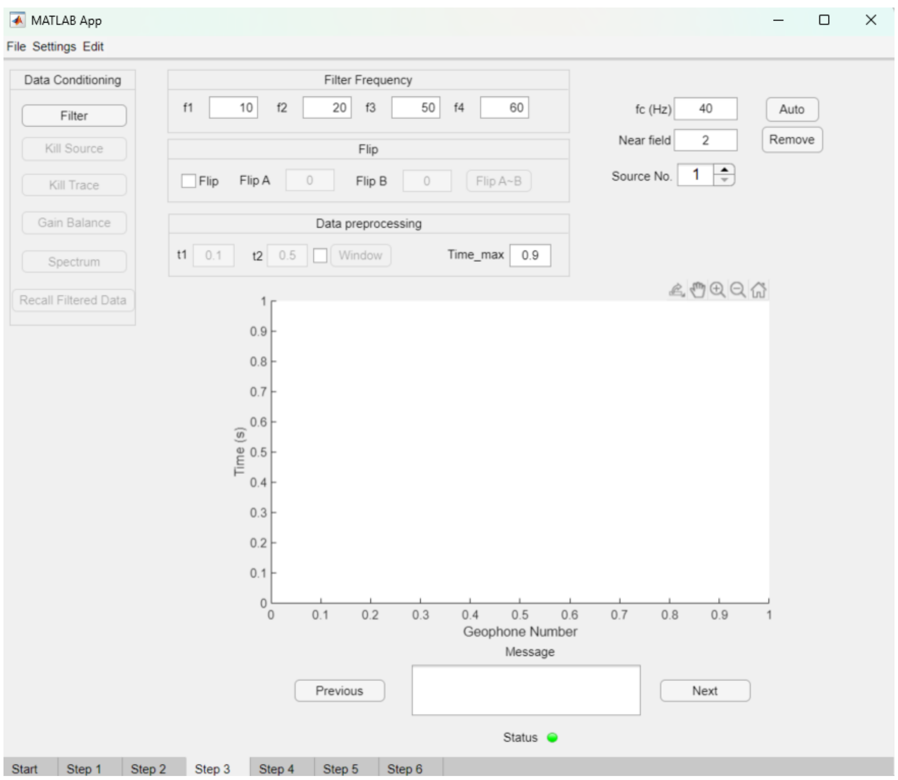

Figure 8. Preprocessing data page

Users perform the following steps:

1. **Set Filtering Frequencies:** Provide filter values f1, f2, f3, and f4 (Hz) to define the filtering bandwidth for data processing and inversion requirements. Then click “Filter” to apply filter (see Figure 9). *(Mandatory step)*

2. **Flip Receiver Order:** The source numbers in this software are always defined from left to right. If the first signal arrives at the geophones in the opposite direction, use the 'Flip' option to correct the alignment. Skip this step if they are already correctly aligned (as shown in Figure 10).

3. **Window Data:** Enter t1 and t2 values, then click "Window" to select a time window for the data.

4. **Manage Poor Profiles:** Use "Kill Source" to remove or restore poor profiles.

5. **Remove Data and Account for Near Field Effects:** Input values in the "Remove" and "Near Field" boxes to exclude unwanted data and account for damping effects (recommended: 2 channels; Figure 11). *(Mandatory step)*

6. **Kill Poor Channels:** Select "Kill Trace" to identify and remove channels with poor signals (Figure 12). Use this step to analyze all sources individually.

7. **Calculate Central Frequency:** Click "Auto" to compute the central frequency of the processed data (Figure 13).

8. **Balance Gain:** Use "Gain Balance" to visualize the gain-balanced profile.

9. **Check Frequency Spectrum:** Select "Spectrum" to view data in frequency domain.

10. **Recall Filtered Data:** Click "Recall Filtered Data" to restore the preprocessed data.

11. **Set Maximum Time Duration:** Adjust “Time_max” (seconds) to trim the input data's time duration. Sometimes, the data recorded after the main wave propagation consists only of noise and is not useful for analysis.

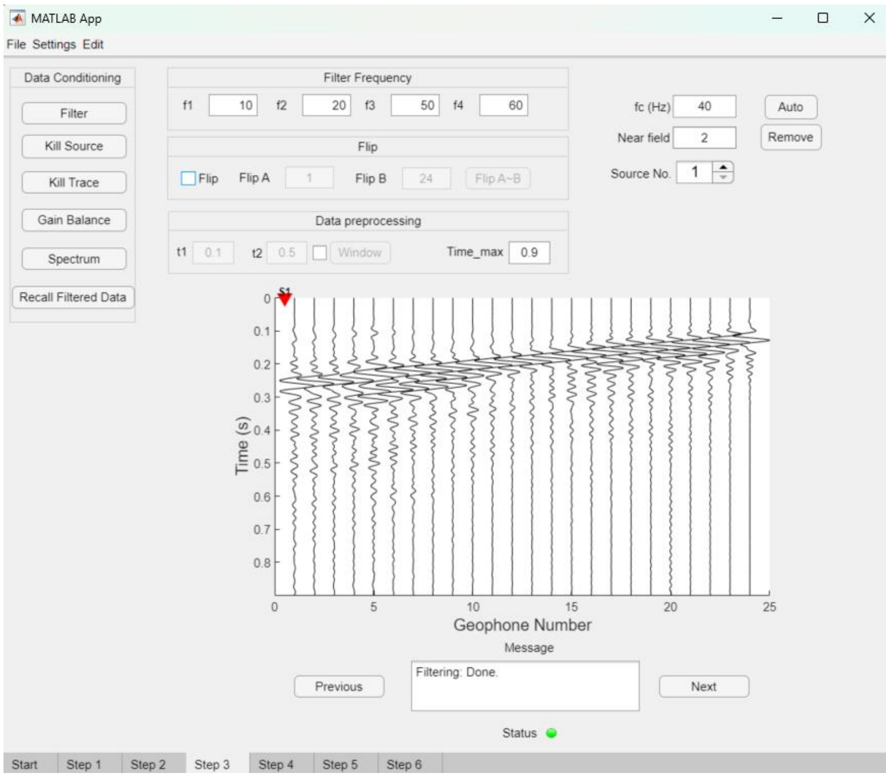

Figure 9. Filter data

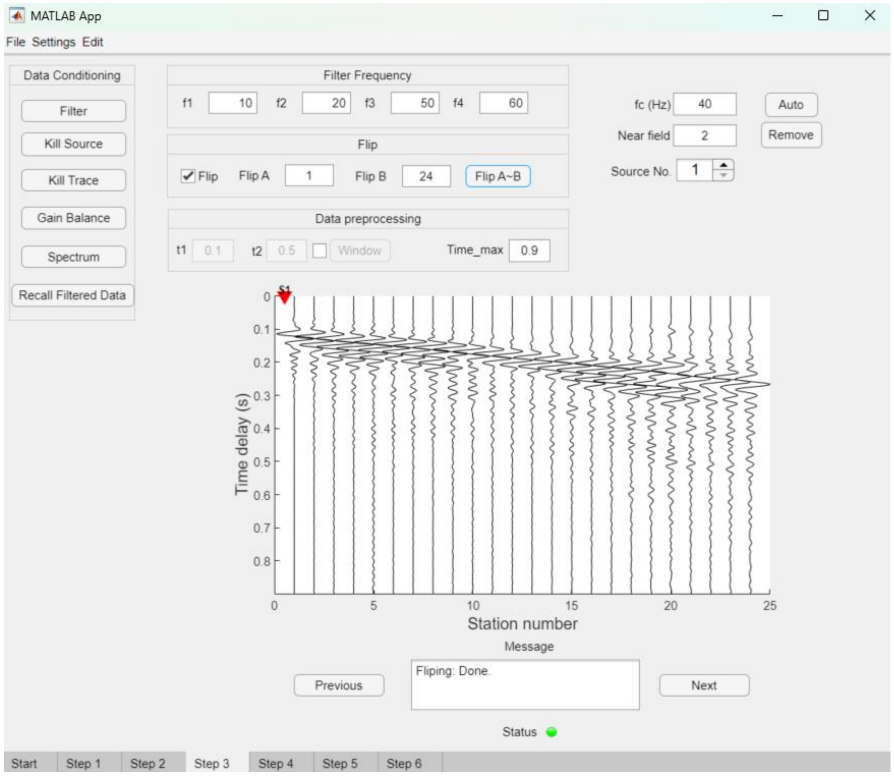

Figure 10. Flip data

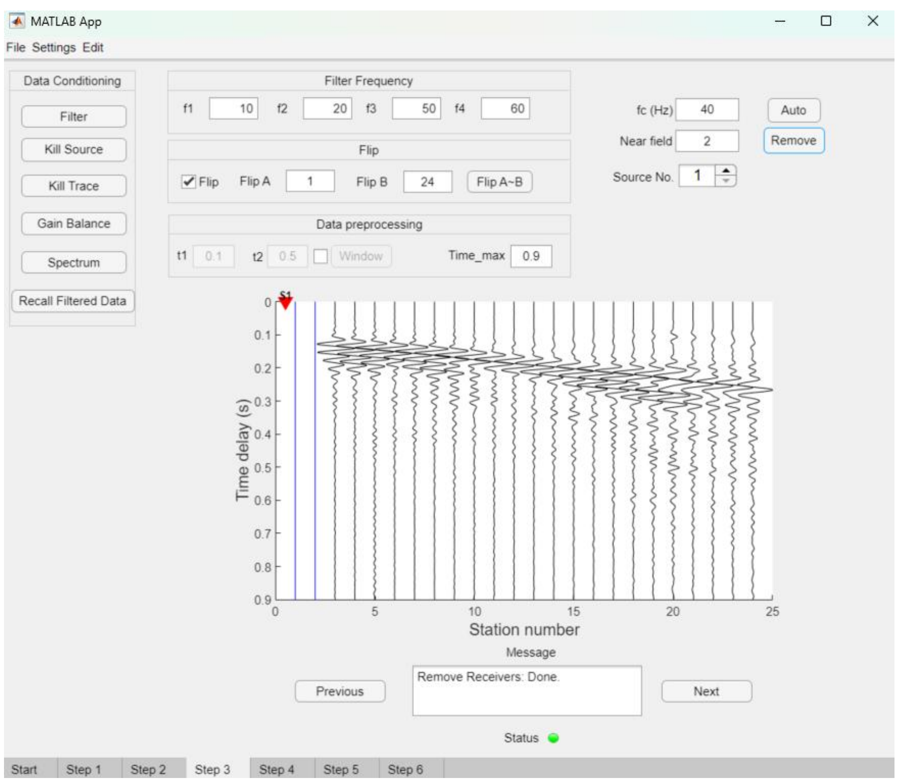

Figure 11. Remove near field data at source 11 (Blue Line).

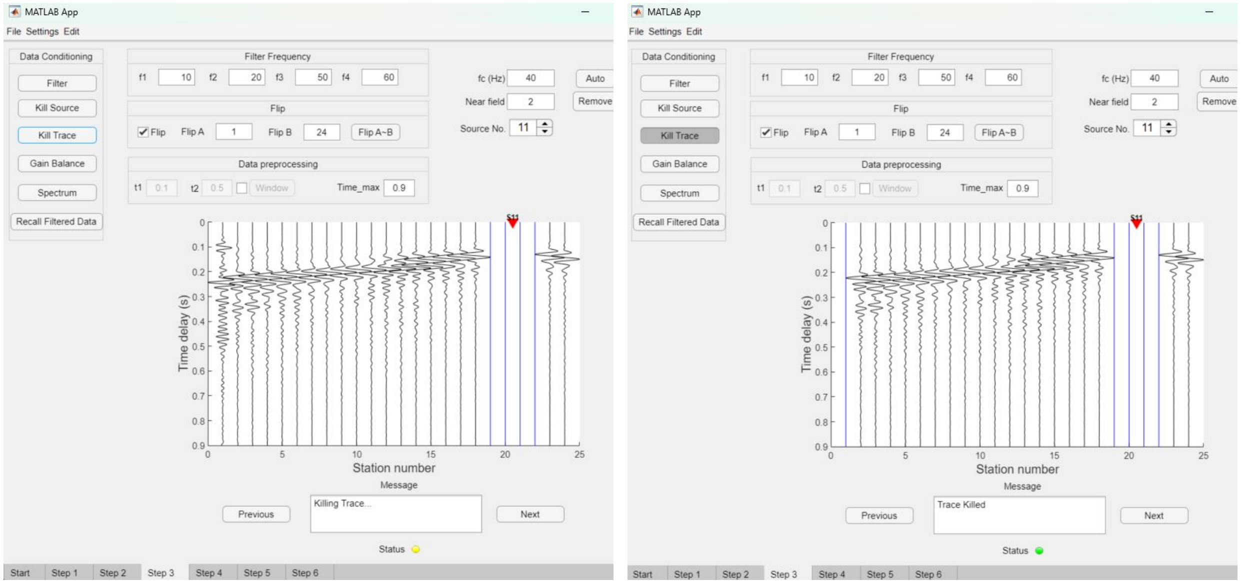

Figure 12. Kill trace at source 11 (blue line after clicking on the first channel).

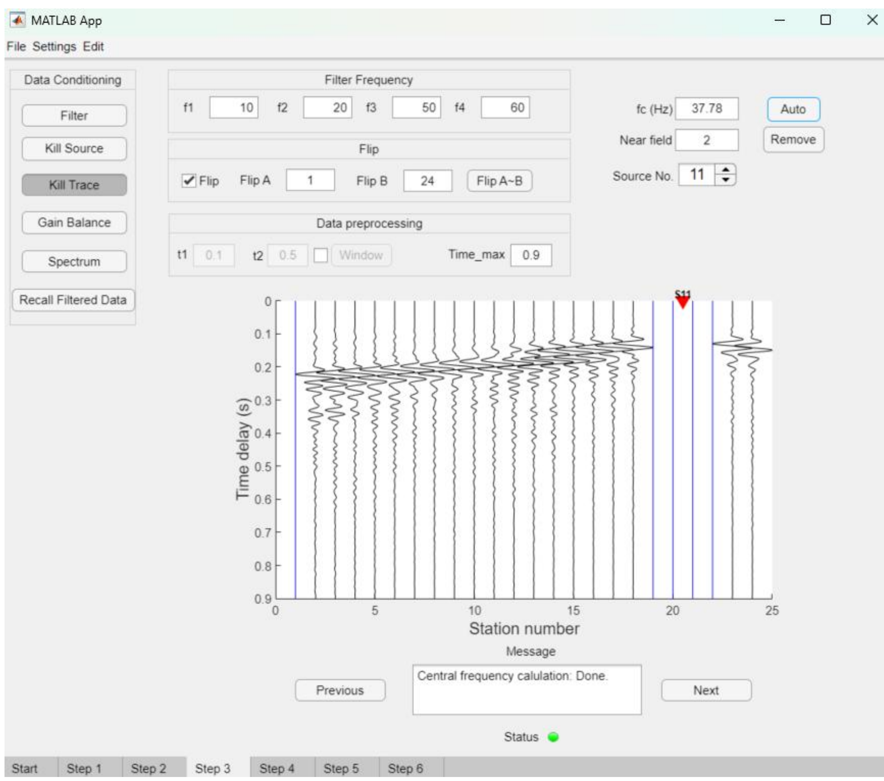

Figure 13. Calculate central frequency.

5. Spectral analysis

Step 4 of the SH-Love FWI is to do the spectral analysis. To do this, choose either:

1. Settings > Spec Analys.
2. Click the “Next” button in the “Step 3” tab.
3. Click “Step 4” at the bottom of the app.

To do this analysis, follow the steps below:

1) Select the source to analyze using the 'Select Source no.' box. (Figure 14).
2) Specify **"Velocity"** (e.g., 1000 m/s) and **"Frequency"** (e.g., 50 Hz) values for analysis.
3) Click **"Analyze"** to compute the dispersion curve.
4) Click **"Phase Velocity"** to identify the maximum phase velocity on the dispersion curve between **f_min** and **f_max**. Use this for the linear or multichannel analysis of surface wave (MASW) initial model in Section 7.
5) To remove unsmooth points, click **"Remove point"**, then select the point on the curve (Figure 15).

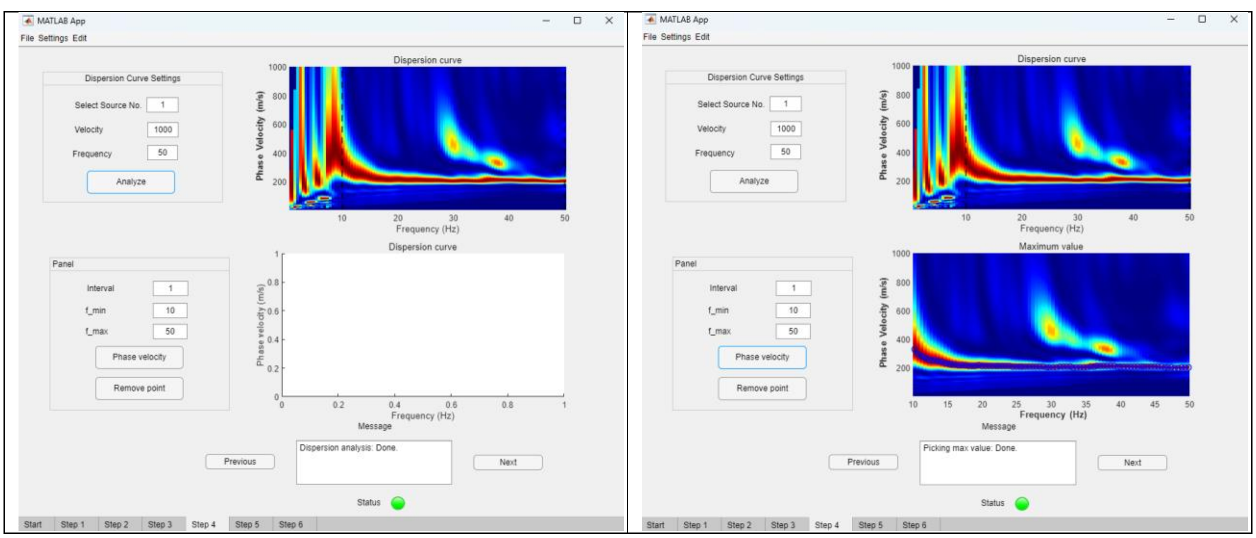

Figure 14. Dispersion analysis page.

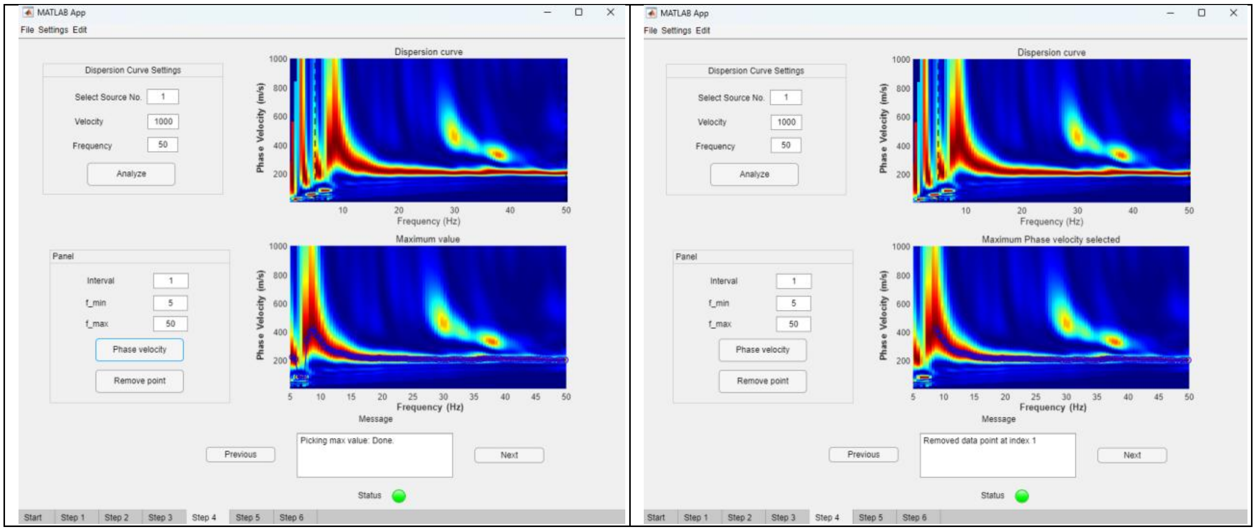

Figure 15. Removing wrong points on dispersion image.

6. Initial model

Step 5 of the SH-Love FWI is to generate the initial model. To do this, choose either:

1. Settings > Initial Model
2. Click the "Next" button in the "Step 4" tab.
3. Click "Step 5" at the bottom of the app.

Then:

1. On "Initial Model Type", two options are available for generating the initial model: **Linear** (create an initial linear Vs Model, as shown in Figure 16) or **MASW** (invert dispersion curve for initial Vs model, as shown in Figure 17).

   Linear *option is used when measured field data is high quality, and* **MASW** *is only used when field data is low quality.*

2. Click 'Generate' to create the initial model.

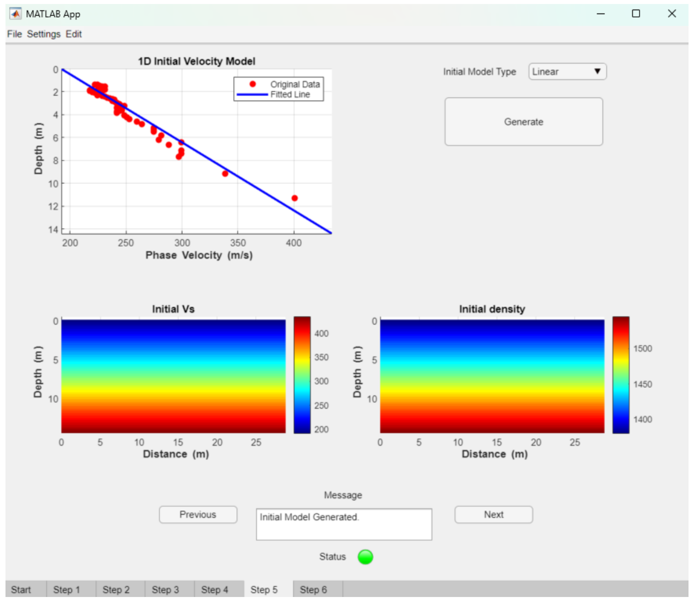

Figure 16. Initial model for Vs and density (Linear).

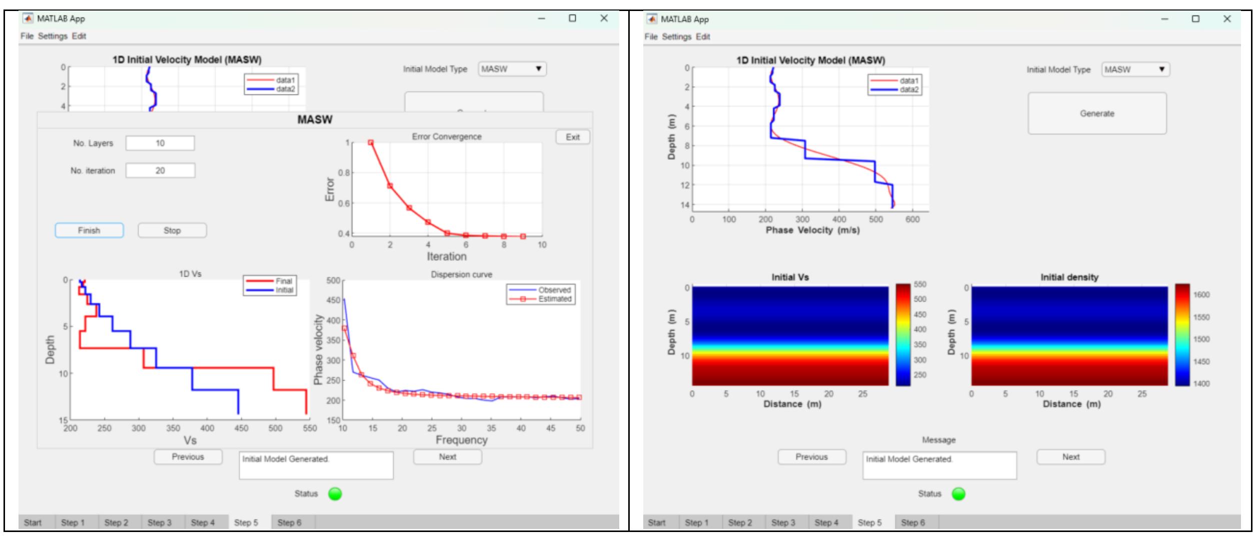

Figure 17. Initial model for Vs and density (MASW).

7. Inversion

Run inversion

The final step (Step 6) of the SH-Love FWI is to invert the Vs (shear wave velocity) and rho (density) profiles. This iterative process updates the initial models to match modeled data with field data, producing the final Vs and rho models.

To do this step, choose either:

1. Settings > Inversion
2. Click the "Next" button in the "Step 5" tab.
3. Click "Step 6" at the bottom of the app.

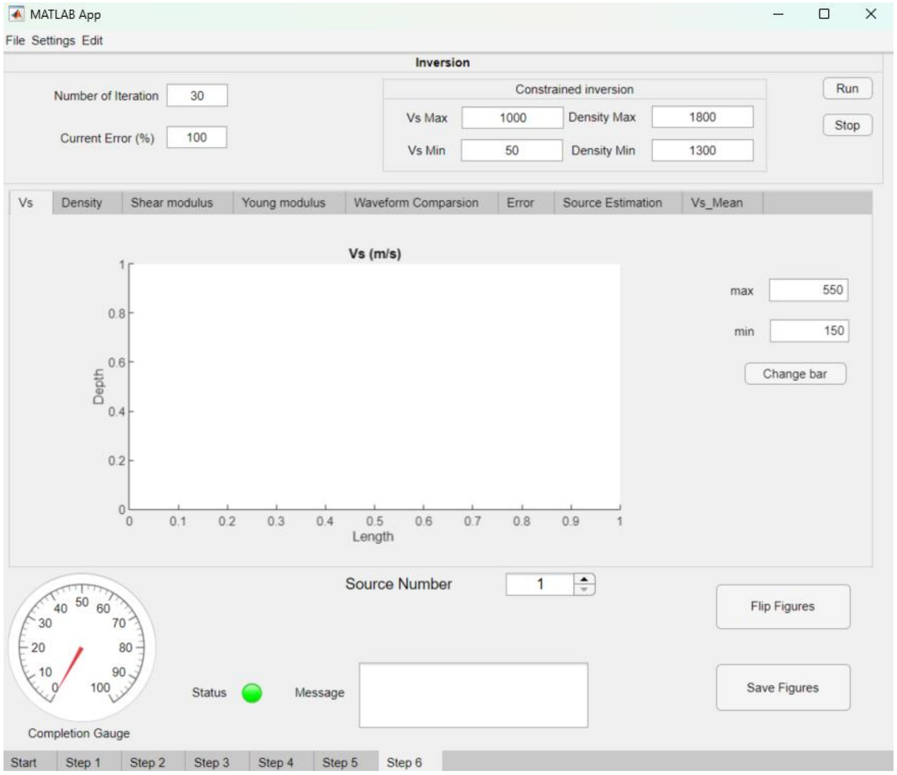

Figure 18. Inversion page

As shown in Figure 18, users do the following:

1) In the "**Inversion**" box: Enter the **number of iterations**.
2) **Vs Max**, **Vs Min**, **rho Max**, and **rho Min** are constraints; it is generally not recommended to modify these unless necessary.
3) Click the "**Run"** button to start the inversion analysis.
4) To stop the analysis, click the "**Stop"** button. (Important: The stop action may take effect only after the current step is completed).

Monitor Results:

- During and after the inversion process, the following outputs will be displayed:

- Updated Vs and rho models for each iteration.
- Shear modulus, Young's modulus, waveform comparisons, estimated source, and error values.
- A Mean-2D-to-1D model.

Post-Inversion Tools:

- **Change Color Bar:** Adjust the color range by selecting the desired **minimum** and **maximum**, then click **Change Bar**.
- **Flip View:** Click "**Flip Figures"** to invert the display orientation of the results.

  Refer to Figure 19 to 26 for visual representations of these results.

Save Results:

- To save all the figures in inversion step, click "**Save Figures"**. Results will be stored in the "InversionResults" folder as .jpg.
- If users wish to save specific outputs, use the "**Save"** introduced in the next section.

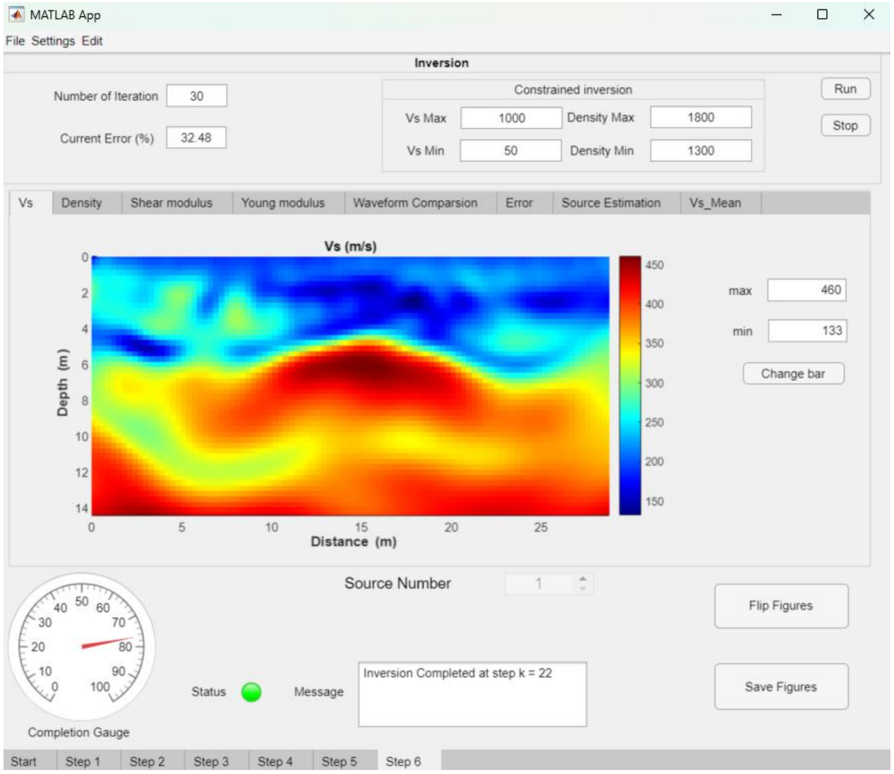

Figure 19. Inverted Vs Model

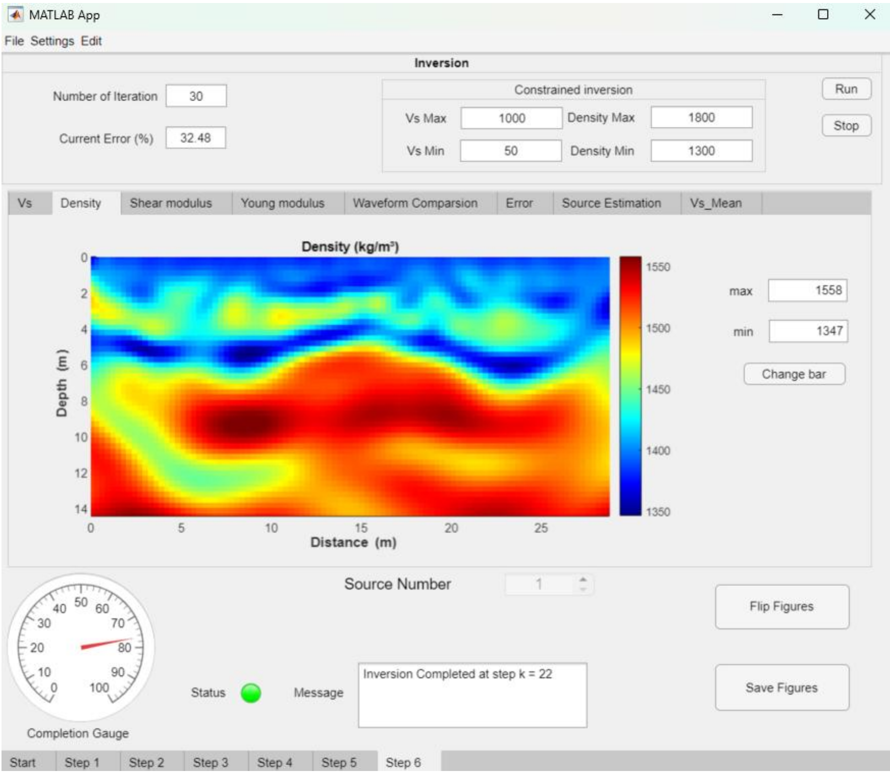

Figure 20. Inverted Density Model

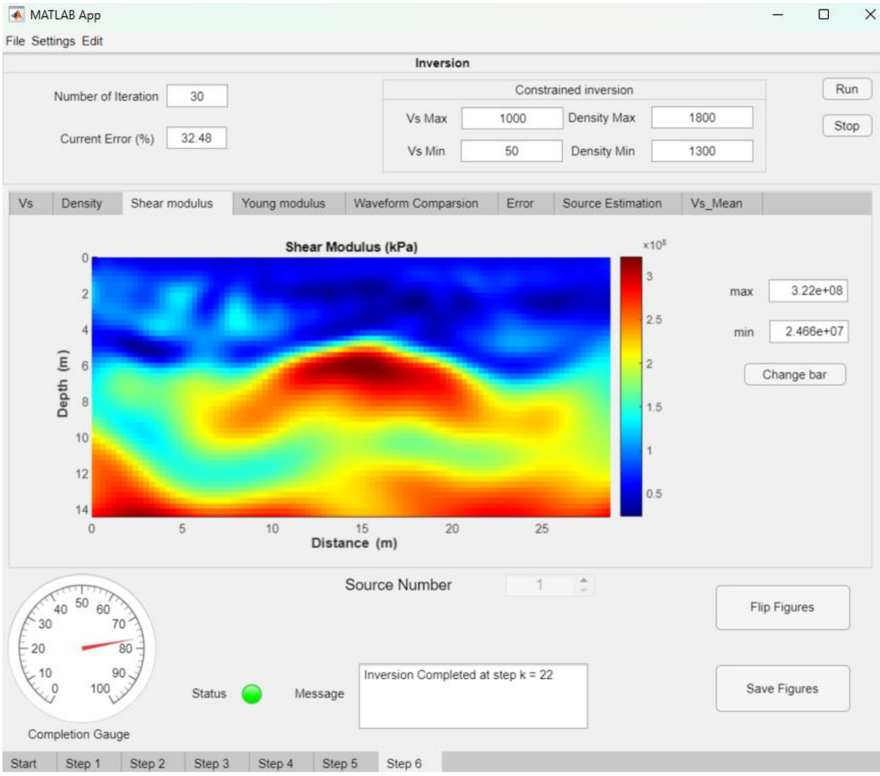

Figure 21. Inverted Shear Modulus

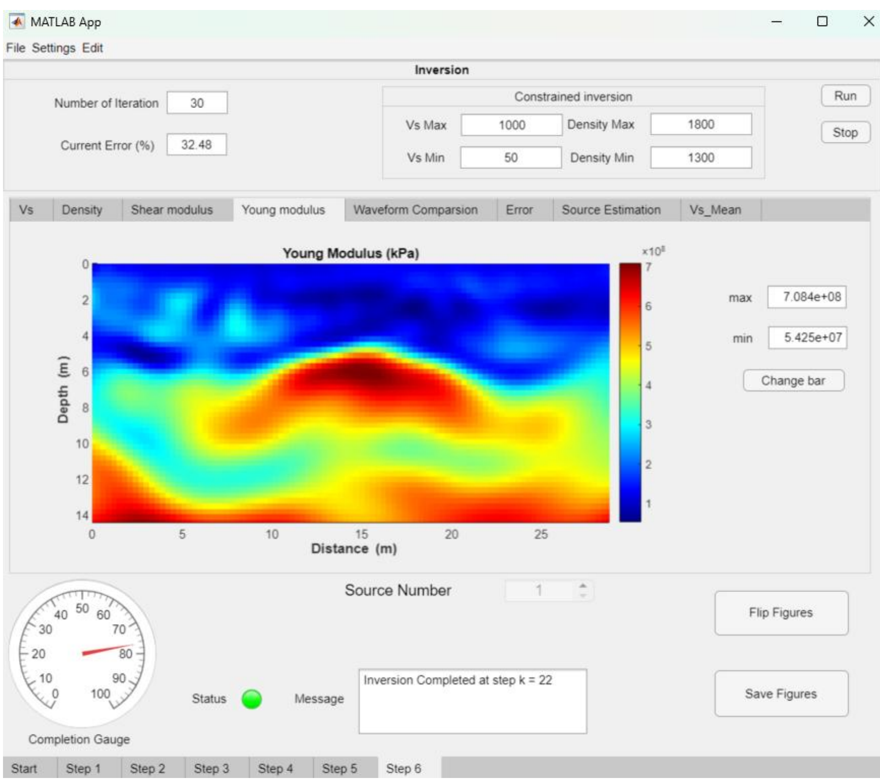

Figure 22. Inverted Young's Modulus

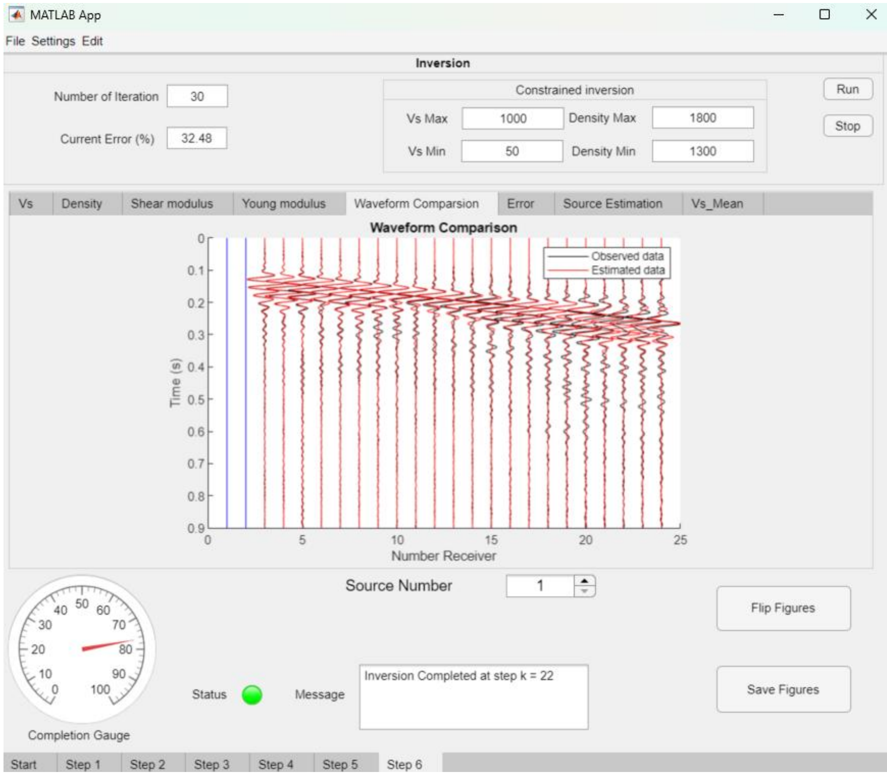

Figure 23. Waveform comparison

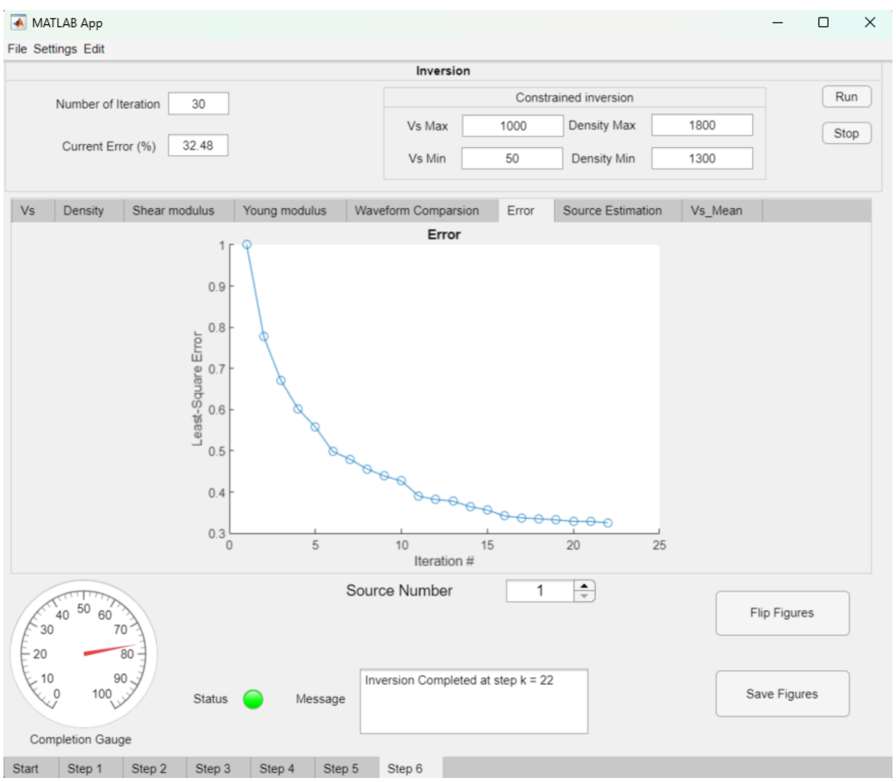

Figure 24. Error

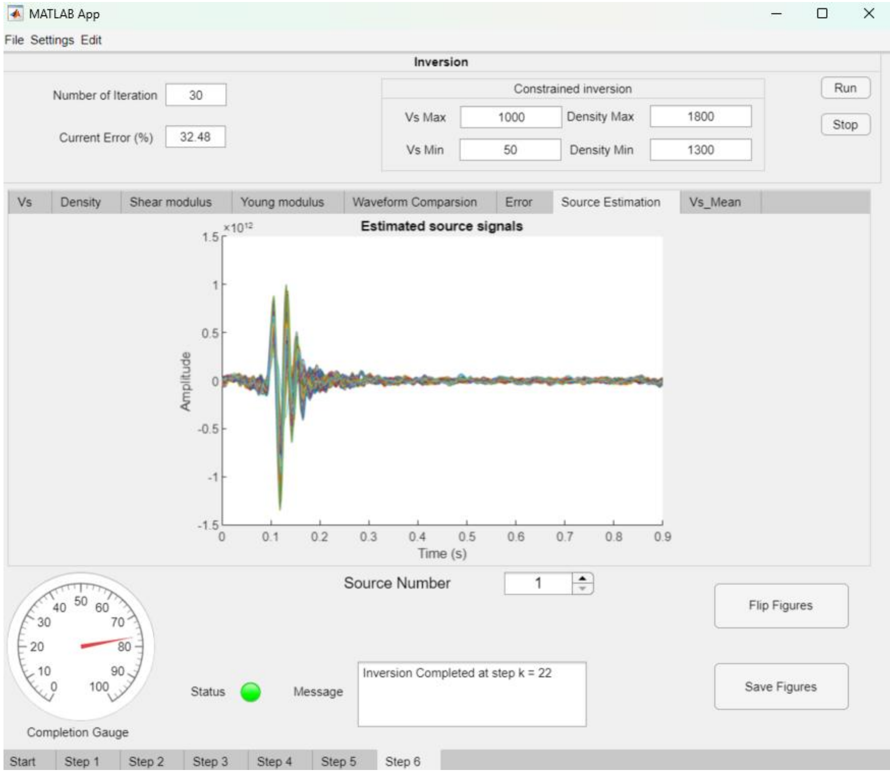

Figure 25. Estimated Sources

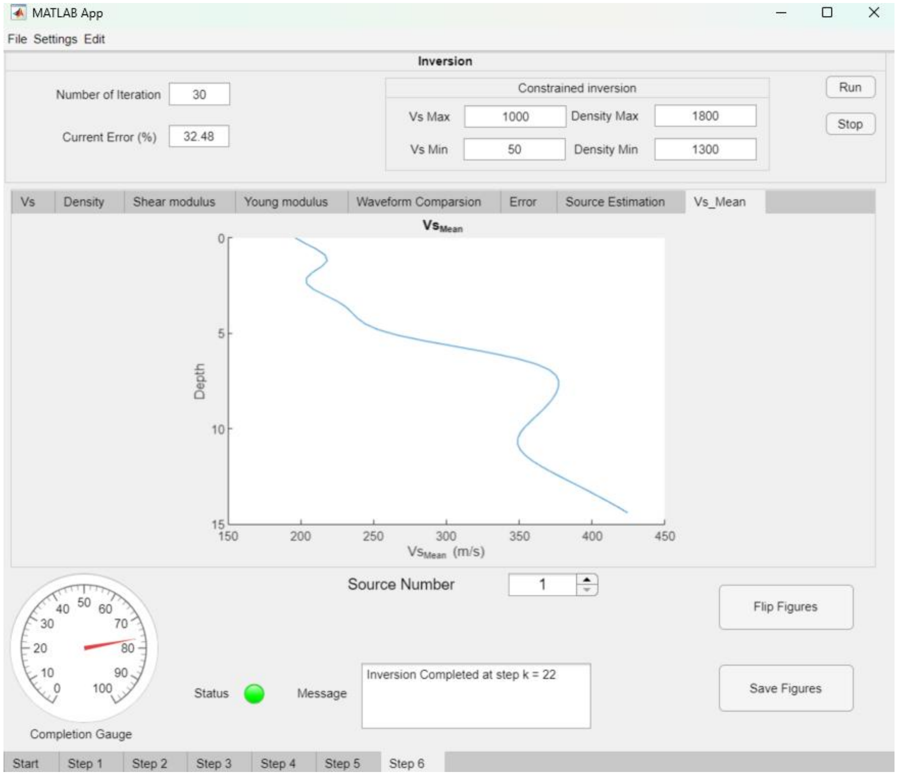

Figure 26. Mean-2D-to-1D Vs model.

Multiple runs

Normally, only one inversion run (first run) is needed for data analysis. However, an additional run (second run) can be done at higher frequency to improve characterized resolution. For multiple runs, whether adjusting the filter settings or modifying other parameters, follow these steps:

Choose either:

1. Settings > Preprocessing
2. Click the “Step 3” button.
3. Skip “Step 4 and 5”
4. Move to “Step 6” and run again as illustrated in **Section 8**.

8. Save and open inversion projects

a) Save

The input parameters, preprocessed data, and inversion results can be saved in **.txt** format after completing the inversion analysis. To ensure accurate saving of the working space, users must first provide the necessary data/parameters and execute all the corresponding project steps.

File > Save, or File > Save as

to save the current working space.

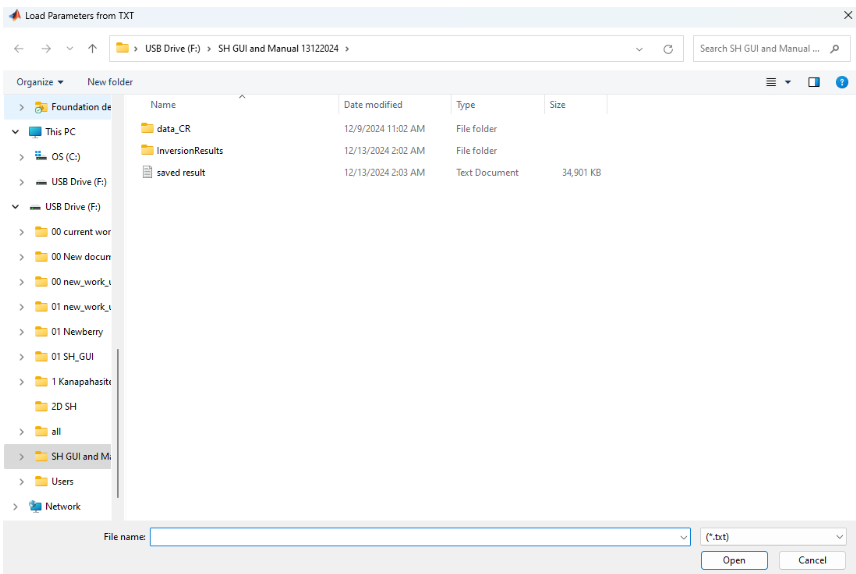

Figure 27. “Save” data.

b) Export

To export a specific project in **.xlsx** format, go to **File > Export**. This action opens a new window where users can select the save location and enter a filename. Once the filename is provided, the corresponding object will be exported in **.xlsx** format.

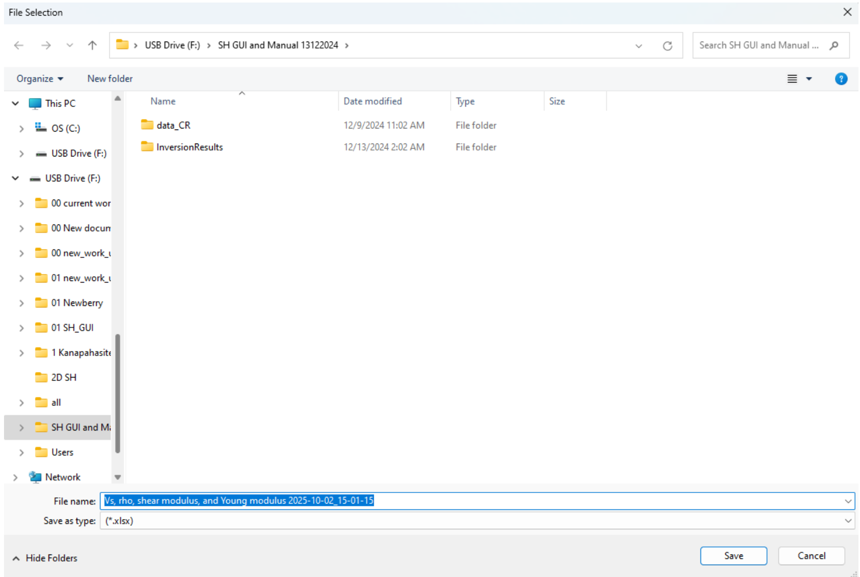

Figure 28. Export data.

c) Open

To open a saved project file, go to **File > Open**. This action opens a new window where users can select and load a saved **.txt** project file. For example, users can load a previously saved project.

Note: After loading a saved project, users can:

- Load additional datasets or files.
- Adjust the preprocessing setup or modify the inversion parameters (Steps 3, 4, 5, and 6).
- Click Run button to re-run the analysis with the updated settings or perform a second run using Vs and density results obtained from the first run.

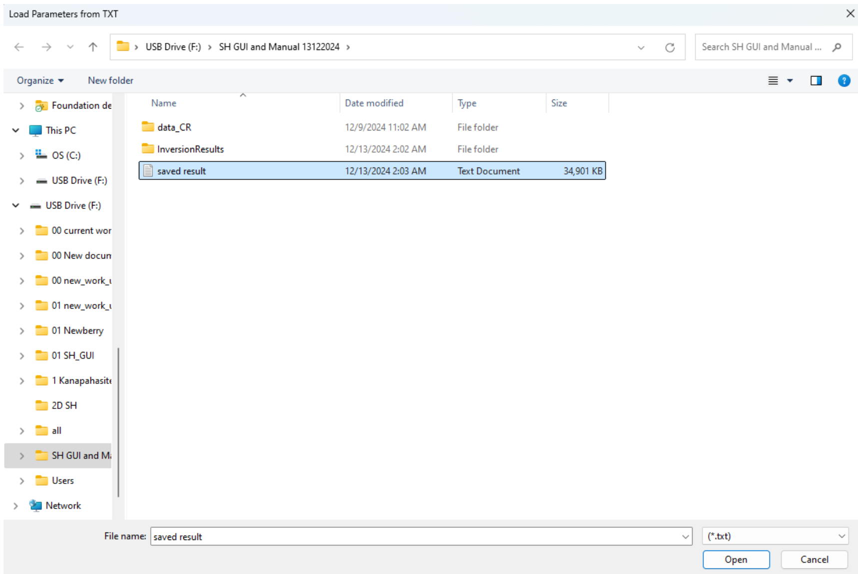

Figure 29. Load saved data.

d) Save Figures

To save all figures as both ***.pdf** and ***.jpg** files, users can click the "Save Figures" button in the application. Upon clicking, the application will save each one in both file formats in the directory.